STRUCTURAL STUDIES OF LAYERED CUPRATES AND BISMUTHATES

Christopher Jon Milne

A Thesis Submitted for the Degree of PhD
at the
University of St Andrews

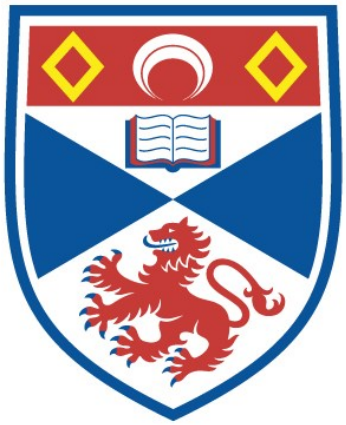

2002

Structural Studies of Layered Cuprates and Bismuthates

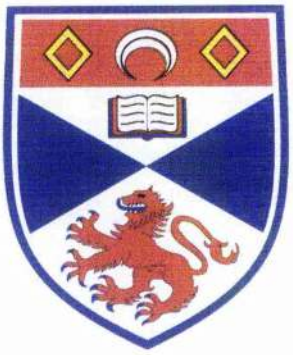

A thesis submitted to the University of St. Andrews as part fulfilment for the degree of Doctor of Philosophy.

Christopher Jon Milne
January 2002

Th E94

Declarations

I, Christopher Jon Milne, hereby certify that this thesis, which is approximately 18,000 words in length, has been written by me, that it is a record of work carried out by me and that it has not been submitted in any previous application for a higher degree.

Date 07 – 01 – 02 Signature of candidate :

I was admitted as a research student in October 1994 and as a candidate for the degree of Ph.D. in September 1995: the higher study for which this is a record was carried out at the university of St. Andrews between 1994 and 2002.

Date 07 – 01 – 02 Signature of candidate :

I hereby certify that the candidate has fulfilled the conditions of the Resolution and Regulations appropriate for the degree of Ph.D. in the University of St, Andrews and that the candidate is qualified to submit this thesis in application for that degree.

Date 07 – 01 – 02 Signature of supervisor :

In submitting this thesis to the University of St. Andrews I understand that I am giving permission for it to be made available for use in accordance with the regulations of the University Library for the time being in force, subject to any copyright vested in the work not being affected thereby. I also understand that the title and abstract will be published, and that a copy of the work may be made and supplied to any bona fide library or research worker.

Date 07 – 01 – 02 Signature of candidate :

Acknowledgements

I wish to thank the many students and staff of St. Andrews University whose help has made this work enjoyable. Special thanks go to my supervisor Dr. Phil Lightfoot for his patience.

I would also like to mention Drs. Richard Gover and Susan Blake whose shared wisdom has been invaluable.

Help has also been received from Mr. Alan Snedden and Mr. Tim Coombs when my computer skills were lacking.

Most of all I wish to acknowledge the support of my mother, father, sister and grandmother whose love made this possible.

Finally I would like to thank the University of St. Andrews for awarding me a studentship.

Abstract.

Studies have been undertaken trying to produce new high T_c superconducting cuprates. As a mechanism for superconductivity in these materials is sought, it is important to produce new materials with new structural features. Studies were carried out on three systems : bismuthates, quadruple perovskites and ruthenates.

Bismuthate work was aimed at trying to intergrow Sillen type phases with layered cuprate phases. This work yielded four new Sillen related structures: $CaBiO_2Cl$ [$P2_1/m$: a = 7.7311(1)Å, b = 4.1234(1)Å, c = 6.3979(2)Å and ß = 105.21(1)^0] has a puckered halide layer due to the lower co-ordination preference of the small Ca^{2+} ion. $SrBiO_2Cl$ [Cmcm : a = 5.7109(2)Å, b = 12.4081(5)Å, c = 5.5888(2)Å] is a Sillen X1 type material with an ordering of Sr and Bi in the double fluorite layers as previously observed in $BaBiO_2Cl$. Bi_2LaO_4Cl [I4/mmm : a = 3.9547(1)Å and c = 9.1275(3)Å] has triple fluorite layers with ordering such that La occupies the central layer only. These layers are separated by planar Cl layers. Isostructural Bi_2NdO_4Cl and Bi_2YO_4Cl have also been prepared. $Bi_6Ca_5O_{11}Cl_6$ [Cmcm : a = 3.865(6)Å, b = 12.57(2)Å and c = 43.05(7)Å] has an X1 related, Arppe type structure, with undulating (M_2O_2) layers, determined from microcrystal diffraction data. Microcrystals formed on reaction of the stoichiometry $Bi_{1.7}Ca_{2.7}O_{4-y}Cl_4$ were shown to possess a Sillen X1X3 type structure, confirming a previous report.

Work on perovskites involved doping studies of the Quadruple Perovskite series $Ln_2Ba_2Cu_2Ti_2O_{11}$ (Ln = Nd, Gd and Tb). Investigation of Sr doping for Ba in this series is reported, as is Cu substitution for Ti in the Nd system.

Work on trying to extend the observation of both superconductivity and ferromagnetism in the ruthenate $RuSr_2GdCu_2O_8$ involved investigation of $RuSr_2TbCu_2O_8$ 1-2-1-2 and quadruple perovskite $Ln_2Ba_2Cu_2Ru_2O_{11}$ (Ln = La, Nd, Gd and Tb) and $NdBa_3Cu_2TiNb_{1-x}Ru_xO_{11}$ systems.

Publications

Milne C.J., Lightfoot P., Short S. and Jorgensen J.D., *Journal of Materials Chemistry* **5(9)**, 1419 (1995).

Fray S.M., Milne C.J. and Lightfoot P., *Journal of Solid State Chemistry* **128**, 115 (1997).

Chapter Summary

Contents

Contents

Contents

Contents

Contents

Contents

1. INTRODUCTION

1.1 The Discovery of Superconductivity

In the early years of the twentieth century, Heike Kammerlingh Onnes worked at the Leiden Institute of Physics on the electronic properties of metals at low temperatures. His work on very pure samples of gold and platinum had shown the resistivity of samples decreasing with temperature with a reduction of the rate of decrease as the temperature falls. He concluded that there were three possibilities to the behaviour at even lower temperatures :

1. The resistance could continuously fall to zero as the temperature is reduced. (Figure 1.1, curve 1)
2. It could fall to a fixed limiting value. (Figure 1.1, curve 2)
3. It could pass through a minimum and approach infinity at very low temperatures. (Figure 1.1, curve 3).

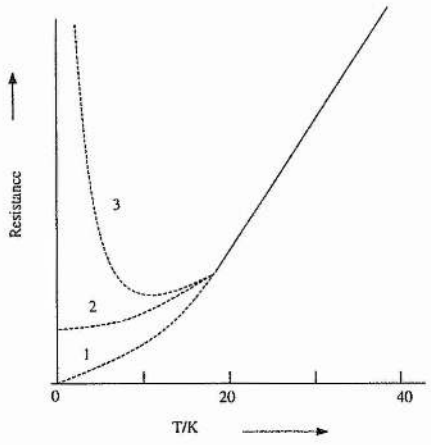

Figure 1.1. The three possible curves for the resistance of metals at low temperatures.

In 1908 Onnes succeeded in liquifying helium [1] which made temperatures in the vicinity of absolute zero (1K - 10K) accessible. With these lower temperatures Onnes found that the resistivity of pure forms of gold and platinum corresponded to Curve 2. i.e. The resistance fell to a residual value which depended on the degree of purity of the sample.

These results were described at the 3rd International Congress of Refrigeration in Chicago in 1913. There he postulated :

"Allowing a correction for the additive resistance I came to the conclusion that the resistance of absolutely pure platinum would have vanished at the boiling point of helium."

To test his hypothesis Onnes decided to measure the low temperature resistance of mercury. Mercury could be made very pure, by multiple distillations, resulting in a reduced residual resistance. His first experiments appeared to confirm this theory with the resistance immeasurably small below 4.2 K. However further experiments with improved apparatus undermined his postulation. He noted :

"At this point (somewhat below 4.2 K) within some hundredths of a degree came a sudden fall not foreseen by the vibrator theory of resistance, that had framed, bringing the resistance at once less than a millionth of its original value at the melting point....., Mercury has passed into a new state which on account of its extraordinary electrical properties may be called the superconductive state." [2]

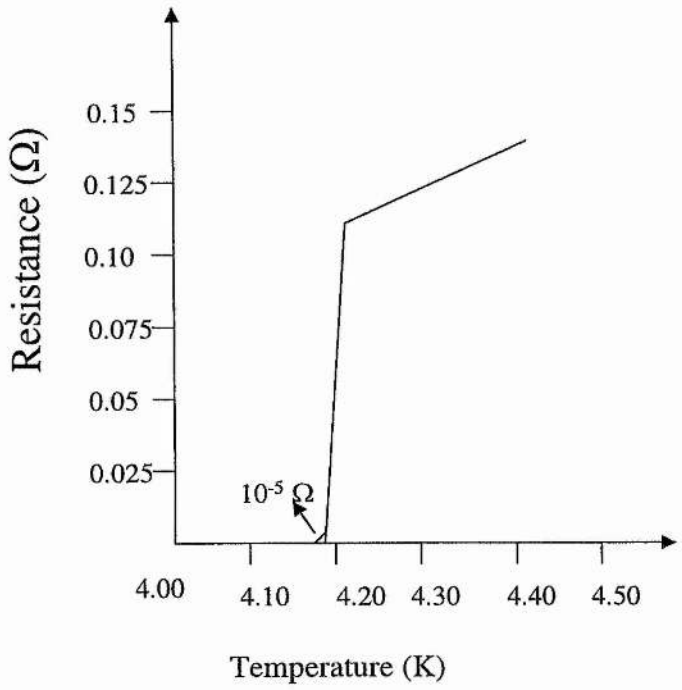

Figure 1.2. Resistivity v's Temperature for Hg [3].

1.2 Definitions and Properties

The phenomenon of superconductivity is therefore the sudden and complete disappearance of the electrical resistance of a substance when it is cooled below a certain temperature. This temperature is known as the critical transition temperature and is denoted by T_c.

It was discovered in 1933 that this loss of electrical resistance in the material is accompanied by the complete expulsion of magnetic fields from its interior (Figure 1.3). This formation of a perfect diamagnet with the total expulsion of magnetic flux is known, after its discoverers, as the Meissner-Ochsenfeld effect [4].

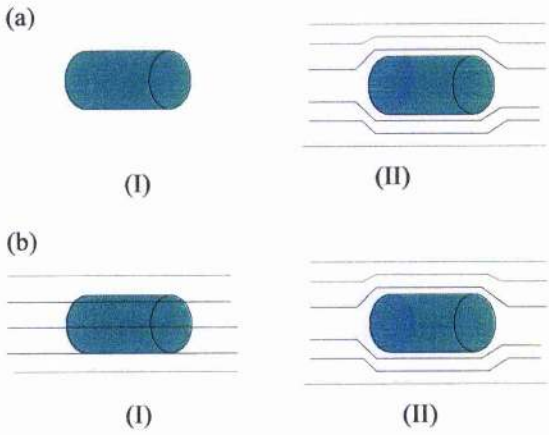

Figure 1.3. (a) (I) Shows a superconductor with no magnetic field. When a field is applied in (II) the magnetic flux is excluded. (b) (I) shows a superconductor above T_c in a magnetic field. When cooled to below T_c as in (b) (II) the flux is expelled from the sample. Both these effects are Meissner effects.

It has also been found that the value for T_c changes in the presence of a magnetic field. It has been shown that the critical temperature drops as the applied field is increased. It follows from this observation that a superconducting material can be made non-superconducting by the application of a large enough field. The minimum value of magnetic field required to bring about the transition (Figure 1.4), known as the critical field strength, is denoted by H_c. The value of H_c is dependent on the type of material and the temperature [5]. A further observation, known as the Silsbee effect, is that if the current passed through a superconductor exceeds a critical value then the superconductivity is destroyed. This value, denoted by J_c, is known as the critical current and is dependent on the material and its geometry [5].

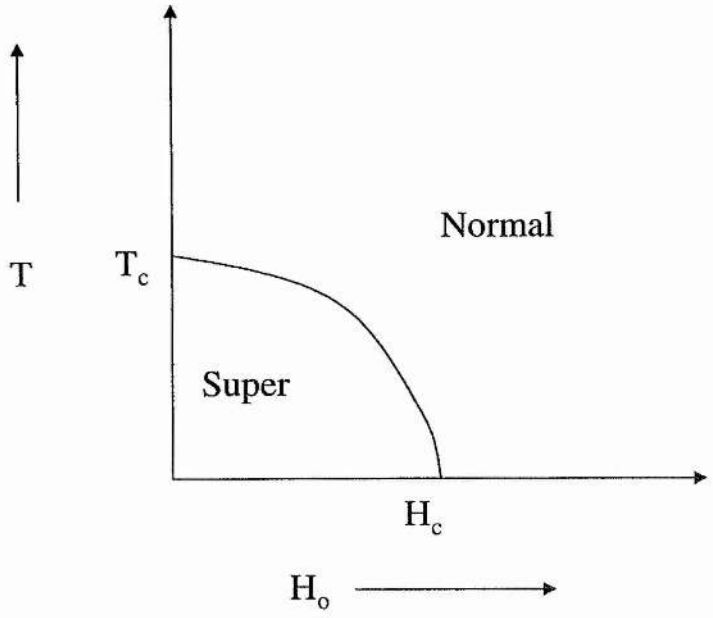

Figure 1.4. The breakdown of superconductivity upon exposure to a magnetic field exceeding H_c. Note that this is for a type I superconductor (see section 1.4).

1.3 The Evolution of Oxide Superconductors

For more than half a century research into superconductivity focussed on elemental and binary metallic systems. The highest T_c for a material of such a class was 23 K, which is observed for Nb_3Ge [6]. Recently however MgB_2 has been shown to superconduct at 39 K [7]

In the early 1960's the first oxide superconductors were discovered. Reduced phases of perovskitic strontium titanate, $SrTiO_{3-x}$, were found to superconduct at ~0.7K. [8]

The perovskite structure is named after the mineral $CaTiO_3$. Perovskites are of general formula ABX_3.In this structure the B cation is octahedrally co-ordinated by the anion X. These octahedra then share corners as shown overleaf in Figure 1.5 :

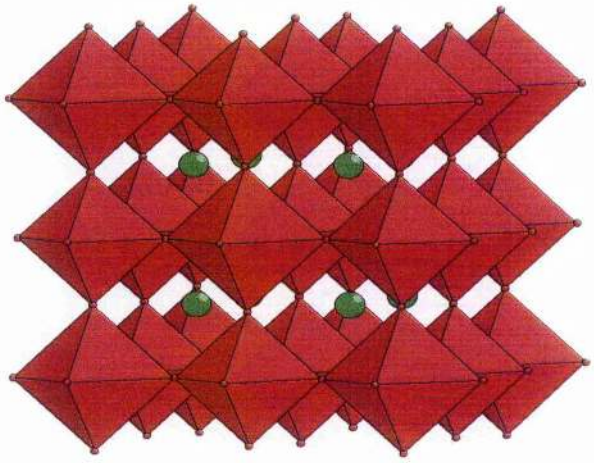

Figure 1.5. The perovskite structure, with BX_6 octahedra shown as red and the A cations shown as green.

The A cation resides at the centre of each set of eight octahedra as shown above. This means that there are twelve anions X co-ordinating the A cation.

Research into oxide systems continued and realised improved T_c's with the synthesis of tungsten, molybdenum and rhenium bronzes. These materials showed a T_c onset between 4K and 6K. [9][10]

The bronzes are similar to the perovskite structure, in that they are again comprised of corner sharing octahedra. In these cases we have tungsten, molybdenum or rhenium co-ordinated by six oxygens comprising the octahedra. This corner sharing lattice provides tunnels in which alkali metals can be located. The resultant crystal structure depends on the amount of alkali metal incorporated. Tungsten, molybdenum and rhenium bronzes can be cubic (and perovskite like) (Figure 1.5), tetragonal (Figure 1.6) or hexagonal.

A.R. Sweedler *et al.*, studied the Na_xWO_3 system and found that varying x allowed the formation of a cubic form and two tetragonal forms. The cubic and

tetragonal II materials are non-superconducting. However they found that the tetragonal I form, at x = 0.2, is superconducting at 0.5 K [9]. They concluded that superconductivity was a general property of non – cubic tungsten bronzes.

Hexagonal superconducting Tungsten bronzes include : K_xWO_3, Rb_xWO_3, Cs_xWO_3, Ca_xWO_3, Sr_xWO_3, Ba_xWO_3, $(NH_4)_xWO_3$, In_xWO_3, Tl_xWO_3 and Li_xWO_3.

Tetragonal superconducting Tungsten bronzes include : K_xWO_3 and Ba_xWO_3.

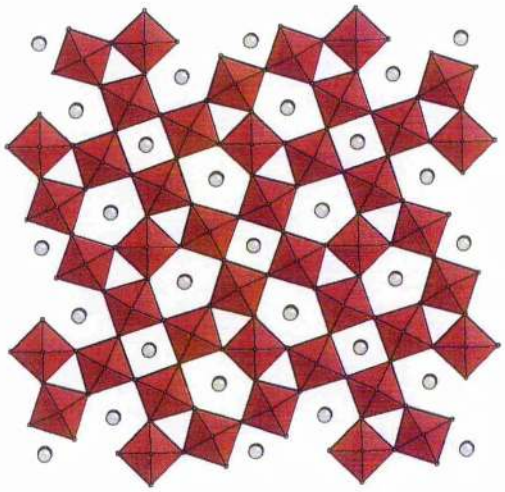

Figure 1.6. The tetragonal tungsten bronze structure of K_xWO_3 with WO_6 octahedra shown as red and the K^+ ions shown as grey. Note the K^+ ions occupying the sites within the four and five sided channels whilst the three sided channels are vacant.

Sleight et al., produced Rhenium and Molybdenum bronzes and showed the hexagonal $K_{0.3}ReO_3$ to be a 3.6K superconductor, whilst the tetragonal $K_{0.5}MoO_3$

shows a T_c of 4.2K [10]. Cubic Na_xMoO_3, K_xMoO_3, Na_xReO_3 and ReO_3 were shown to be non-superconducting.

The gradual increase in T_c continued into the 1970's. $LiTi_2O_4$, with its spinel type structure (Figure 1.7) showed a superconducting transition at 13K [11], while the $BaPb_{1-x}Bi_xO_3$ system, with its perovskite structure, gave a similar T_c value [12].

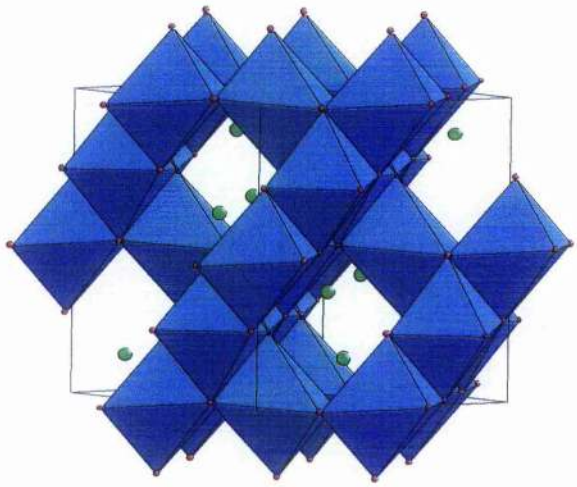

Figure 1.7. The Spinel structure of the $LiTi_2O_4$ superconductor. TiO_6 octahedra are shown in blue with Li green.

There was then a quiet period in which little advance was made in the search for materials with higher values of T_c. In 1986 however, a significant breakthrough was made. During their study of the La-Ba-Cu-O system, Bednorz and Muller found that the oxide ceramic $La_{2-x}Ba_xCuO_4$ was a superconductor at 30K [13]. This discovery marked the beginning of an unprecedented surge in activity in the field. Within the next few months a massive jump in the record value of T_c occurred with the synthesis of another copper oxide material

$YBa_2Cu_3O_{7-\delta}$ [14]. With its T_c of 93K, this compound took superconductivity above the boiling point of liquid nitrogen (77K), and from a laboratory phenomenon to a technology with important practical applications [15].

1.4 Classification of Superconductors.

Superconductors are classified as either Type I or Type II, with all the superconducting elements other than vanadium, technetium and niobium comprising the Type I superconductors. Sometimes called soft superconductors, these have the lowest values of T_c and have a characteristic sharp transition to the superconducting state.

All other superconductors are classified as Type II or hard superconductors. They have a broad transition to the superconducting state through which they exist in a mixed state (Shubnikov State). In this mixed state vortices of superconducting current surround cores of normal state material.

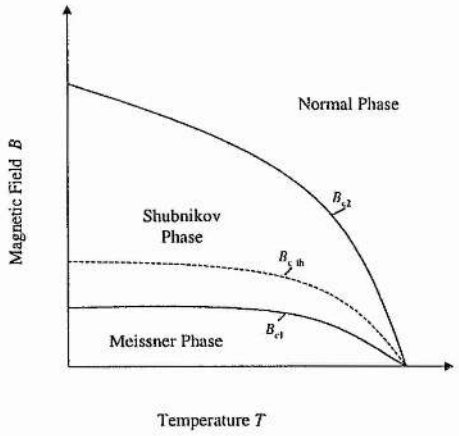

Figure 1.8. The breakdown of superconductivity, through a mixed state, on application of an increasing magnetic field for a Type II superconductor.

In 1957 John Bardeen, Leon Cooper and John Schrieffer published their Theory of Superconductivity which has since been named after each of them as BCS theory [16]. This explains the origins of superconductivity and the properties of superconducting elements and simple alloys. The basis of superconductivity is said to be the charge carriers, which in BCS superconductors are pairs of electrons known as Cooper pairs. These pairs move cooperatively through the material, unaffected by thermal vibrations below T_c. Electrons normally repel each other but are made to attract each other through an electron – phonon interaction in the superconductive state.

If we consider an electron moving through a lattice of positive metal atoms it follows that the lattice will contract towards this electron. This distortion (or phonon) causes an area of increased positive charge to be set up around the electron causing a second electron to be attracted to it. These attracting electrons are the Cooper pair which move cooperatively through the structure unaffected by thermal vibrations below T_c.

BCS theory cannot explain superconductivity at temperatures above ~35 K (making MgB_2 especially interesting) and hence a new theory is required. However it is known that in all superconductors the charge carriers are Cooper pairs, be they pairs of electrons or pairs of electron holes. What is required is thus an explanation of the pairing mechanism of the charge carriers at the elevated temperatures characteristic of cuprate superconductors.

1.5 Features of Cuprate Superconductors

Since the Nobel Prize winning discovery of superconductivity in the $La_{2-x}Ba_xCuO_4$ system, a huge number of new superconducting cuprate materials have been made. A publication by Tokura and Arima [17] states that although these cuprate superconductors are often compositionally quite complex they share a number of structural similarities. The cuprate superconductors can be classified as either oxygen deficient perovskites (eg $YBa_2Cu_3O_7$) or intergrowths (eg La_2CuO_4) both of which are layered.

Different layers within these cuprate superconductors contribute different factors to the observation of superconductivity. Firstly we have a copper oxide layer with four oxygen ions surrounding a copper ion lending to a square planar type coordination. These squares are corner sharing and form an infinite two dimensional lattice in the crystallographic a-b plane. The O-Cu-O linkages are approximately 3.8-3.9 Å and it is within these sheets that the superconductivity occurs. The sheets are separated by a varying number of insulating block layers. These blocks are often composed of simple metal or metal oxide units. ie :

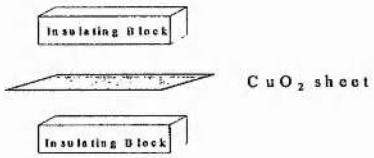

Figure 1.9. Tokura and Arima's classification of cuprate superconductors

A further requisite, for the observation of superconductivity in cuprate systems, is that the Copper in the CuO_2 planes must be of mixed valence. ie. Cu^{2+}/Cu^{3+} or Cu^{2+}/Cu^{+}. If the material is partially oxidised to give Cu^{2+}/Cu^{3+} character then it is said to be a p-type superconductor with the charge carriers

deemed to be pairs of positive holes. On the other hand a material reduced to give Cu^{2+}/Cu^{+} character is called an n-type superconductor with negatively charged electron pairs acting as the charge carriers. A maximum value of T_c is obtained for average oxidation states for copper of 2.15 in p-type superconductors and 1.85 in n-type superconductors.

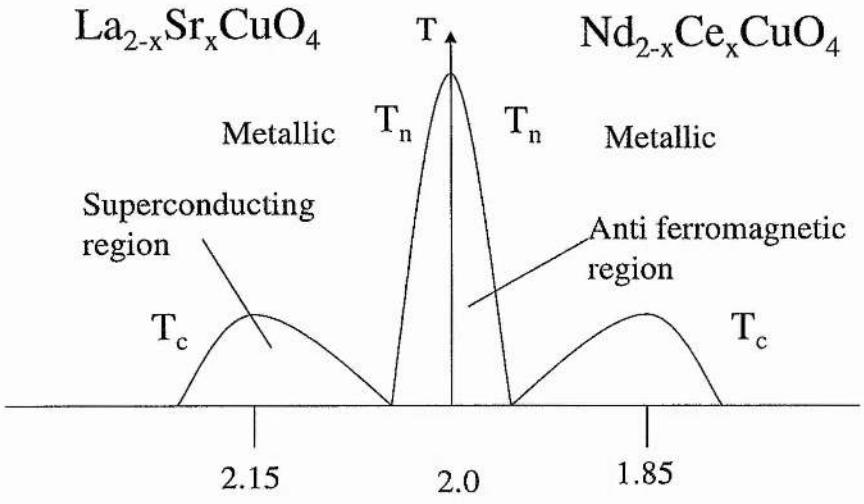

Figure 1.10. Electronic phase diagram for cuprate superconductors, showing their existence to be near a metal – insulator transition.[18]

This mixed valence is achieved by altering (doping) the insulating block layers. An insulating/semiconducting CuO_2 sheet consists of Cu^{2+} and O^{2-} and hence has an overall charge of –2. It follows therefore, for the maintenance of charge neutrality, that the block layers must have a sum charge of +2. The valence of the copper in the CuO_2 planes can therefore be modified by changing the sum charge of the insulating block layers by aliovalent ion substitution, or control of oxygen stoichiometry, within these block layers.

If the block layers are large with respect to the CuO_2 planes then the planes will be under tension. It follows that any action which will reduce the bonding character of the O-Cu-O linkages is favoured in this situation.

The highest occupied energy band is primarily of Cu 3d character and is antibonding with respect to the in plane O-Cu-O bonds. Thus large interplanar blocks favour n-type doping which adds electrons to the antibonding highest energy band.

Conversely, small interplanar blocks place the CuO_2 planes under compressive stress. Thus p-type doping, and the increase in bonding character of the O-Cu-O bonds alleviates this stress. Hence:

Requisites for superconductivity in Cuprates:

1. Stoichiometric CuO_2 planes with O-Cu-O linkages of dimensions ~3.8-3.9A
2. Insulating block layers separating the CuO_2 planes
3. Mixed valence of Cu obtained by aliovalent substitution, or control of oxygen stoichiometry, in the block layers.

1.6 Some Cuprate superconductors

1.6.1 $La_{2-x}Ba_xCuO_4$

The parent, undoped, La_2CuO_4 (Figure 1.11) is the first in the so called Ruddlesden-Popper series [19] of rocksalt-perovskite intergrowth structures of general formula ($AO(ABO_3)_n$), with rocksalt type blocks stacked on perovskite units. This T structure lends to a six fold coordination of the copper , with four in plane copper-oxygen bonds and two, slightly longer , apical copper-oxygen

bonds. The La^{3+} ion is in a ninefold coordination environment characteristic of a cation at the boundary of a rocksalt-perovskite intergrowth.

La_2CuO_4 has no superconductivity and is instead antiferromagnetic. The crystal structure of this stoichiometry contains Cu^{2+} (d^9) ions and the unpaired electrons on these ions align their spins antiparallel to each other throughout the structure. The presence of this interaction locks the electrons to the lattice and inhibits conduction and superconductivity.

However if some Ba^{2+} is substituted for some La^{3+} then in order to retain electrical neutrality in the structure there has to be some charge compensation. ie. For every Ba^{2+} introduced into the structure then one Cu^{2+} must oxidise to Cu^{3+}. This oxidation breaks up the alignment of the unpaired spins and when the average oxidation state of the copper reaches a critical value of ~+2.15 then the antiferromagnetism is replaced by superconductivity.(Figure 1.10)

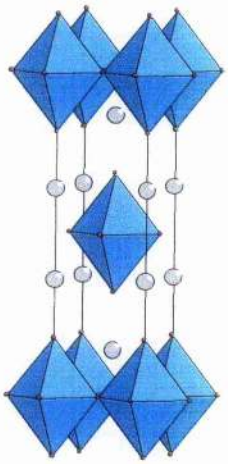

Figure 1.11. The structure of La_2CuO_4. La is shown as grey with CuO_6 octahedra shown as cyan.

This structure is also observed in the material of composition $Ca_2CuO_2Cl_2$. In this case there is retention of the perovskite like CuO_2 planes whilst the rocksalt layers are of composition CaCl. This lends to Cl^- ions occupying the apical position in the octahedral anion coordination of the copper ions. This material is an antiferromagnetic insulator that becomes superconducting upon partial substitution of Ca^{2+} by Na^+ [20].

1.6.2 $Nd_{2-x}Ce_xCuO_4$

Nd_2CuO_4 is of general formula $AO(ABO_3)$, however because of the reduction in size on going from La^{3+} to Nd^{3+} (La^{3+} = 1.216 Å Nd^{3+} = 1.163 Å [21]) it assumes a different structure. In this case the Nd^{3+} ion is in a lower coordination of eight oxygens giving rise to a fluorite type block layer.

Examination of this structure type shows that these fluorite type block layers do not lend to apical oxygens, and hence we have a copper ion coordinated solely by the four in-plane oxygens. This structure type of fluorite – perovskite intergrowth is known as the T′ structure and is shown overleaf. (Figure 1.12)

Nd_2CuO_4 has resisted attempts to yield superconductivity on oxidation of the Cu^{2+} by substitution of divalent ions for Nd^{3+} (p-type doping). This structure was however made superconducting by substitution of Nd^{3+} with Ce^{4+}[22] (n-type doping). This causes a reduction of the copper and, for x: $0.15 \leq x \leq 0.18$ in the formula $Nd_{2-x}Ce_xCuO_4$, antiferromagnetism is replaced by superconductivity.

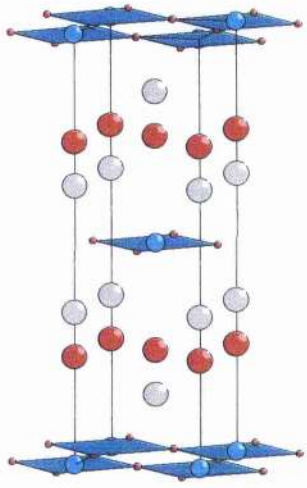

Figure 1.12. The structure of Nd_2CuO_4. Nd^{3+} are shown as grey, CuO_2 sheets are shown as cyan and oxygens are shown as red.

Although Nd^{3+} is smaller than La^{3+} the CuO_2 planes in the T' structure of Nd_2CuO_4 are actually under tension, making them amenable to n-type doping. This is because there is an increase in the electrostatic repulsions between oxygen ions in the fluorite type block causing an increase in the size of the a-b plane.

1.6.3 $Nd_{2-x-y}Ce_xSr_yCuO_{4-\delta}$

In 1988 Akimitsu et al. discovered superconductivity at 28K whilst investigating the Nd-Ce-Sr-Cu-O system[23]. The phase responsible was shown to be of the composition $Nd_{2-x-y}Ce_xSr_yCuO_{4-\delta}$. Due to the difference in size of the Ce^{4+} (0.97 Å) and Sr^{2+} (1.31 Å)[21] these ions substitute for Nd^{3+} on two distinct sites. The larger Sr^{2+} ions prefer a higher coordination and form a nine coordinate, rocksalt type block layer on one side of the CuO_2 planes. Conversely

the smaller Ce^{4+} ions lend to the formation of a lower, eight fold, coordinated fluorite type block layer on the other side of the CuO_2 planes.

This structure can thus be considered as a 1:1 intergrowth of the T and T' structures and is known as the T* structure and is shown below (Figure 1.13). The Sr^{2+} (green) containing, rocksalt type, block layer lends an apical oxygen to the CuO_2 planes while the Ce^{4+} (blue) containing, fluorite type layer does not. Thus we have copper in a five fold, square pyramidal, coordination.

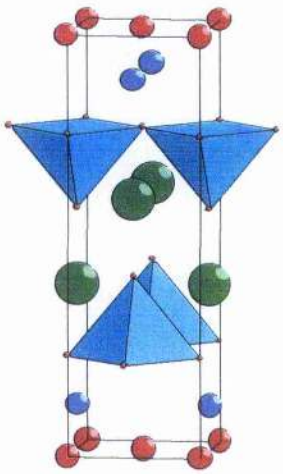

Figure 1.13. The structure of $Nd_{2-x-y}Ce_xSr_yCuO_{4-\delta}$. The Nd^{3+} sites partially substituted for by Sr^{2+} are shown as green while the Nd^{3+} sites partially substituted by Ce^{4+} are shown as blue. CuO_5 pyramids are shown in cyan with oxygen shown as red.

Within this T* structure, superconductivity can be induced by varying the ratio of divalent and tetravalent substituents. With both rock-salt and fluorite blocks adjacent to the CuO_2 planes one might consider that both n and p type

superconductivity can be induced in this structure. However only p-type superconductivity has been achieved by this method in this structure type.

1.6.4 $YBa_2Cu_3O_{7-\delta}$

The superconducting T and T' structures and the T* structure have been described as intergrowths. However the layered type materials required for the observation of superconductivity in cuprates, can also be created from the perovskite structure by means of creating and ordering oxygen vacancies.

$YBa_2Cu_3O_{7-\delta}$, known as the 1-2-3 superconductor is an example of this type of layered material.

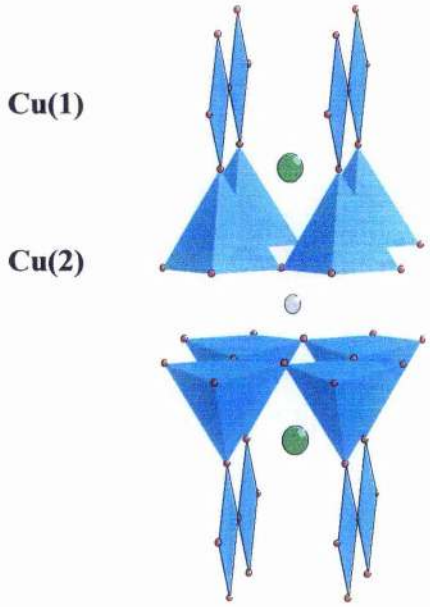

Figure 1.14. Crystal structure of $YBa_2Cu_3O_7$ with CuO_5 pyramids and CuO_4 chains shown as cyan, Ba shown as green and Y shown as grey.

We see from Figure 1.14 that in $YBa_2Cu_3O_{7-\delta}$, for $\delta=0$, the copper resides in two distinct sites :

Cu(1) 4 fold coordinate units, extending in the b-direction, between the Ba-O layers. (Ba shown as green)

Cu(2) 5 fold coordinate units, extending in the a-b plane, either side of the Y ion. (Y shown as grey)

For samples with $\delta>0$ the additional oxygen vacancies are formed in the chains of CuO_2 that extend in the b-direction, ie. (0,0.5,0).

Variable temperature, *in-situ* neutron powder diffraction experiments [24] have shown that :

(1) Oxygen is lost from the sample as temperature is increased.

(2) There is migration of oxygen from the (0,0.5,0) site to the (0.5,0,0) site.

As the occupancies of these two sites become equal then the symmetry of the system changes from orthorhombic to tetragonal. At this symmetry change the value of δ is always 0.5.

ie. For $YBa_2Cu_3O_x$

orthorhombic for $6.5<x=<7.0$

tetragonal for $6.0=<x<6.5$

Note:

(1) On heating of the tetragonal system oxygen is lost equally from the (0,0.5,0) and (0.5,0,0) sites.

(2) Only the orthorhombic form is superconducting with the associated oxygen content doping holes into the CuO_2 sheets

The tetragonal 1-2-3 structure is shown below :

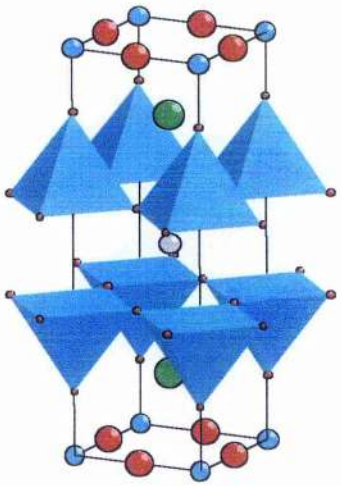

Figure 1.15. The crystal structure of teragonal $YBa_2Cu_3O_{6.5}$ with CuO_5 pyramids and Cu ions shown as cyan, Ba shown as green, Y shown as grey and O shown as red. The oxygen sites shown as red are equally occupied.

1.6.5 $Tl_mBa_2Ca_{n-1}Cu_nO_{2n+m+2}$ (the ToBaCCo series)

For m = 1 in this general formula we can form members such that n = 1,2,3,4. These compounds, like the T, T'and T* structures, can be described as layered intergrowths, however their structures are slightly more complex.

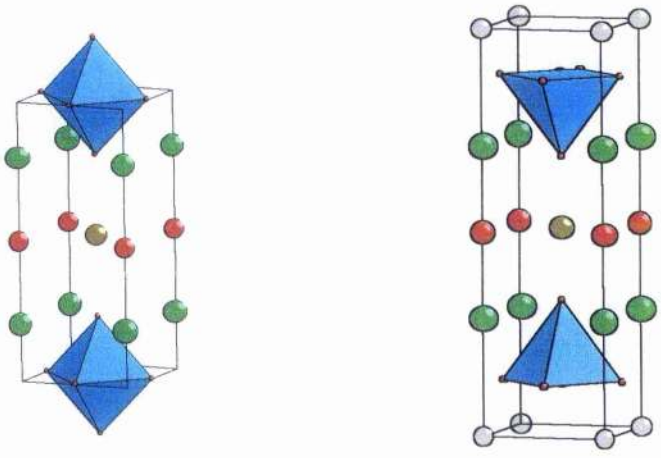

Figure 1.16. Members of the Tl – Ba – Ca – Cu – O series with m = 1 and n = 1 and 2. [25][26]

We can see from Figure 1.16 that for m = 1 and n = 1 we have perovskitic CuO_2 sheets with rocksalt type Ba-O layers on either side lending to a six fold coordinated Cu ion. This sequence is split by a third layer, Tl – O, also with a rocksalt geometry.

For m = 1 and n = 2 we see that the two CuO_2 sheets are separated by a Ca layer which contains no oxygen (as in the Y layer in the 1-2-3 structure). Thus we have perovskitic CuO_2 sheets with rocksalt Ba-O layers on one side and oxygen deficient, perovskitic Ca layers on the other. This lends to a five fold, square pyramidal coordination of the copper.

For m = 1 and n = 3 and 4 we have a layer sequence of :

(a) n=3

$[TlO][BaO][CuO_2][Ca][CuO_2][Ca][CuO_2][BaO]$

and

(b) n=4

$[TlO][Ba\text{-}O][CuO_2][Ca][CuO_2][Ca][CuO_2][Ca][CuO_2][BaO]$

These higher members of the series have both square pyramidal and square planar co-ordinated Cu ions.

A number of phases of general formula $(AO)_mM_2Ca_{n-1}Cu_nO_{2n+2}$ have been made such that A= Tl, Bi or Pb, or a mixture of these, and M= Sr or Ba.

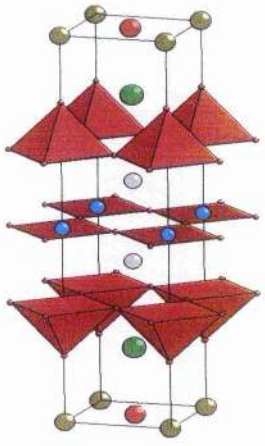

Figure 1.17. Member of the Tl – Ba – Ca – Cu – O series for m = 1 and n = 3. [28] Tl is shown as brown, CuO_2 sheets and CuO_5 pyramids shown as red, Ba shown as green and Ca is shown as grey.

1.6.6 $ACuO_2$.

This is the simplest superconducting cuprate structure. There is an infinite stacking of CuO_2 planes separated by A^{2+}. $CaCuO_2$ itself cannot be prepared, however the structure can be stabilised by partial replacement of Sr for Ca, ie. $Ca_{1-x}Sr_xCuO_2$: $0.13=<x=<0.17$ [28]. High pressure synthesis can extend the stoichiometry range over which the phase is formed.

Larger alkaline earth metals can be incorporated in this system, as far as $Ba_{0.33}Sr_{0.66}CuO_2$ beyond which the complex $BaCuO_2$ structure is obtained.

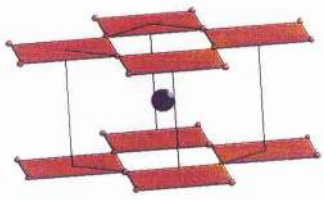

Figure 1.18. The structure of the infinite layer compound $ACuO_2$. A ion site is shown in purple with the CuO_2 sheets shown as red.

Superconductivity in this structure was induced in 1991 when Smith et al. observed a T_c of 40K in $Sr_{1-x}Ln_xCuO_2$: Ln= Nd, Pr [29]. The range of x over which superconductivity is observed is very narrow, ie. $0.14=<x=<0.16$. It is enough however to make this only the second type of cuprate superconductor in which the charge carriers are negatively charged, ie. n-type doping.

It is interesting to note that superconductivity has been reported in the phase $(Sr_{1-x}Ca_x)_{1-y}CuO_2$: ($0.3=<x=<0.6$, y~0.1) containing alkaline earth vacancies [30]. These vacancies introduce holes into the CuO_2 sheets, making the infinite layer the first structure to exhibit both p and n type superconductivity.

ie. $Sr_{1-x}Ln_xCuO_2$ = larger a axis : strain on CuO_2 planes : n type

$(Sr_{1-x}Cax)_{1-y}CuO_2$= smaller a axis : compression of CuO_2 planes : p type.

1.7 Summary and Aims

The structures of cuprate superconductors are a mixture of simplicity and complexity. They may contain up to seven elements and yet may be simplified to layered structures with different blocks contributing different factors to the superconductivity

The aim of this project at the outset was to investigate new intergrowth systems as potential superconductors. I hoped to produce superconducting materials with novel structural features and determine the effect of these novel features on properties such as T_c, J_c and H_c.

Chapter two will outline the experimental techniques employed for the synthesis and characterisation of materials while the remaining chapters will be used to relay the results of my research into various potentially superconducting systems and any conclusions reached.

References for Chapter 1.

[1] Onnes H.K., *Comm. Leiden Nr. 108, Proc. Roy. Acad. Amsterdam* **11**, 168 (1908).

[2] Onnes H.K., *Comm. Leiden, Suppl. Nr.* **34** (1913).

[3] Onnes H.K., *Comm. Leiden* **120b** (1911).

[4] Meissner W. and Ochsenfeld R., *Naturwissenschaften* **21**, 787 (1933).

[5] Smart L. and Moore E., "The magnetic properties of superconductors" in Solid State Chemistry an Introduction, Second Edition, Chapman and Hall (1995).

[6] Geballe T.H. and Hulm J.K., *Science* **239**, 367 (1983).

[7] Nagamatsu J., Nakagawa N., Muranaka T., Zenitani Y. and Akimitsu J., *Nature* **410**, 63 (2001)

[8] Scholey J.J., Hosler W.R. and Cohen M.L., *Phys. Rev. Lett.* **12**, 474 (1964).

[9] Sweedler A.R., Raub C. and Matthias B.T., *Phys. Lett.* **15**, 108 (1965).

[10] Sleight A.W., Bither T.A. and Bierstedt P.E., *Solid State Comm.* **7**, 299 (1969).

[11] Johnston D.C., Prakash H., Zachanisen W.H. and Viswanathan R., *Mater. Res. Bull.* **8**, 777 (1973).

[12] Sleight A.W. Gibson J.L. and Bierstedt P.E., *Solid State Comm.* **17**, 27 (1975).

[13] Bednorz J.G. and Muller K.A., *Z. Physik.*, **B64**, 189 (1986).

[14] Wu W.K., Ashburn J.R., Tong C.J., Hor P.H., Meng R.L., Huang Z.J. and Wang Y,Q., *Phys. Rev. Lett.* **58**, 405 (1987).

[15] Campbell A.M. in "High Temperature Superconductivity", Proceedings of the 39th Scottish Universities Summer School in Physics, ed. D.P. Tunstall, St. Andrews p.86 (1991).

[16] Bardeen J., Cooper L.N. and Schrieffer J.R., *Phys. Rev.* **108**, 1175 (1957).

[17] Tokura Y. and Arima T., *Japanese Journal of Applied Physics* **29**, 2388 (1990).

[18] Sleight A.W. in "Electronic Structure and Valency in Oxides Superconductors", Chemistry of Superconductor Materials, ed. Vanderah T., Noyes Publications (1992).

[19] Ruddlesden S.N. and Popper P., *Acta Cryst.* **10**, 538 (1957).

[20] Argyriou D.N., Jorgensen J.D., Hitterman R.L., Hiroi Z., Kobayashi N. and Takano M., *Phys. Rev.* **B51**, 8434 – 8437 (1995).

[21] Shannon R.D. *Acta Cryst.* **A32**, 751 (1976).

[22] Tokura Y., Takagi H. and Uchida S., *Nature* (London), p. 337 – 345 (1989).

[23] Akimitsu J., Suzuki S., Watanabe M. and Sawa H., *Jap. J. Appl. Phys.* **27**, 1859 (1988).

[24] Jorgensen J.D., Beno M.A., Hinks D.G., Soderholm L., Volin K.J., Hitterman R.L., Grace J.D., Schuller I.K., Segre C.U., Zhang K. and Kleefisch M.S., *Phys. Rev.* **B36**, 3608 (1987).

[25] Mathies D.P. and Snyder R.L., *Powder Diffraction* **1**, p. 8 – 24 (1990).

[26] Hervieu M., Maignan A., Martin C., Michel C., Provost J. and Raveau B., *J. Solid State Chem.*, **75**, p212 - 215 (1988).

[27] Liang J.K., Zhang Y.L., Huang J.Q., Xie S.S., Che G.C., Cheng X.R. and Ni Y.M., *Modern Physics Letters B*, **7**, p561 – 569 (1989).

[28] Siegrist T., Zahurak S.M., Murphy D.W. and Roth R.S., *Nature* **334**, 231 (1988).

[29] Smith M.G., Manthiram A., Zhou J., Goodenough J.B. and Markert J.T., *Nature,* **351,** 549 (1991).

[30] Azuma M., Hiroi Z., Takano M., Bando Y. and Takeda Y., *Nature* (London), **356**, 775 (1992).

2. EXPERIMENTAL

The aim of this project was to produce new superconducting materials and characterise them. The characterisation of these materials would involve the presentation, and interpretation, of structural, electrical and magnetic data. From these data we hoped to determine the influence of novel structural features on superconducting properties.

In this chapter I shall outline the experimental techniques employed throughout my work.

2.1 Sample Preparation

Samples were prepared using the conventional solid state method. This involves the direct reaction of a mixture of solid starting materials. Solids do not usually react with each other at room temperature and thus it is necessary to heat them.

The amount of starting materials required was determined from the formula of the desired product.

Consider:

$Bi_2Ca_2CuO_4Cl_4$ F.W.= 767.66 $gmol^{-1}$

: as a desired intergrowth of the Sillen X2 and the Ruddlesden- Popper n=1 ($Ca_2CuO_2Cl_2$) phases.

If we require 2g of product this is equal to (2/FW) moles.

Thus we require 2 x (2/FW) moles of Bi

2 x (2/FW) moles of Ca

1 x (2/FW) moles of Cu

4 x (2/FW) moles of O

4 x (2/FW) moles of Cl

The reaction of :

2 x (2/FW) moles of BiOCl

2 x (2/FW) moles of $CaCO_3$

and (2/FW) moles of $CuCl_2$

: provides the correct amounts for the production of 2g of $Bi_2Ca_2CuO_4Cl_4$.

In order to form the product from the starting materials sufficient heat must be provided such that the ions have sufficient thermal energy to jump from their initial lattice site, diffuse and recrystallise as product. The temperature to which the reaction mixture is heated is set at some 10 – 20K below the lowest melting point.

Before heating, the starting materials were intimately mixed. This was done by grinding them in an agate mortar and pestle. The increased intimacy, which decreases the distances of diffusion that must occur, was further enhanced by pressing the ground mixture into a pellet.

The powder was placed in a die and subjected to a static pressure of 4 Ton for 10 – 15 minutes. The pellet was then placed on platinum foil, placed in an

alumina boat and heated to the appropriate temperature in a furnace. If side reactions with oxygen were deemed to have any adverse effect on the realisation of the desired product then the sample was heated in an inert atmosphere. This was achieved using a tube furnace set up, shown below :

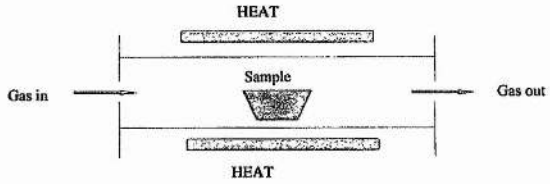

Figure 2.1. Tube furnace experiment.

2.2 Product Structural Characterisation

Crystalline solids consist of regular arrays of atoms, ions or molecules. These regular arrays are based on small units which repeat in all directions. The smallest repeating unit that shows the full symmetry of an array is known as the unit cell. Structural characterisation involves the determination of the size and shape of this unit cell and the location of its contents. This has been achieved with the use of diffraction techniques.

During my project I have employed three diffraction techniques : powder x-ray diffraction, powder neutron diffraction and microcrystal x-ray diffraction.

2.2.1 Optical Diffraction

Optical diffraction occurs when a beam of light is allowed to pass through a grating. A grating consists of a piece of glass on to which a large number of lines have been drawn. These lines are drawn such that they run parallel to each other

and they are equally spaced by a distance a little more than the wavelength of the light.

As light strikes the grating the lines act as secondary sources of light which is radiated in all directions. As this light leaves each line, interference occurs between the waves. In certain directions the beams are in phase and constructive interference occurs to give diffracted beams in these directions.

2.2.2 X-ray Diffraction by Crystals.

In 1912 Von Laue postulated that if crystalline materials could be regarded as having a regular repeating structure and if X-rays were electromagnetic radiation then crystals should act as a 3 dimensional grating and diffraction of x – rays should take place. He was proved correct when W. Friedrich and P. Knipping observed the x-ray diffraction of a copper sulphate crystal. Subsequent work by the father and son team of W.H. and W.L. Bragg led to the use of x-ray diffraction as a means of structural characterisation.

W.L. Bragg went on to postulate an alternative view of the diffraction process in crystals. He showed that diffraction could be modelled as reflections of the incident beam by planes in the crystal which are related to the unit cell.

2.2.3 Lattice Planes.

These planes, which 'reflect' the x-rays, exist in sets where each member runs parallel to the next with a separation of a distance (usually given in Angstroms) known as the d – spacing. Each set is labelled d_{hkl}, d is obviously the d spacing value, while h, k and l values, for each set, are known as the Miller Indices. These indices label the orientation of each set of planes and are derived by taking

the reciprocal value of the fraction of the unit cell axis that the plane next to that which passes through the origin intercepts at.

2.2.4 Bragg's Law

Each plane is said to act as a semi-transparent mirror with some x-rays being reflected [angle of incidence = angle of reflection], whilst the rest continue through the structure to be reflected by other planes. ie.

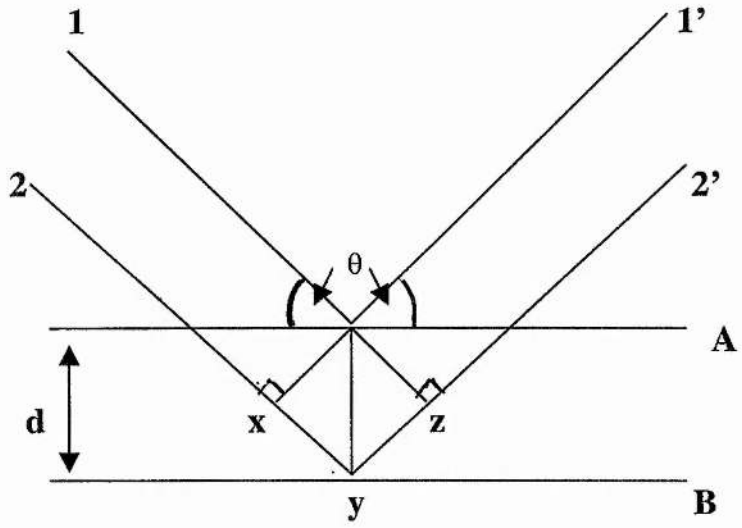

Figure 2.2. Derivation of Bragg's Law.

If we consider the two adjacent planes A and B, in Figure 2, reflecting beams 1 and 2 to give 1' and 2'. We see that beams 1' and 2' will be in phase if the distance xyz equals a whole number multiple of the wavelength of the incident beam.

From Figure 2.2 we see that :

$$xy = yz = d\sin\theta$$

therefore

$$xyz = 2d\sin\theta$$

For constructive interference :

$$xyz = n\lambda$$

therefore

$$\underline{\mathbf{n\lambda = 2d\sin\theta}}$$

This last equation is known as Bragg's Law.

When Bragg's law is satisfied the reflected beams are in phase and interfere constructively. At angles other than the Bragg angle (θ) the reflected beams are out of phase and destructive interference or total cancellation occurs. In real crystalline systems there are of course thousands of lattice planes and hence in phase reflected beams are very intense. Bragg's law actually imposes stringent conditions on the angles at which reflection may occur. If the angle of incidence is but a few tenths of a degree out then the destructive interference of the reflected beams is usually complete and no beam is detected. Thus by measuring the angle θ at which a beam is reflected we can determine the d – spacing, of the set of planes reflecting, from Bragg's equation.

2.2.5 Factors Affecting Intensity of Reflections

The intensity I, of the reflection for any given d_{hkl} is related to the so called structure factor F_{hkl}. This is the result of the different scatterings of the ions in the structure. X – ray diffraction occurs with the interaction of the x – rays and the electrons on the ion in the structure, such that ions having more electrons have higher scattering powers.

Knowledge of the unit cell composition and the location of the ions allows the calculation of F_{hkl} and production of a theoretical pattern. Conversely, knowledge of F_{hkl} can be used to determine the location of ions in the unit cell. For us to obtain knowledge of the structure we must know the magnitude of F_{hkl} and its phase (+ or -).

The problem with diffraction is that the intensity of the reflection is not directly proportional to the structure factor F_{hkl}, but rather :

$$F_{hkl} \propto \sqrt{I}$$

This means that we can derive a value for F_{hkl} but we cannot determine the phase. This is known as the phase problem. Fortunately techniques exist to overcome this problem as will be outlined in this chapter.

There are also other factors that affect the intensity of reflections and these must be accounted for when trying to determine F_{hkl} :

1. Polarization factor – fall off of signal with 2θ due to finite size of electron cloud.
2. Lorentz factor – geometric factor dependent on type of instrument that varies with θ. Usually considered with (1.) as L_p factor.

3. Multiplicities – the number of reflections that contribute to an observed reflection. See Section 2.2.12
4. Temperature factor – thermal motion of ions in a material results in a decrease of intensity and an increase in background scattering.
5. Absorption factor – dependent on sample and instrument.
6. Preferred Orientation – occurs when there is a non random distribution of crystallite orientation.
7. Extinction – near perfect crystals have a reduced diffracting power, unimportant in powder diffraction.

2.2.6 Powder X-ray Diffraction

The work done on diffraction by Von Laue and messers Bragg and Bragg required large single crystals with few imperfections. However things were to change after work done by Debye and Scherrer and independently by A.W. Hull.

They showed that a polycrystalline material (or powder), placed in a monochromatic x-ray beam gave a distinctive diffraction pattern as a series of diffraction cones. They reasoned that because of the high number of crystallites in a powder, for every set of planes present some will be orientated such that the Bragg condition is achieved. Rotation of the sample ensures that reflecting planes are present in nearly equal amounts.

A powder x – ray diffraction experiment is outlined below in Figure 2.3 :

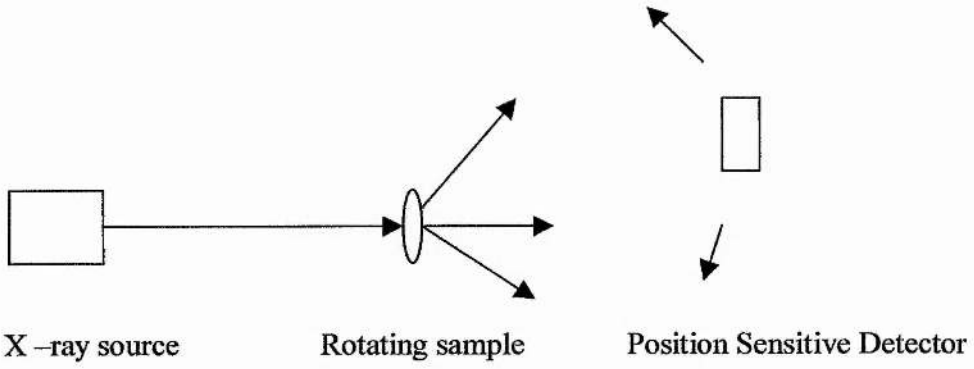

Figure 2.3. Schematic of a powder diffraction experiment.

A position sensitive x – ray detector sweeps through the cones and records intensities at different values of θ (or more commonly 2θ). A typical diffractogram is shown below :

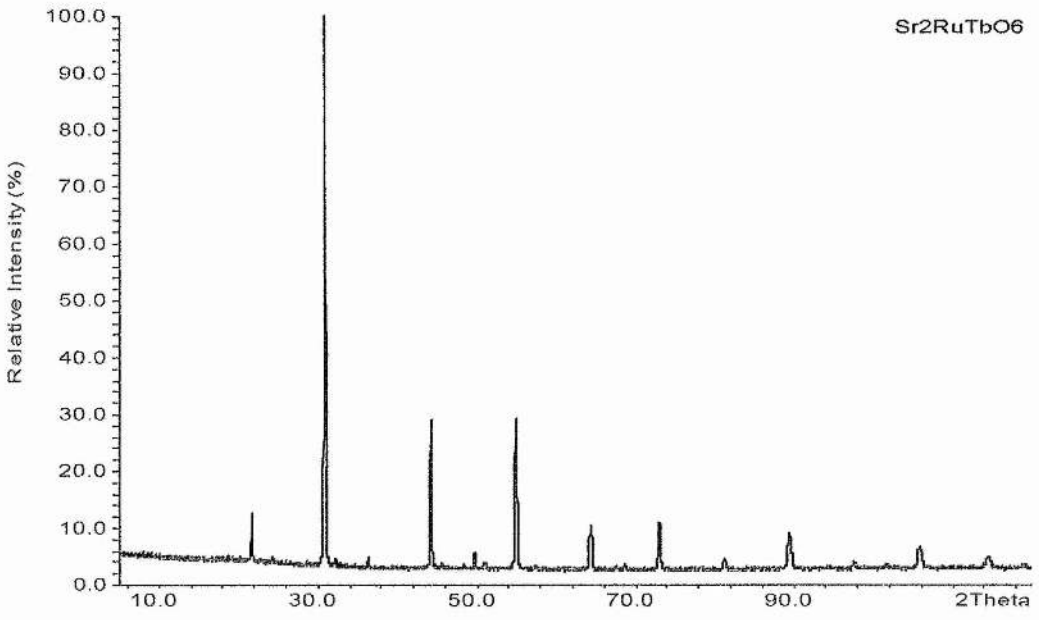

Figure 2.4. Powder x – ray diffractogram.

Peak positions in a diffractogram are thus determined by the size and shape of the unit cell, in accordance with Bragg's law, while the intensities of the peaks are determined mainly by the contents of the unit cell, their location and their scattering powers.

2.2.7 Powder Diffraction as a Fingerprint Technique

Powder diffraction is a powerful tool with its most useful application being as a fingerprint technique. An x – ray diffraction pattern can be checked against a standard pattern to determine the success of a reaction. Peak positions can also be used to drive search engines to determine compounds with similar peaks.

During this project such fingerprint analysis was used routinely with most of the experiments undertaken with a view to achieving a known desired structure. X – ray data of products was collected on a STOE STADI-P diffractometer.

A pattern for the desired structure was produced (peak positions from cell and space group data and intensities from unit cell composition) and the diffractogram of the product checked against this. On occasion however the realised pattern was not of that desired with non – identifiable phases present. In such cases I would determine if the product was a single phase by trying to index the pattern.

2.2.8 Indexing a Powder Pattern.

Indexing a powder pattern involves allocating h, k, and l values to the observed reflections. Successful accomplishment of this allocation allows the determination of the unit cell shape and size. This was achieved during this work with the use of the TREOR program [1]. This program goes through the various

unit cell shapes and sizes systematically, and generates peak positions which are checked against the observed reflections until a match within defined error limits is achieved.

The successful indexing of a pattern means that almost unequivocally you have a single phase. The next stage in product characterisation is the allocation of the correct space group.

2.2.9 Space Groups.

Unit cell shapes are a consequence of symmetry in the structure, with the shapes (crystal systems) and their associated symmetry summarised in Table 2.1.

Table 2.1. Crystal systems and the minimum symmetry they possess.[2]

Crystal System	Essential Symmetry
Cubic	4 x 3 fold axis
Hexagonal	1 x 6 fold axis
Rhombohedral	1 x 3 fold axis
Tetragonal	1 x 4 fold axis
Orthorhombic	3 x 2 fold axis or 3 x mirror planes
Monoclinic	1 x 2 fold axis or 1 x mirror plane
Triclinic	None

The posession of other symmetry elements and / or centering of the unit cell causes certain reflections to be 'systematically absent'. Some of the rules governing these absences are listed below in Table 2.2.

Table 2.2. Systematic absences due to lattice centering.[2] Additional rules apply if space symmetry elements are present.

Lattice type	Rule for reflection to be observed
Primitive, P	None
Body Centered, I	hkl; h + k + l = 2n
Face Centered, F	hkl; h, k, l either all odd or all even
Side Centered eg C	hkl; h + k = 2n
Rhombohedral, R	hkl; -h +k +l = 3n or (h – k + l = 3n)

Once a material has been successfully indexed and systematic absences determined one can usually allocate one of 230 space groups which summarise the symmetry in the product (although space group allocation is not always totally unambiguous, one can usually narrow the choice down to two or three).

2.2.10 Structure Determination.

The work of the solid state chemist is to correlate structure and properties. Thus the location of the ions in the unit cell is of paramount importance. In section 2.2.5, I outlined the relationship between the intensity of a reflection with a structure factor F_{hkl}. ie

$$F_{hkl} \propto \sqrt{I}$$

Complicated Fourier transform mathematics can relate the sum of structure factors for different h,k,l to the electron density of the unit cell. Acquisition of electron density information allows the positions of ions in the unit cell to be determined.

The determination of F_{hkl} values (sign and magnitude) can readily be achieved if a good starting model is known. The technique by which F_{hkl}, and hence the structure of the product, are determined from a starting model is Rietveld refinement.

2.2.11 Rietveld Refinement

Rietveld refinement is a least squares pattern treatment procedure whereby starting values for F_{hkl} are calculated via the starting model and then parameters within this model are varied, with the new F_{hkl} calculated, so as to fit the pattern of the model with the collected data. Rietveld refinement during this work was carried out using the G.S.A.S.[3] system. The parameters that can be varied in a Rietveld refinement with this system are :

1. The half width of reflections.
2. Zero point.
3. Unit cell parameters.
4. Asymmetry parameter.
5. Preferred orientation
6. Scale factor
7. Overall isotropic temperature factor.

8. The fractional coordinates of the ions in the unit cell.
9. Atomic thermal parameters (isotropic or anisotropic).
10. The fractional occupancy of a site.
11. Components of the magnetic vector of atoms in the unit cell.

Parameters are varied so as to achieve the best fit between the collected data and the proposed model. The degree of fit is quantified by the **R – factors**. These R – factors are a comparison of y (intensity) values of the product's diffractogram and those of the model.

The most commonly used R –factors are R_p and R_{wp} known as the R – factor and weighted R – factor respectively [4]:

$$\mathbf{R_p} = \frac{\Sigma \left| y_i(obs) - y_i(calc) \right|}{\Sigma\, y_i(obs)}$$

$$\mathbf{R_{wp}} = \left\{ \frac{\Sigma\, w_i(yi(obs) - y_i(calc))^2}{\Sigma\, w_i(y_i(obs))^2} \right\}^{1/2}$$

Another measurement of fit is that of χ^2 (Chi – squared)

:

$$\chi^2 = \left\{ \frac{Rwp}{Rexp} \right\}^2$$

Where $R_{exp} = [(N-P)/\Sigma_i\, w_i y_i(obs)^2]^{1/2}$ [4].

If the pattern of a product has been indexed but no suitable starting model is known then overcoming the phase problem for structure solution is more difficult. The technique employed for such an eventuality are known as Direct Methods.

Direct methods are a statistical approach to determination of the phase of F_{hkl} from intensity data for given reflections. SIR88 [5] was the direct methods package used in this project.

2.2.12 Limitations of Powder x – ray diffraction.

Although modelled as reflections from lattice planes x – ray diffraction is the result of the interaction of x – rays with the electrons in a structure. Elements with more electrons (higher atomic number) dominate the scattering of the x – rays and hence accurate location of lighter elements is not possible. X – ray intensity also falls off at high angles of 2θ due to the finite size of the electron clouds.

A further limitation of powder diffraction is that there is a loss in dimensionality in the experiment when compared to single crystal diffraction. This means that there is an overlap of peaks. The number of reflections that contribute to an observed powder line is known as the multiplicity. If reflections of different (h,k,l) contribute to the same diffraction peak then intensity data is more complicated and structure determination becomes more difficult.

For precise determination of the positions of lighter atoms and information at high angles of 2θ the when no single crystals are available complimentary use of powder neutron diffraction is advisable.

2.2.13 Neutron Diffraction.

High energy neutrons are said to have a wavelength determined by the de Broglie relationship:

$$\lambda = h / mv$$

with h = Plancks constant ($6.6 * 10^{-34}$ Jsec), m = mass of neutron ($1.6749 * 10^{-27}$ Kg) and v = velocity of neutron.

Neutrons with wavelengths ~1 Å are suitable for diffraction experiments and they obey Bragg's Law. The difference between neutrons and x – rays in diffraction terms is that the neutrons are diffracted by the nuclei (scattering lengths are not related to atomic number) of the ions in the crystal structure and hence heavy ions do not dominate the scattering. There is also no fall off of signal at high angles of 2θ due to the small size of the nucleas.

Neutron diffraction experiments in this work were carried out at the Intense Pulsed Neutron Source, Argonne, Illinois, U.S.A. and at the ISIS facility at the Rutherford Appleton Laboratories, Didcot, U.K.. Both these facilities produce neutrons by spallation.

2.2.14 Neutron Diffraction Experiment at ISIS.

An ion source produces H^- ions when Hydrogen gas is mixed with hot Caesium vapour. The H^- ions are then accelerated from the source to the start of a linear accelerator by the potential difference between the source (-665 keV) and the linear accelerator (ground potential). The ion beam is then accelerated down

the linear accelerator by high intensity radio – frequency fields to an energy of 70 MeV.

From the linear accelerator the H^- ions pass through a 0.3 μm aluminium oxide film which strips these ions of both electrons to yield protons. These protons are then accelerated, using a synchotron, to 800 MeV before being fired at a Tantalum target. This high energy collision causes the Tantalum to be broken up (spallation) with huge numbers of neutrons produced.

The neutrons produced interact with moderators and reflectors which surround the target. Neutrons continually bounce around the moderators and reflectors until they escape in the direction of the open neutron port to be used in experiments.

The moderated neutrons escaping through the open port are diffracted by the sample contained in a Vanadium can and resolved, using fixed position detectors, by time of flight.

2.2.15 Time of Flight Neutron Diffraction

Neutrons in the experiment outlined above are released in short pulses which allows the separation of the different wavelengths of neutrons by the Time of Flight (T.O.F.) method. The diffracted 'white' neutrons are analysed at the fixed position detectors on the basis of how long they take to arrive.

The T.O.F. of a neutron can be converted to the equivalent d – spacing using a combination of the de Broglie relationship and Bragg's Law :

$$\lambda_n = h/m_n v_n$$

$$= ht/m_n l$$

(λ = the de Broglie wavelength, h = Planck's constant ($6.6 * 10^{-34}$ Jsec), m_n = mass of neutron ($1.6749 * 10^{-27}$ Kg), v_n = velocity of the neutron, t = time of flight and l = path length of the neutron.)

This results in :

$$ht/m_n l = 2d\sin\theta$$

$$\Rightarrow \quad d = ht/2m_n l\sin\theta$$

2.2.16 Microcrystal Diffraction

The best way to structurally characterise materials is, if possible, to grow crystals which may allow diffraction data to be taken in 3 dimensions with a 4 circle diffractometer. Often however even if crystals are produced they are too small (ie <0.1mm) for structure determination using laboratory single crystal x – ray diffractometers.

Recently however the use of synchotron radiation, with its ability to produce a high intensity of x – rays, has allowed the determination of the structure of small 'microcrystals'[6]. During this work some crystallites of a small nature were produced and data collected from them using microcrystal diffraction at the Synchotron Radiation Source at Daresbury, U.K..

2.2.17 Synchotron Radiation

Acceleration of electrons in a magnetic field causes them to emit electromagnetic radiation over a wide spectrum. Synchotrons exploit this by accelerating electrons in a ring of high field magnets which gives of electromagnetic radiation perpendicular to the ring. Monochromators comprising of single crystals, often Silicon or Germanium, allow a narrow range

of wavelength to be used. Synchotron radiation wavelengths can be varied by changing the monochromator which allows tunability of the wavelengths produced and further enhances the power of this technique.

2.2.18 Structure Solution from Microcrystal Data

Initial atomic positions were determined by Direct methods and the basic structure completed by minimising the difference between the intensity data (F_{obs}) and the refined model structure (F_{calc}).

Correctness of the model structure is determined by its R – factor (R) or its weighted R – factor (wR)[7] :

$$\mathbf{R} = \frac{\Sigma \left| |F_{obs}| - |F_{calc}| \right|}{\Sigma |F_{obs}|}$$

$$\mathbf{wR} = \frac{\Sigma\, w\, (F_{obs} - F_{calc})^2}{\Sigma\, w\, F_{obs}^{\,2}}$$

References for Chapter 2.

[1] Werner P.–E., Eriksson L. and Westdahl M., *J. Appl. Crystallogr.* **18**, 360 (1989).

[2] West A.R. in "Solid State Chemistry and its Applications", John Wiley and Sons (1984).

[3] Larson A.C. and Von Dreele R. B., Los Alamos National Laboratory Report No. LA-UR-86-748 (1987).

[4] Young R.A. in "The Rietveld Method", Oxford Science Publications (1995).

[5] Burla M.C., Camalli M., Cascarano G., Giacovazzo C., Polidori G., Spagna R. and Viterbo D., *J. Appl. Crystallogr.* **22**, 389 (1989).

[6] Clegg W., *J. Chem. Soc., Dalton Trans.* **19**, 3223 (2000).

[7] Clegg W. in "Crystal Structure Determination", Oxford Science Publications (1998).

3. New Bismuth Oxyhalide Intergrowths.

3.1 Background.

Some superconducting copper oxides and oxyhalides were described as intergrowths in Chapter 1. Different building blocks such as perovskite, rock salt and fluorite are stacked to give the layered structures of cuprate superconductors.

Another well defined class of materials that may be considered as intergrowth structures are the bismuth oxides and oxyhalides. These materials are generally tetragonal with an a-axis of approximately 3.8 – 3.9 Å making them a suitable size for intergrowth with blocks containing CuO_2 sheets of suitable dimensions for superconductivity.

These materials have a $[Bi_2O_2]^{2+}$ fundamental building block and exist in two main families, the Sillen phases and the Aurivillius phases.

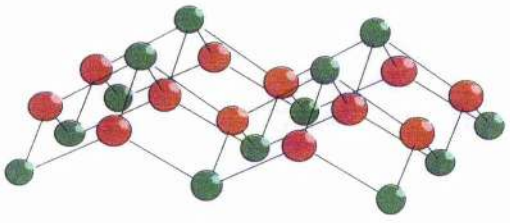

Figure 3.1. The Bi_2O_2, double fluorite, layer with oxygen red and bismuth green. These ions form corner sharing square pyramids with O in the four basal positions and Bi at the apex. Adjoining pyramids are inverted.

3.1.1 Sillen Phases

In the late 1930's and early 1940's L.G. Sillen and co-workers synthesised and characterised the first complex bismuth oxyhalides [1-7]. Their structure is based on the double fluorite bismuth oxide layers, shown in Figure 3.1, separated by a planar layer (or layers) of halide.

Substituting aliovalent metals for Bi^{3+} in the $[Bi_2O_2]^{2+}$ layer allows the variation of the charge on this block and incorporation of different numbers of halide layers. X1 structures contain a single halide layer between the bismuth oxide layer, X2 structures contain two halide layers and the X3 structures three halide layers. These are shown below :

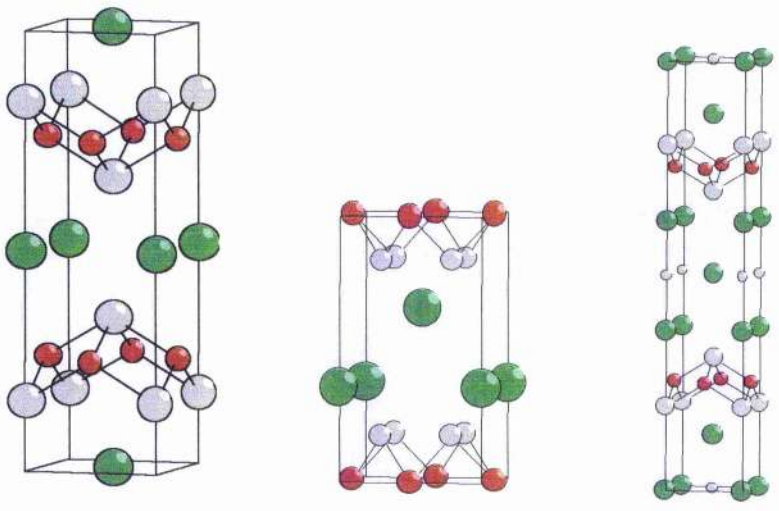

Figure 3.2. Structures of X1, X2 and X3 Sillen phases, with partially substituted Bi_2O_2 layers and and varying numbers of interleaving halogen layers. The halogen is shown as green, oxygen shown as red and the bismuth (or partially substituted bismuth) shown as grey. Note the metal site in the central halogen layer of the X3 phase shown as blue.

More complex members exist with $SrBi_3O_4Br_3$ adopting an X1X2 type structure with the metal oxide, double fluorite, layers alternatively interleaved by a single and then a double halogen layer [5].

3.1.2 Aurivillius Phases

In the 1950's Bengt Aurivillius discovered the series of layered mixed metal oxides of general formula $[Bi_2O_2]^{2+}$ $[A_{n-1}M_nO_{3n+1}]^{2-}$. These consist of intergrown layers of double fluorite Bi_2O_2 and a varying number of perovskite layers indicated by n [8].

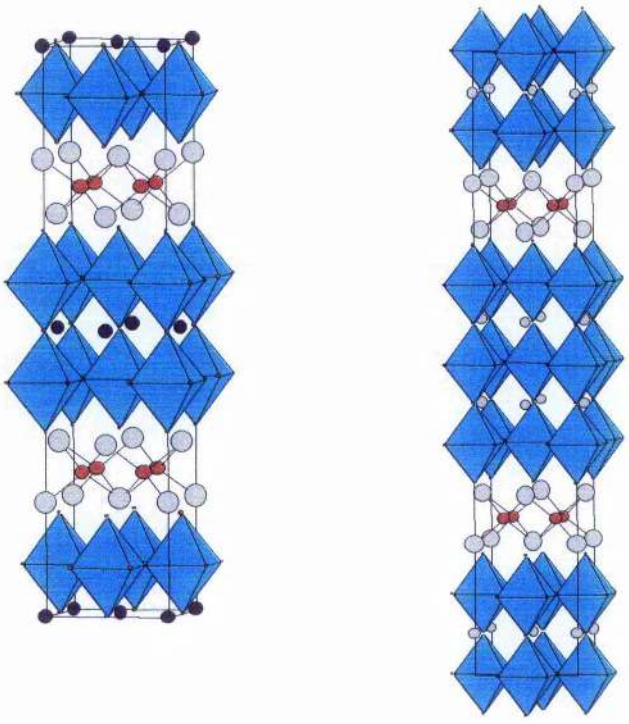

Figure 3.3. Structures for n = 2 and 3 Aurivillius phases.

3.1.3 BIPOX phases

J.F. Ackerman demonstated the adaptability of these Sillen and Aurivillius phases by designing, synthesising and characterising a series of **bi**smuth **p**erovskite **ox**ychlorides. These are Aurivillius – Sillen intergrowth materials with Bi_2O_2 layers separated alternately by perovskite and halide layers [9]. These materials are labelled as A_nX_m with n indicating the number of perovskite layers and m the number of halide layers.

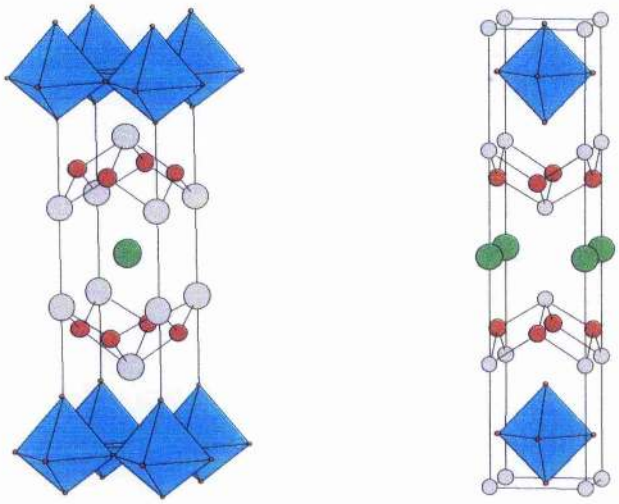

Figure 3.4. A_1X_1 and A_2X_1 BIPOX structures [9,10].

My work on oxyhalides was based on trying to intergrow Sillen phases with the Ruddlesden – Popper superconductors. The feasibility of such intergrowths was suggested in a publication by Zhu et al. [11] who reported the synthesis of a new Sillen X1X3 phase $Bi_{1.7}Ca_{2.7}O_{4-y}Cl_4$, together with a new copper containing phase $Bi_{2.4}Ca_{3.1}CuO_{6-y}Cl_5$. The proposed structures for these two phases are shown overleaf :

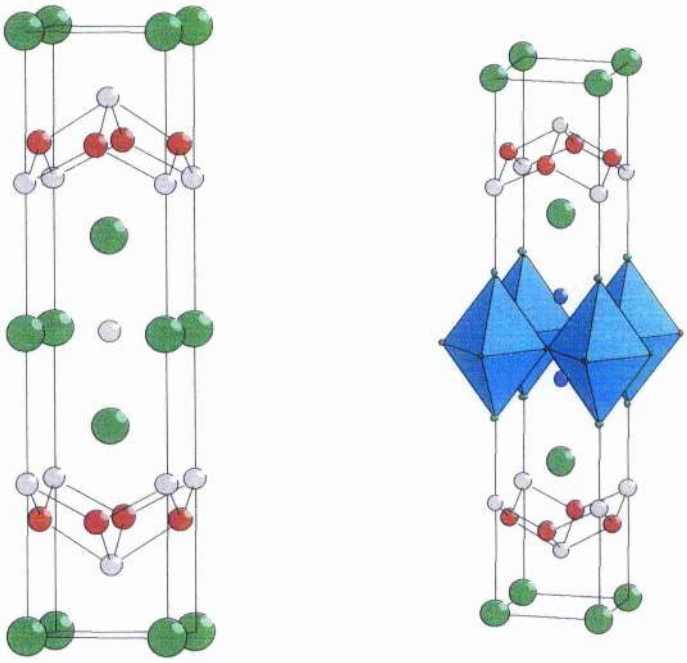

Figure 3.5. The two structures published by Zhu et al.[11]. Cl are shown as green, O as red and the Ca / Bi site in the Bi_2O_2 layers are shown as grey. Additional Ca positions, in the central halogen layer of the X3 section of the X1X3 structure and in the rock – salt type, CaCl, layer of the right hand structure are shown as blue. The right hand structure shows cyan octahedra surrounding Cu ions with four in plane oxygens and two apical chlorides.

The latter phase can be regarded as an intergrowth of Sillen X1X2 and Ruddlesden – Popper n=1 phases. The ideal layer sequence of such an intergrowth can be thought of as :

$[(Bi/Ca)_2O_2]$

$[Cl]$

$[(Bi/Ca)_2O_2)]$

$[Cl]$

$[Ca_2CuO_2Cl_2]$

$[Cl]$

From this structure it is feasible to envisage a series of Sillen / Ruddlesden – Popper intergrowths with a $Ca_2CuO_2Cl_2$ unit incorporated between two halogen layers in Sillen phases with an X2 section e.g. X2 and X1X2. Partial substitution of Na^+ for Ca^{2+} in $Ca_2CuO_2Cl_2$ yields superconductivity [12].

Here I present the results of my attempts to produce such structures.

3.2 $Bi_3Ca_3CuO_6Cl_5$ (air synthesis)

Stoichiometric amounts of BiOCl, $CaCO_3$ and $CuCl_2$ corresponding to the above formula were reacted. This is the formula for the ideal Sillen X1X2 / Ruddlesden – Popper n = 1 intergrowth with a R.P. unit of $Ca_2CuO_2Cl_2$ and the X1X2 configuration accounted for by a composition of $Bi_{1.5}Ca_{0.5}$ in the M_2O_2 layers.

In the paper by Zhu et al.[11] reaction was carried out at 730°C in an inert atmosphere of flowing argon. My first attempts at synthesis were carried out in air to see if this simpler experimental procedure realised the same product.

The composition was reacted at 730°C for 48 hrs in air with one intermediate regrinding. The resulting x – ray diffraction pattern is shown in Figure 3.6.

CuO was identified as an impurity but the rest of the peaks in the x – ray pattern for this reaction were indexed using TREOR [13] and gave a primitive monoclinic cell with a = 7.73 Å, b = 4.12 Å, c = 6.40 Å and β = 105.2°. The only clearly resolved 0k0 peak (010) was absent suggesting the centrosymmetric $P2_1/m$ as the space group. Structure solution was started using x-ray data with integrated intensities extracted using the LeBail profile-fitting technique [14]. These were used in the SIR88 direct methods computer program with the three strongest peaks identified as Bi, Cl and Ca.

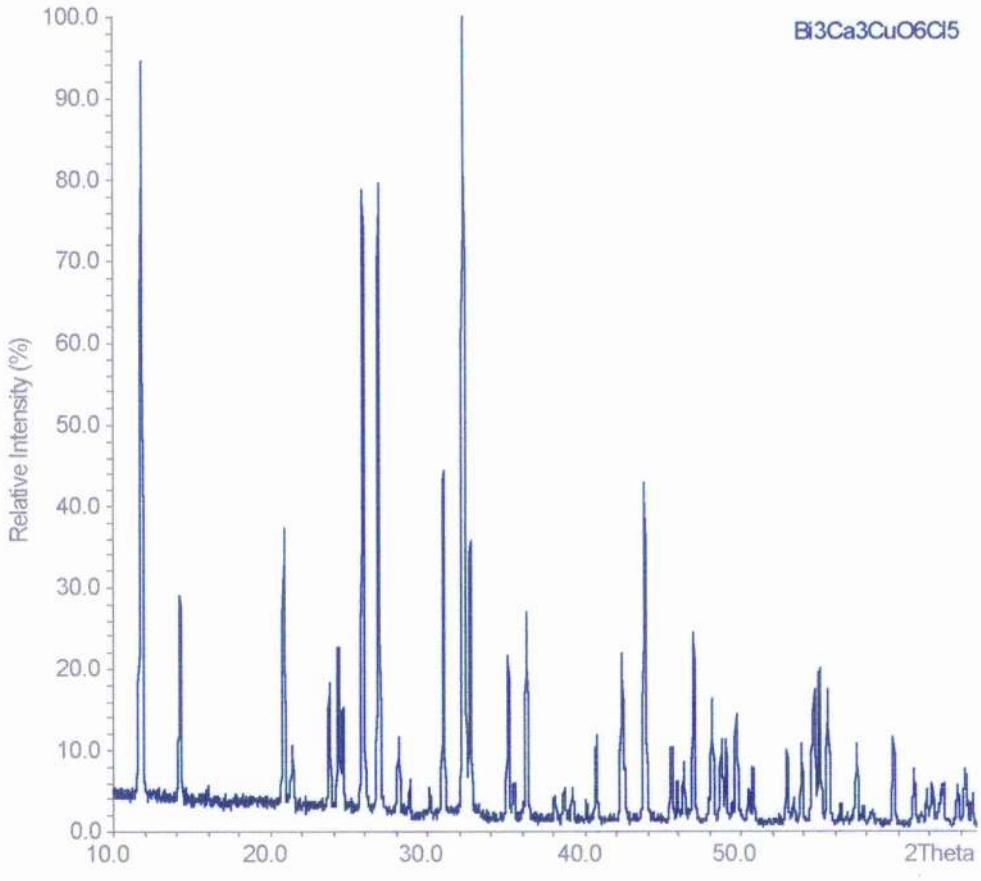

Figure 3.6. X – ray diffraction pattern of '$Bi_3Ca_3CuO_6Cl_5$' reacted in air.

Rietveld refinement of this partial model followed by the generation of difference Fourier maps revealed the additional oxygen positions and allowed successful completion of the structure.

Precise location of the lighter atoms and a generally better structure determination was obtained by simultaneous refinement against both x – ray and neutron powder diffraction data. Neutron diffraction data was collected for a 5g sample of "$Bi_3Ca_3CuO_6Cl_5$" on the Polaris instrument at the ISIS facility, Chilton, UK. The refinement data showed the major phase to be of a composition $CaBiO_2Cl$ with a distorted Sillen X1 structure [15].

Table 3.1. Crystal Data and Details of Structure Solution and Refinement.

Empirical Formula	$CaBiO_2Cl$
Formula weight	316.513 $gmol^{-1}$
Crystal system	Monoclinic
a (Å)	7.7311(1)
b (Å)	4.1234(1)
c (Å)	6.3979(2)
β	105.21(1)°
Space group	$P2_1/m$
T (°C)	25
X – ray data	
λ (Å)[Cu Kα]	1.540562
2θ range	5° – 85°
No. of reflections	203
No. of data points	3988
*R_{wp}, *R_p	13.6%, 9.9%
Neutron data	
d-spacing range (Å)	0.64 – 3.02
No. of reflections	1042
No. of data points	3079
*R_{wp}, *R_p	3.35%, 5.90%
No. of parameters	63
Combined *χ^2	9.58

* see section 2.2.11

Table 3.2 Final Atomic Parameters for $CaBiO_2Cl$

Atom	Site	x	y	z	$U_{11}/Å^2$	$U_{22}/Å^2$	$U_{33}/Å^2$	$U_{13}/Å^2$
Bi	2e	0.5914(2)	0.25	0.3237(2)	0.0103(7)	0.0179(7)	0.011(1)	0.0017(6)
Ca	2e	0.0778(4)	0.25	0.3245(5)	0.017(2)	0.007(1)	0.006(2)	0.005(1)
O1	2e	0.4043(3)	0.25	0.5293(5)	0.011(1)	0.004(1)	0.009(2)	0.009(1)
O2	2e	0.8531(3)	0.25	0.5096(6)	0.0034(9)	0.003(1)	0.015(2)	0.006(1)
Cl	2e	0.8197(2)	0.75	0.0604(4)	0.0151(9)	0.0287(9)	0.007(1)	0.0031(8)

Note : $U_{12} = U_{23} = 0$

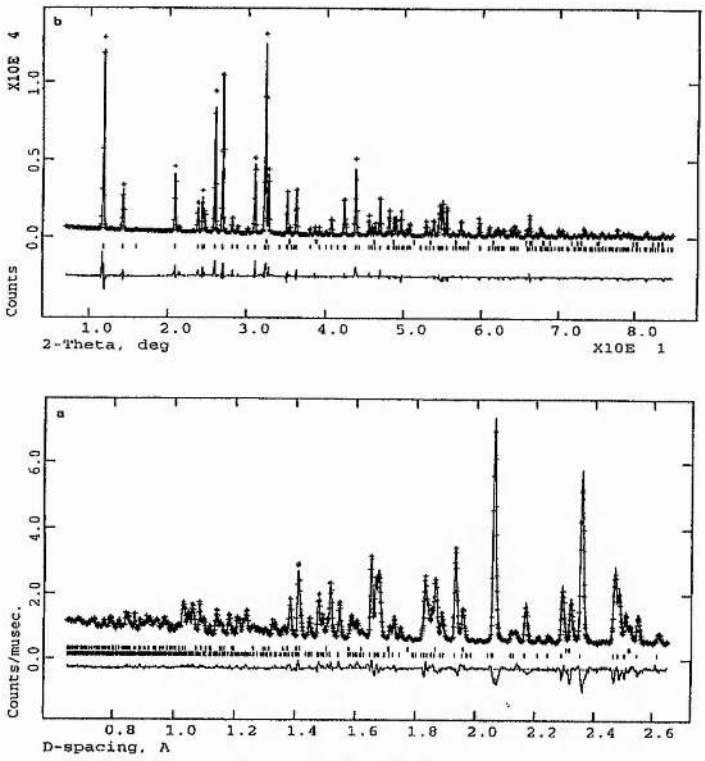

Figure 3.7. Rietveld fits for $CaBiO_2Cl$. Top fit is for x – ray data, bottom fit is for neutron data.

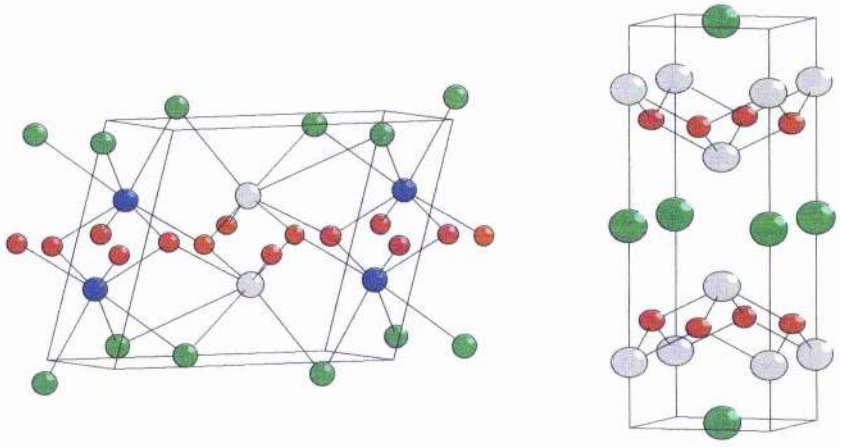

Figure 3.8. $CaBiO_2Cl$ and the ideal Sillen X1 phase. $CaBiO_2Cl$ is shown with Bi positions given as grey and Ca positions shown as blue to show their ordering.

The view in Figure 3.8 shows the ordering of the Ca and Bi ions in the $[M_2O_2]$ layers of $CaBiO_2Cl$. We also see that the Cl layer is puckered resulting in a reduction in the coordination of the M ions. The above structures also show that in the Sillen X1 phase each ion M is coordinated by 4 oxygens and 4 chlorides, whereas in $CaBiO_2Cl$ M is coordinated by 4 oxygen and 3 chloride. This is due to the smaller size of the Ca^{2+} resulting in the replacement of the chloride "square", of the ideal square antiprism, with a triangle.

Table 3.3 Selected Bond Distances for $CaBiO_2Cl$

Bi – Cl x2	3.430(2) Å	Ca – Cl x2	3.053(3) Å
Bi - Cl	3.470(2) Å	Ca – Cl	2.778(4) Å
Bi – O(1) x2	2.263(1) Å	Ca – O(1)	2.520(4) Å
Bi – O(1)	2.196(3) Å	Ca – O(2) x2	2.316(2) Å
Bi – O(2)	2.060(2) Å	Ca – O(2)	2.346(4) Å

3.3 $SrBiO_2Cl$

Having made $CaBiO_2Cl$ we then synthesised $SrBiO_2Cl$ by reaction of appropriate amounts of $SrCO_3$ and BiOCl at 800°C for 36 hours in air. Analysis of the x – ray profile showed a relationship with the supercell seen in $BaBiO_2Cl$ [16]. The structure for $BaBiO_2Cl$ was therefore used as a starting model for refinement of the $SrBiO_2Cl$ data. Rietveld refinement of these data showed the $BaBiO_2Cl$ model to be correct .

Table 3.4 Crystal Data and Details of Structure Refinement

Empirical formula	$SrBiO_2Cl$
Formula weight	364.051 $gmol^{-1}$
Crystal system	Orthorhombic
a (Å)	5.7109(2)
b (Å)	12.4081(5)
c (Å)	5.5888(2)
Space group	Cmcm
T (°C)	25
λ (Å) [Cu Kα]	1.540562
2θ range	5° – 85°
No. of reflections	93
No. of data points	3989
*R_{wp}, *R_p	12.7%, 9.4%
No. of parameters	27
*χ^2	6.66

* see section 2.2.11

Table 3.5 Final atomic parameters for $SrBiO_2Cl$.

Atom	Site	x	y	z	$U_{11}/Å^2$	$U_{22}/Å^2$	$U_{33}/Å^2$	$U_{iso}/Å^2$
Bi	4c	0	0.0824(1)	0.25	0.037(1)	0.043(1)	0.026(1)	
Sr	4c	0	0.3879(2)	0.25	0.022(3)	0.034 (3)	0.029(2)	
O	8c	0.241(2)	0	0				0.045(5)
Cl	4c	0	0.7442(6)	0.25				0.048(3)

Note : Since only x – ray data was used it was only possible to derive isotropic temperature factors for the light O and Cl ions.

Table 3.6 Selected bonnd distaces for $SrBiO_2Cl$

Bi – Cl x 2	3.527(5) Å
Bi – Cl x 2	3.491(4) Å
Bi – O x 4	2.211(7) Å
Sr – Cl x 2	3.240(4) Å
Sr – Cl x 2	3.367(4) Å
Sr – O x 4	2.465(7) Å

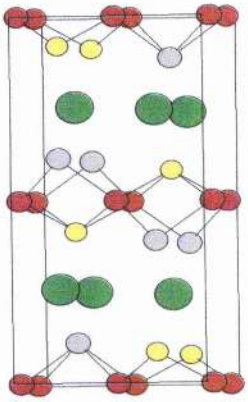

Figure 3.9. Structure of $SrBiO_2Cl$ [15]. Bi positions are shown as grey with Sr positions shown as yellow. Cl and O are shown as green and red respectively.

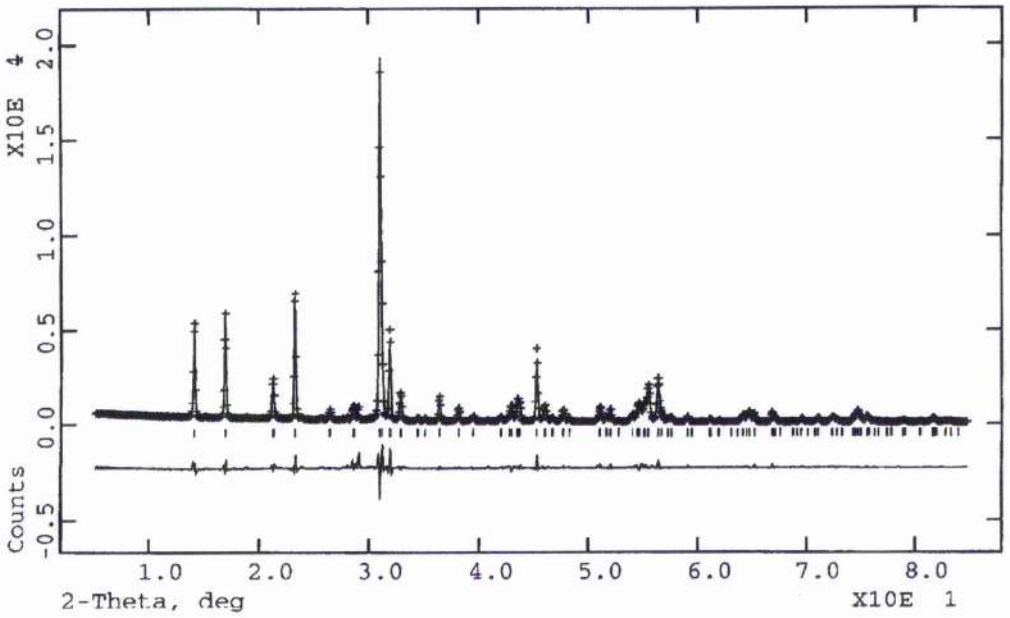

Figure 3.10. Rietveld fit for x – ray data of $SrBiO_2Cl$.

3.4 $Bi_3Ca_3CuO_6Cl_5$ (N_2 synthesis).

Having showed that reaction of the above stoichiometry in air did not produce the desired intergrowth structure we tried the synthesis in an inert atmosphere of flowing nitrogen. The sample was heated at 650°C for 2 hours and 730°C for 48

hours as reported in the literature. A typical diffraction pattern for the product of such a reaction is shown below.

From the diffractogram in Figure 3.11 we see that the reaction appears to be yielding a mixture of the two phases postulated by Zhu et al.. It was thought that perhaps some $CuCl_2$ was being lost in the reaction and thus 1.3 molar equivalents of $CuCl_2$ were added to the sample, based on the approximation that the sample was entirely the copper free X1X3 phase. This mixture was then heated at 730°C for 24 hours. The diffractogram obtained when the green product was x – rayed is shown in the top profile of Figure 3.12.

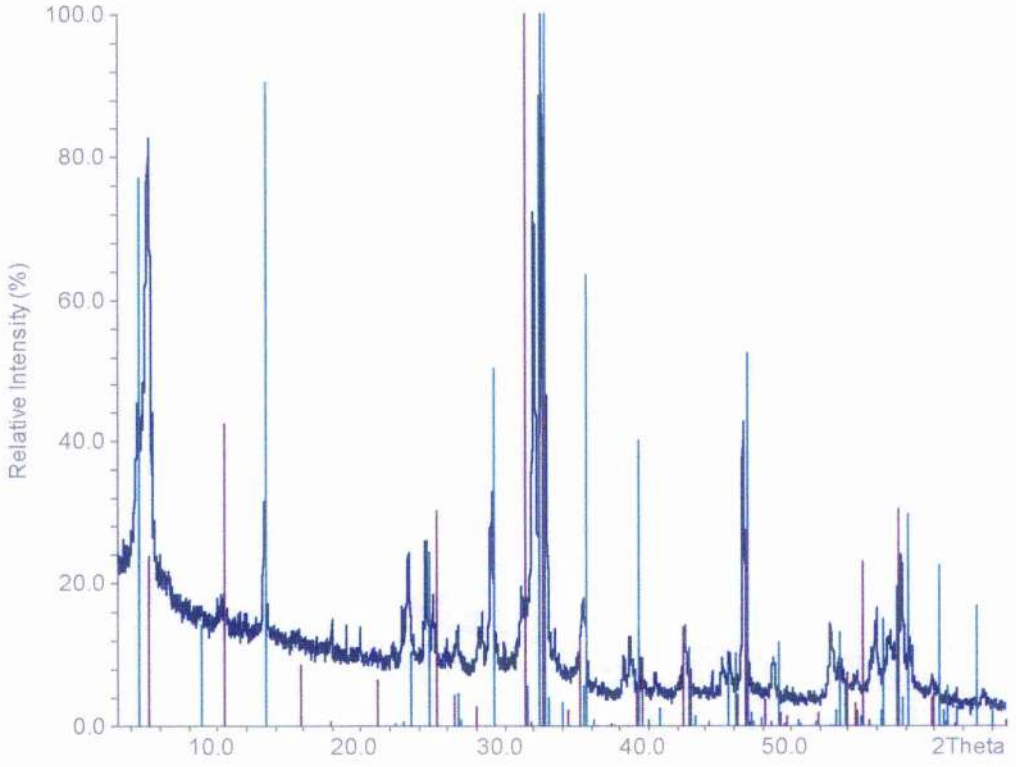

Figure 3.11. Diffraction profile of reacted $Bi_3Ca_3CuO_6Cl_5$ in N_2 and the peak files for the two structures postulated by Zhu et al..

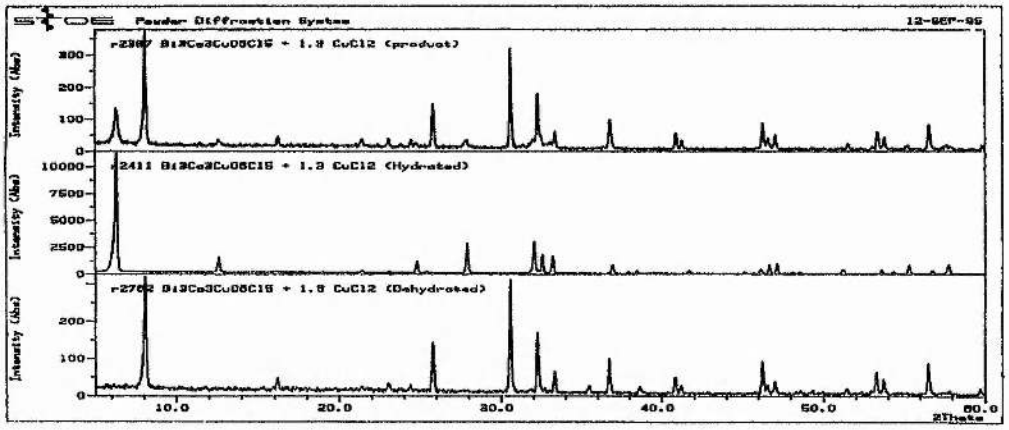

Figure 3.12. Diffractograms of (1)product of $Bi_3Ca_3CuO_6Cl_5$ + 1.3 $CuCl_2$, (2) product after hydration, (3) product after dehydration.

It was noted that the green sample in the mortar and pestle rapidly coagulated and went a darker shade of green. Subsequent analysis, of this dark green material, by powder x – ray diffraction realised the middle diffractogram shown in Figure 3.12. From this pattern we could index the peaks on the basis of a tetragonal unit cell with a = 3.8771 Å, c = 28.0588 Å. Examination of the observed reflections showed that all the peaks belonged to the subgroup {h+k+l = 2n}. There were no other absences and hence a space group of I 4/mmm was assigned.

The realisation of this product on standing in air suggested that we were observing the formation of a hydrated phase. I therefore heated the sample at 100°C for 48 hours and took another x – ray pattern (the bottom profile in Figure 3.12). The dehydrated sample could be indexed as a tetragonal phase with a ~ 3.9 Å and c ~ 21.7 Å. Analysis of observed reflections inferred the same I 4/mmm space group.

A search of the Daresbury Laboratory Chemical Database revealed the cell dimensions of the dehydrated phase to be similar to those of the I4/mmm, Sillen X3 structure of $Bi_{1.5}Ca_{1.25}O_2Cl_3$ [6]i.e. a = 3.897 Å and c = 21.69Å

Observation of this hydration prompted a reexamination of the $Bi_3Ca_3CuO_6Cl_5$ sample. It was noted that on standing in moist air the sample had darkened (light grey to dark grey) so the sample was x – rayed again and the pattern below was realised.

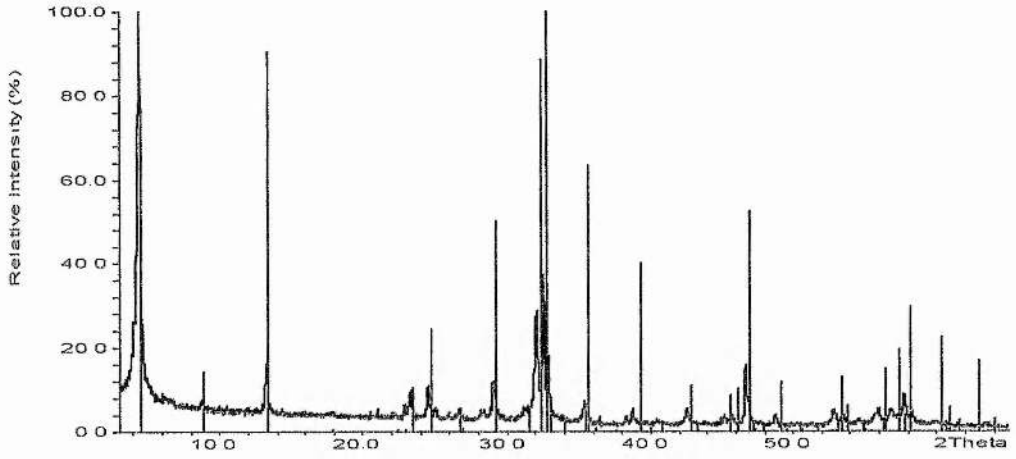

Figure 3.13. $Bi_3Ca_3CuO_6Cl_5$: heated at 650°C for 5 hours under N_2 then exposed to air. Comparison with the peak file of the pattern expected for successful production of $Bi_{2.4}Ca_{3.1}CuO_{6-y}Cl_5$ shows there to be a good match. ie.

$$Bi_3Ca_3CuO_6Cl_5 \xrightarrow[N_2]{650^{o}C} \text{mixture of Zhu phases} \xrightarrow[air]{moist} \text{Single Phase } Bi_{2.4}Ca_{3.1}CuO_{6-y}Cl_5$$

This is highly improbable and rather suggests that the single phase we achieve is some form of hydrate.

What is noticed in this reaction under N_2 is that there is no sign of the characteristic CuO peaks at d = 2.5283 Å and 2.3330 Å. This suggests that Cu is incorporated into the X1X3 structure.

The most obvious place for the copper to exist would be in the central halogen layer of the X3 section of the structure.

This X1X3 phase thus appears to undergo an intercalation of water to give a crystalline, hydrated product with an electron distribution similar to that of the proposed intergrowth system. This hydration is reversible with the original X1X3 structure restored on heating at 90°C for 5 hours :

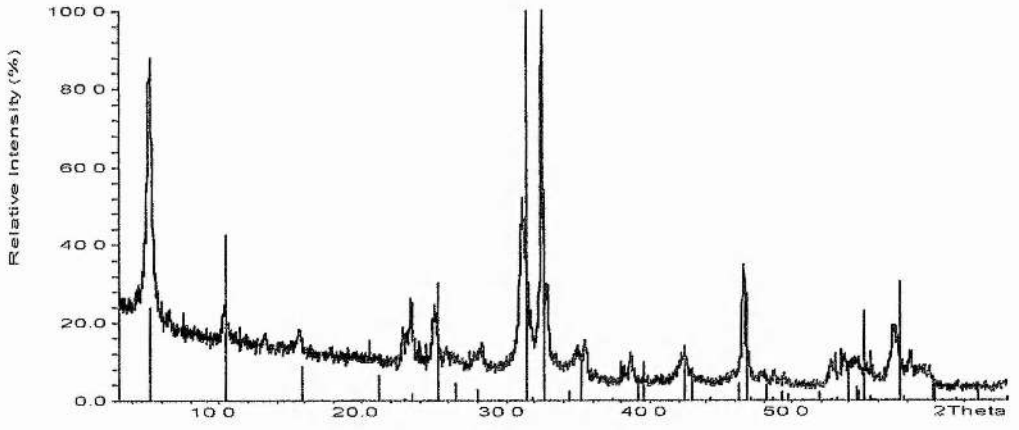

Figure 3.14. '$Bi_3Ca_3CuO_6Cl_5$' product following hydration and then reheating. The peak file shown is that of the X1X3 phase outlined by Zhu et al.

It is likely that the water molecules are entering the structure in the X3 section when we consider the hydration observed in the Sillen X3 product of $Bi_3Ca_3CuO_6Cl_5$+1.3$CuCl_2$.

3.5 $BiCaCuO_2Cl_3$

Having observed the formation of an X3 structure on addition of $CuCl_2$ to a stoichiometry of $Bi_3Ca_3CuO_6Cl_5$ I attempted to produce a stoichiometric X3 phase by reaction of precursors weighed out to give a formula of $BiCaCuO_2Cl_3$. ie. A layer sequence of :

$[BiCaO_2]$

$[Cl]$

$[CuCl]$

$[Cl]$

These precursors were reacted at 650°C for five hours. The sample yielded was coated with small crystals that were too small for normal laboratory single crystal analysis but suitable for microcrystal diffraction.

Data was collected at the Synchotron Radiation Source, Daresbury.

The structure was solved with the product shown not to be the desired X3 structure but rather related to the Arppe structure [17]. With a Bi:Ca ratio of 6:5 on all metal sites the product is of nominal stoichiometry $Bi_6Ca_5O_{11}Cl_6$.

Table 3.7 Crystal Data and Details of Structure Solution.

Empirical Formula	$Bi_6Ca_5O_{11}Cl_6$
Formula Weight	1842.998 $gmol^{-1}$
Crystal System	Orthorhombic
a (Å)	3.865(6)
b (Å)	12.57(2)
c (Å)	43.05(7)
Space Group	Cmcm
T (K)	273.2
λ (Å)	0.7107
No. of Reflections	1383
*R – factor (obs)	0.1715
*wR – factor (obs)	0.2446
No. of Parameters	61

* see section 2.2.18

Table 3.8. Final atomic parameters from microcrystal diffraction data for product of reaction of $BiCaCuO_2Cl_3$ ($Bi_6Ca_5O_{11}Cl_6$)

Atom	x	y	z	U_{iso}
Bi/Ca 1	0.5	0.1451(3)	0.01550(7)	0.0090(8)
Bi/Ca 2	0	0.2762(3)	0.07251(7)	0.0074(8)
Bi/Ca 3	0.5	0.0688(3)	0.10519(7)	0.0082(8)
Bi/Ca 4	0	0.2072(3)	0.16051(8)	0.0105(8)
Bi/Ca 5	-0.5	0.0185(4)	0.20006(10)	0.0195(10)
Bi/Ca 6	0	0.1777(6)	0.25	0.024(2)
Cl 1	0	-0.043(2)	0.0422(7)	0.050(6)
Cl 2	0	-0.122(2)	0.1238(7)	0.051(7)
Cl 3	-0.5	0.326(3)	0.2074(8)	0.054(7)
O 1	0	0.238(3)	0.0222(8)	0.001(6)
O 2	0.5	0.171(3)	0.0639(9)	0.005(7)
O 3	0	0.161(4)	0.112(1)	0.011(8)
O 4	0.5	0.108(3)	0.1549(8)	0.000(6)
O 5	0	0.117(4)	0.201(1)	0.019(10)
O 6	-0.5	-0.034(5)	0.25	0.01(1)

Table 3.9 Selected Bond Distances for $Bi_6Ca_5O_{11}Cl_6$

Bond	Distance
(Bi/Ca)1 – O1 x 2	2.28(2) Å
(Bi/Ca)1 – O1	2.17(3) Å
(Bi/Ca)1 – O2	2.12(3) Å
(Bi/Ca)2 – O1	2.24(3) Å
(Bi/Ca)2 – O2 x 2	2.37(2) Å
(Bi/Ca)2 – O3	2.23(5) Å
(Bi/Ca)3 – O2	2.18(3) Å
(Bi/Ca)3 – O3 x 2	2.27(2) Å
(Bi/Ca)3 – O4	2.18(3) Å
(Bi/Ca)4 – O3	2.17(4) Å
(Bi/Ca)4 – O4 x 2	2.31(2) Å
(Bi/Ca)4– O5	2.12(5) Å
(Bi/Ca)5 – O4	2.26(3) Å
(Bi/Ca)5 – O5 x 2	2.28(3) Å
(Bi/Ca)5 – O6	2.25(2) Å
(Bi/Ca)6 – O5 x 2	2.22(5) Å

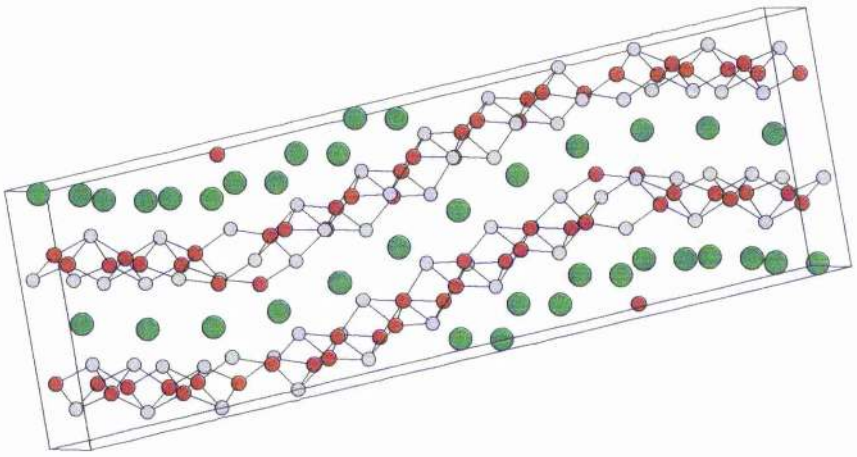

Figure 3.15. Structure of microcrystals realised on reaction of $BiCaCuO_2Cl_3$. Bi/Ca sites are shown as grey, O sites are red and the Cl sites are green.

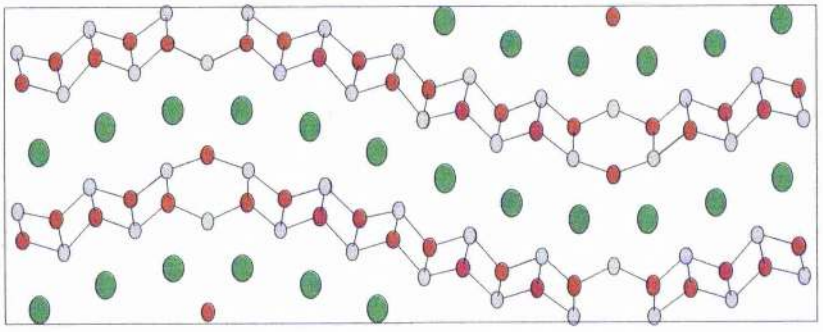

Figure 3.16. View along the a – axis of the unit cell of the compound $Bi_6Ca_5O_{11}Cl_6$.

The view in figure 3.16 shows that the product consists of layers of bismuth oxide type layers separated by a single halogen layer as in a Sillen X1 structure. However we also notice that there is a wave like distortion as observed in the Arppe compound. This new material consists of sets of five halogens and five bismuth oxide pyramids at angles to each other.

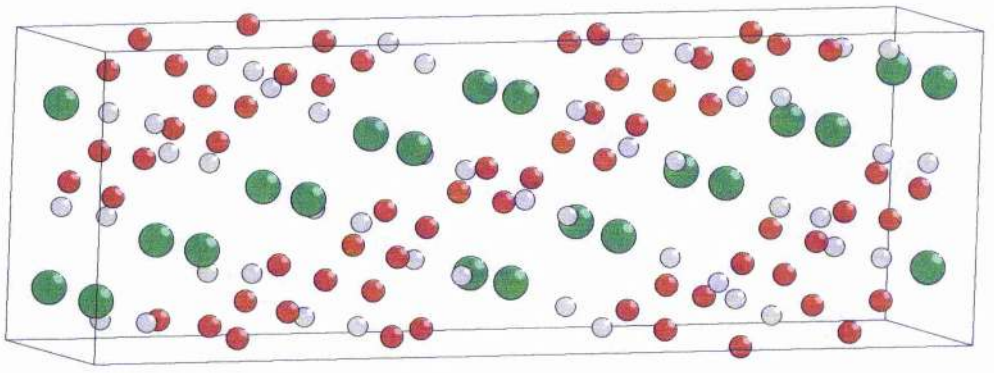

Figure 3.17. Structure of Arppe compound.

3.6 Solid Solution and Hydration in the X1X3 Sillen Phase

From my studies of the sample of '$Bi_3Ca_3CuO_6Cl_5$' it appears that rather than a Sillen / Ruddlesden – Popper intergrowth, we observe an X1X3 and its hydrated analogue. It also appears that there may be Cu located in the structure probably in the octahedral void in the central halogen layer of the X3 section.

To check if it was possible that Cu was incorporated into the structure it was decided to synthesise and compare compounds of the following formulae :

$Bi_{1.7}Ca_{2.7}O_{3.25}Cl_4$

$Bi_2Ca_3O_4Cl_4$

$Bi_2Ca_{2.5}Cu_{0.5}O_4Cl_4$

$Bi_2Ca_2CuO_4Cl_4$

Reaction of the stated stoichiometries at 650°C for 5 hours and 730°C for 48 hours under nitrogen, followed by standing in air to hydrate, realised the patterns shown below in Figure 3.18. There is no sign of the characteristic peaks of CuO at d = 2.5283 Å and 2.3330 Å suggesting incorporation of copper into the phases.

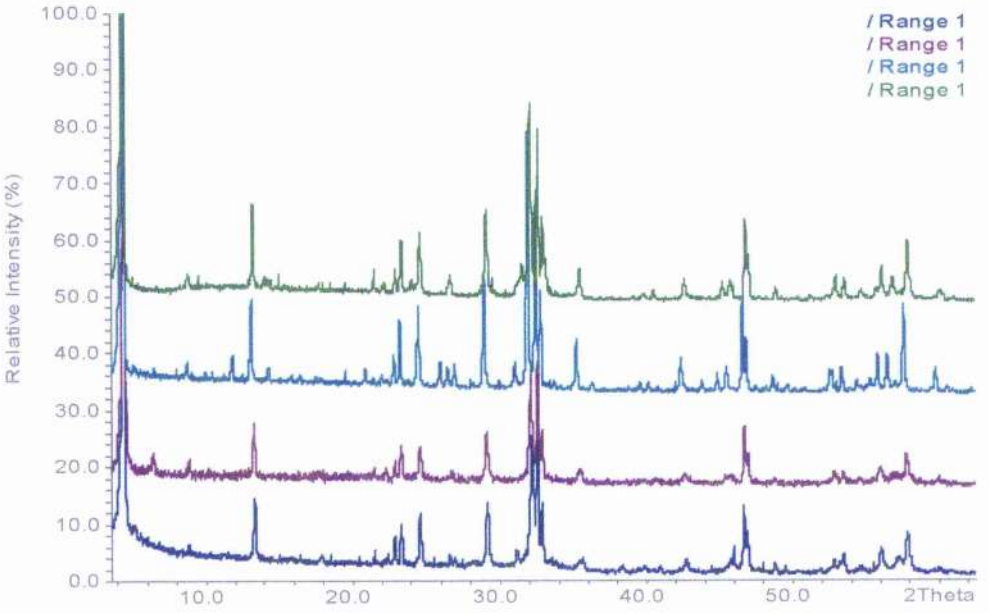

Figure 3.18. X – ray powder diffraction patterns for $Bi_{1.7}Ca_{2.7}O_{4-y}Cl_4$ and $Bi_2Ca_{3-x}Cu_xO_4Cl_4$ with x = 0, 0.5 and 1, after hydration. The $Bi_{1.7}Ca_{2.7}O_{4-y}Cl_4$ trace is at the bottom with increasing x as you move up.

From these patterns we can see that all the stoichiometries yield a similar pattern. Indexing of the major peaks realised the lattice parameters overleaf:

Table 3.10. Lattice parameters of the hydrated X1X3 phases calculated using powder x –ray diffraction data.

Compound	a	c	Volume
$Bi_{1.7}Ca_{2.7}O_{4-y}Cl_4$	3.8787 Å	19.830 Å	298.3 $Å^3$
$Bi_2Ca_3O_4Cl_4$	3.8844 Å	19.991 Å	301.6 $Å^3$
$Bi_2Ca_{2.5}Cu_{0.5}O_4Cl_4$	3.885 Å	20.910 Å	315.6 $Å^3$
$Bi_2Ca_2CuO_4Cl_4$	3.885 Å	21.110 Å	318.6 $Å^3$

From Table 3.10 we can see that with increasing copper content we have an associated increase in the unit cell volume. This implies successful substitution of the larger copper for calcium in the X1X3 structure.

On heating the composition $Bi_{1.7}Ca_{2.7}O_4Cl_4$ to 650°C in nitrogen for 5 hours the realised sample was coated with very fine crystals. Although too small for use on the laboratory single crystal facility they were suitable for microcrystal diffraction.

Microcrystal diffraction data was collected at the Synchotron Radiation Source, Daresbury.

Table 3.11 Crystal Data and Details of Structure Solution

Empirical Formula	$Bi_{1.7}Ca_{2.7}O_{3.25}Cl_4$
Formula Weight	657.294 $gmol^{-1}$
Crystal System	Tetragonal
a (Å)	3.895(1)
c (Å)	16.888(2)
Space Group	P4/mmm
T (K)	273.2
λ (Å)	0.6884(1)
No.of Reflections Observed	268
*R – factor (obs)	0.329
*wR = factor (obs)	0.445
No. of Parameters	20

* see section 2.2.18

Table 3.12 Final Atomic Parameters for $Bi_{1.7}Ca_{2.7}O_{3.25}Cl_4$

Atom	x	y	z	$U_{iso}/Å^2$	$U_{11}/Å^2$	$U_{22}/Å^2$	$U_{33}/Å^2$
Bi(1)	0.5	0.5	0.11542(4)		0.0050(2)	0.0050(2)	0.0079(3)
Ca(1)	0.5	0.5	0.11542(4)		0.0050(2)	0.0050(2)	0.0079(3)
Bi(2)	0	0	0.24912(7)		0.0043(3)	0.0043(3)	0.0116(5)
Ca(2)	0	0	0.24912(7)		0.0043(3)	0.0043(3)	0.0116(5)
Ca(3)	0.5	0.5	0.5	0.023(2)			
Cl(1)	0	0	0		0.026(2)	0.026(3)	0.003(2)
Cl(2)	0	0	0.5		0.027(2)	0.026(6)	0.029(3)
Cl(3)	0.5	0.5	0.3407(2)		0.025(1)	0.025(1)	0.011(2)
O(1)	0.5	0	0.1795(4)	0.008(1)			

Note : $U_{12} = U_{13} = U_{23} = 0$

Table 3.13 Selected Bond Distances for $Bi_{1.7}Ca_{2.7}O_{3.25}Cl_4$

Bond	Length (Å)
(Bi/Ca)1 – O1 x 4	2.228(3)
(Bi/Ca)2 – O2 x 4	2.275(4)
(Bi/Ca)2 – Cl3 x 4	3.159(2)
Ca3 – Cl2 x 4	2.7542(4)

3.7 $Bi_4La_2CuO_8Cl_3$

Stoichiometric oxides and halides corresponding to the above formula were reacted.This composition was intended to be the ideal composition for a Sillen X1X2 / R.P. n = 1 intergrowth with a layer sequence of that shown below :

$[Bi_2O_2]$

$[Cl]$

$[Bi_2O_2]$

$[Cl]$

$[La_2CuO_4]$

$[Cl]$

However, examination of this formula shows that the cation / anion charges do not balance unless the copper ion is assigned a valence of +1. This makes this composition unfeasible as the starting point for induction of superconductivity.

The result of reaction of these quantities at 675°C for 72 hours in an N_2 atmosphere is however significant.

The x – ray diffraction plot given in Figure 3.19 show the realisation of a simple pattern upon repeated heated treatment with no apparent CuO impurity. On obtaining the pattern, and removing the vaseline peaks (vaseline is used to mount the sample), I was able to index the profile on the basis of a tetragonal unit cell of a ~ 3.9 A and c ~ 9.1 A. The lack of any systematic absences allowed the assignment of the highest symmetry tetragonal space group P 4/mmm.

A 3g sample of this product was prepared and sent to Argonne in order to obtain some neutron powder diffraction data. This was collected on the Special Environment Powder Diffraction (S.E.P.D.) instrument. Data analysis was then carried out by the Rietveld method using the G.S.A.S. refinement suite.

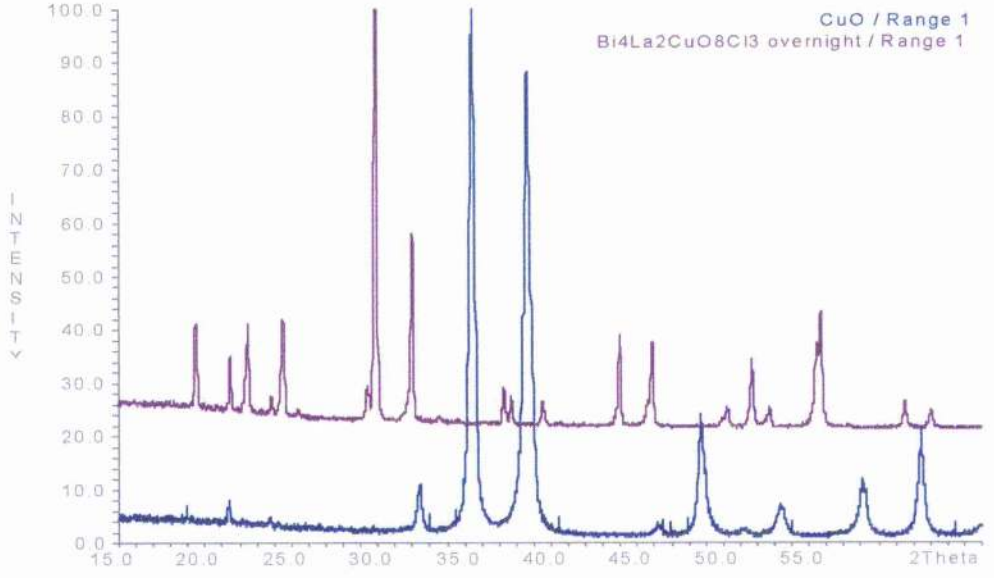

Figure 3.19. Final x – ray diffraction profile for $Bi_4La_2CuO_8Cl_3$, with the CuO pattern to show it's apparent absence as an impurity.

It was noted from preliminary analysis of the neutron data that there was some impurity as all the peaks could not be attributed to the space group assigned from

the x – ray data. This was not too surprising as the size of the unit cell was rather small for the accomodation of the full $Bi_4La_2CuO_8Cl_3$ stoichiometry. These impurities may have been masked in the x – ray data by the high scattering nature of the major phase.

A trial structural model was put into the refinement based on analogy with the Sillen phases, assuming that the structure contained O-Bi-Cl-Bi-O layers along the c – axis. Cl was placed at [0.5, 0.5, 0], hence giving Bi at [0, 0, z~0.2] and O at [0, 0.5, z~0.32]. Initial Rietveld refinement of this partial model gave a reasonable fit and a subsequent difference Fourier map revealed a single dominant peak at [0.5, 0.5, 0.5]. This site is eight fold coordinate with respect to oxygen and clearly represented a second metal atom. Due to the similarity in the neutron scattering lengths of Bi and La the refinement was then carried out against both x – ray and neutron data sets simultaneously. The x – ray data would clearly reveal any site ordering preferences of the two metals over the two sites.

Constrained refinement of the Bi/La occupancies over the two sites , with the Bi : La ratio fixed at two, suggested there was complete ordering of Bi at site (1) and La at site (2) (the refined occupancy factor for Bi on site (1) = 1.04(2)). These site occupancies were therefore kept fixed during the final stages of refinement.

This refinement reveals that the phase present is one of nominal composition Bi_2LaO_4Cl. Examination of the structure, shown in Figure 3.21, shows that instead of the anticipated Bi_2O_2 bilayers we actually have a related, triple fluorite, Bi_2LaO_4 layer [18].

Final refined atomic parameters are given in Table 3.15, detailing the structure shown in Figure 3.20. Rietveld plots are given in Figures 3.21 and 3.23.

Table 3.14 Crystal Data and Details of Structure Refinement

Empirical Formula	Bi_2LaO_4Cl
Formula Weight	656.323 $gmol^{-1}$
Crystal System	Tetragonal
a (Å)	3.9547(1)
c (Å)	9.1275(3)
Space Group	I4/mmm
T (°C)	25
X – ray Data	
λ (Å)(CuKα)	1.540562
2θ range	5° – 85°
No. of Reflections	147
No. of Data Points	3849
$*R_{wp}$	13%
Neutron Data	
d spacing range (Å)	0.5 – 3.5
No. of Reflections	425
No. of Data Points	5252
$*R_{wp}$	7.8%
No. of Parameters	39
Combined $*\chi^2$	2.76

*see section 2.2.11

Table 3.15. Final atomic parameters for Bi_2LaO_4Cl.

Atom	Site	x	y	z	$U_{11}/Å^2$	$U_{22}/Å^2$	$U_{33}/Å^2$
Bi	2g	0	0	0.2103 (2)	0.0060 (6)	0.0060 (6)	0.014 (1)
La	1d	0.5	0.5	0.5	0.0082 (8)	0.0082 (8)	0.009 (1)
O	4I	0	0.5	0.3282 (2)	0.0055 (9)	0.0111 (9)	0.0054 (8)
Cl	1c	0.5	0.5	0	0.0124 (8)	0.0124 (8)	0.016 (2)

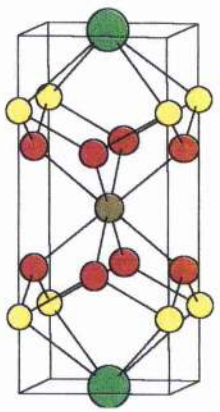

Figure 3.20. Structure of Bi_2LaO_4Cl. Bi is shown as yellow, La is brown, O is red and Cl is green.

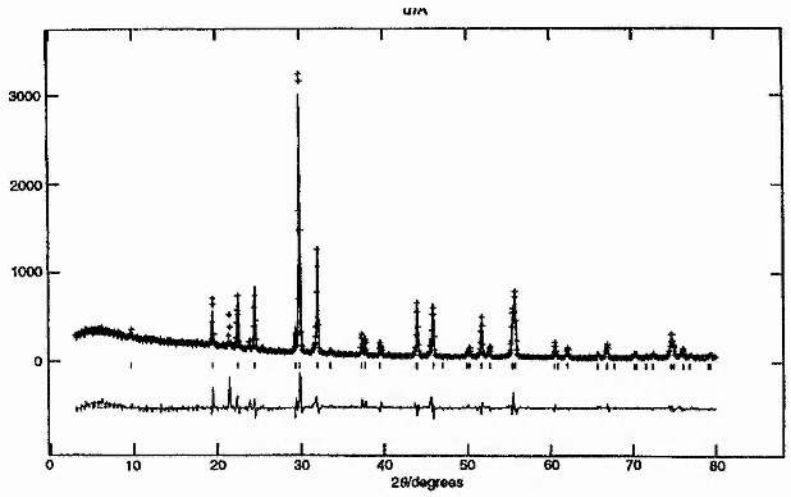

Figure 3.21. Rietveld plot for x – ray data of '$Bi_4La_2CuO_8Cl_3$'.

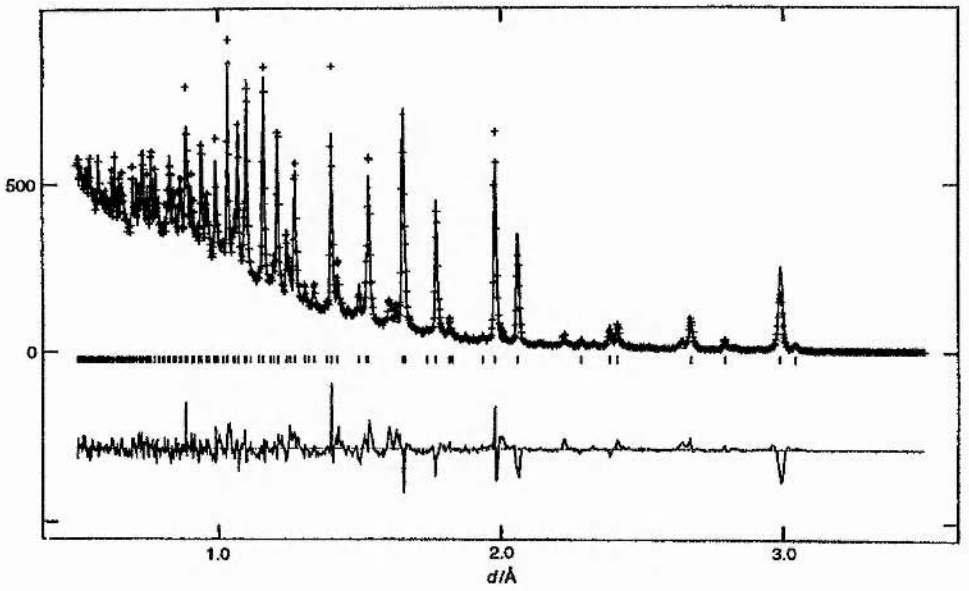

Figure 3.22. Rietveld plot for neutron data of '$Bi_4La_2CuO_8Cl_3$'.

Analysis of the structure, shown in Figure 3.20 shows that lanthanum is in an eight coordinate environment. This prompted the synthesis of the Nd and Y analogues which were prepared by reaction in an N_2 atmosphere at 675°C for 48 and 24 hours respectively. Initial x- ray characterisation of these phases suggests

that they are isostructural with Bi_2LaO_4Cl whilst the reduction in the required reaction time may reflect a greater structural compatability.

The lattice parameters of these phases from preliminary x – ray analysis are :

Bi_2NdO_4Cl a = 3.906(2) A and c = 8.985(6) Å

Bi_2YO_4Cl a = 3.849(1) A and c = 8.894(3) Å

The x – ray diffraction patterns for these phases are shown below in Figure 3.23.

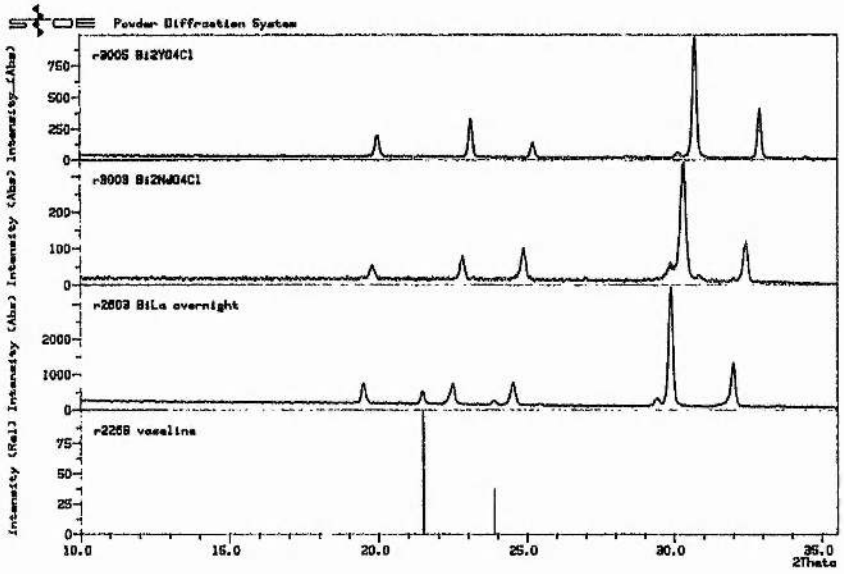

Figure 3.23. X – ray powder diffraction patterns for Bi_2YO_4Cl, Bi_2NdO_4Cl and Bi_2LaO_4Cl. The bottom profile shows the impurity peaks of vaseline used to mount the sample.

Note that the peaks shift towards larger d spacings as the Ln species becomes larger.

3.8 $Bi_4LaSrCuO_8Cl_3$

Stoichiometric amounts of halides and oxides corresponding to the above formula were reacted at 700°C for 60 hours in a nitrogen atmosphere. Substitution of Sr for La allows a formal oxidation state of +2 to be assigned to copper in a desired layer sequence of :

$[Bi_2O_2]$

$[Cl]$

$[Bi_2O_2]$

$[LaSrCuO_4]$

$[Cl]$

The x- ray pattern realised by the product of reaction at 800°Cfor 48 hours and then 850°C for 48 hours is shown in Figure 3.24. The pattern shows very sharp peaks and appears to be of quite a high symmetry due to the low number of peaks.

Attempts to index this pattern were unsuccessful and none of the peaks present could be attributed to any Bi, La, Sr, Cu, O or Cl containing compounds in the Daresbury database. It may be that this is a mixture of unknown phases leading to an inability to index the pattern as a single phase.

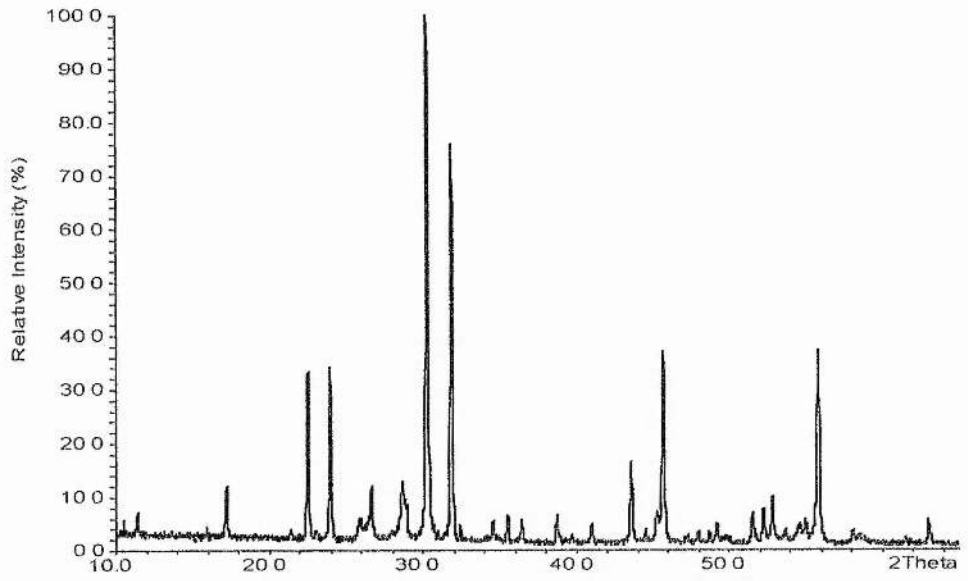

Figure 3.24. X – ray profile following the reaction of $Bi_4LaSrCuO_8Cl_3$.

3.9 $Bi_2La_2CuO_6Cl_2$

Stoichiometric amounts of oxides and halides corresponding to the above composition were reacted at 900°C for 24 hours in a nitrogen atmosphere. The above formula corresponds to the ideal composition of a proposed Sillen X2 / Ruddlesden – Popper n = 1 intergrowth. The layer sequence of the desired product is :

$[Bi_2O_2]$

$[Cl]$

$[La_2CuO_4]$

$[Cl]$

The x – ray profile of the product of this reaction is shown in Figure 3.25. Examination of this x – ray profile shows that the product is mainly composed of the Bi_2LaO_4Cl obtained on reaction of $Bi_4La_2CuO_8Cl_3$.

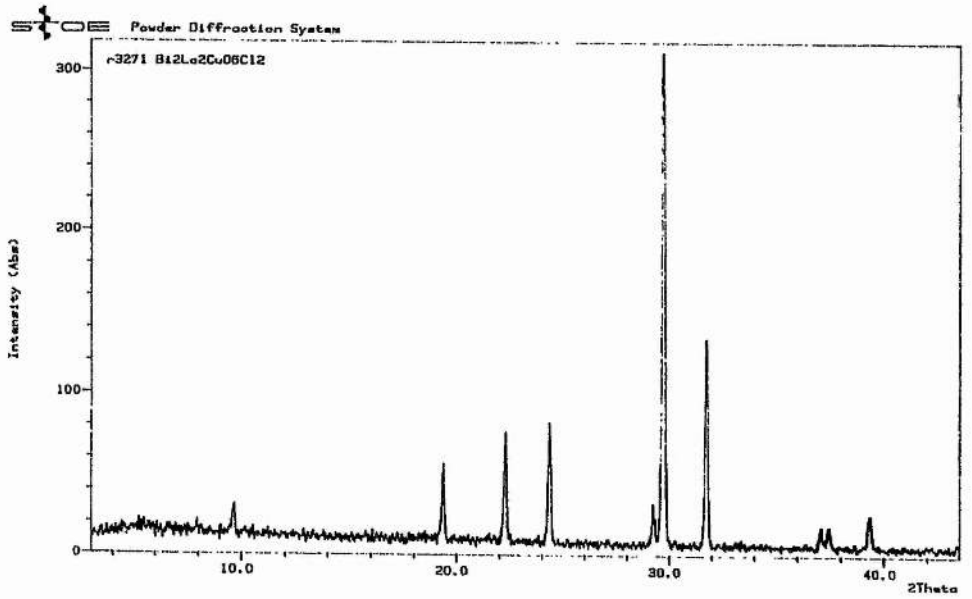

Figure 3.25. X- ray profile of the product of $Bi_2La_2CuO_6Cl_2$.

3.10 $Bi_2Nd_2CuO_6Cl_2$

The above formula corresponds to the ideal composition of a postulated Sillen X2 / Ruddlesden – Popper n = 1 intergrowth with the R – P unit the T' structure of Nd_2CuO_4. The desired structure would have a layer sequence :

$[Bi_2O_2]$

$[Cl]$

$[Nd_2CuO_4]$

$[Cl]$

The above composition was reacted at 900°C for 24 hours under nitrogen and yielded the top x – ray profile shown below :

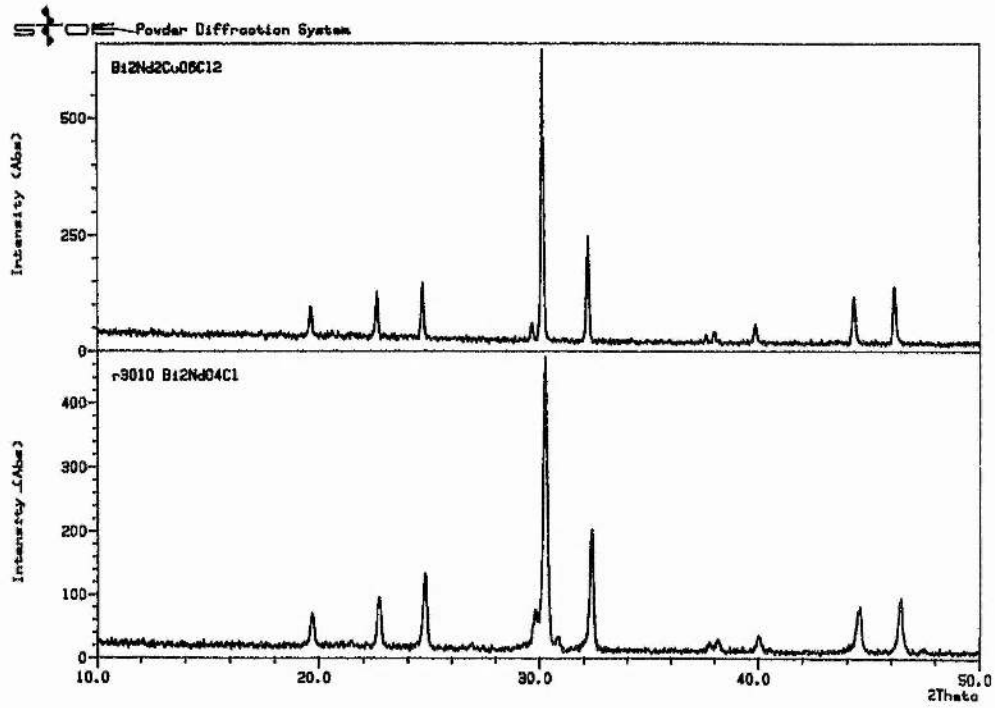

Figure 3.26. Comparison of product obtained on the reaction of precursors of stoichiometry $Bi_2Nd_2CuO_6Cl_2$ with the profile of Bi_2NdO_4Cl.

The comparison in Figure 3.26 shows that Bi_2NdO_4Cl is preferentially produced over the desired structure.

3.11 Discussion and Summary.

In this chapter I have relayed the results of my attempts to incorporate CuO_2 containing units between the halogen layers of the X2 section of Sillen X1X2 and X2 phases.

The ideal formula for a Sillen X1X2 / $Ca_2CuO_2Cl_2$ intergrowth is $Bi_3Ca_3CuO_6Cl_5$. Reaction of this stoichiometry in air does not yield the desired structure but rather a cation ordered, puckered, Sillen X1 related phase $CaBiO_2Cl$

[15]. $SrBiO_2Cl$ was also produced and shown to adopt the same structure as $BaBiO_2Cl$ [16].

Reaction of $Bi_3Ca_3CuO_6Cl_5$ in an inert atmosphere of flowing N_2 yields a Sillen X1X3 phase which hydrates to give a product with a similar x – ray diffractogram as the desired intergrowth. There is no evidence for CuO as an impurity phase suggesting that for the first time Cu has been incorporated in a Sillen phase.

The ideal formula for a Sillen X2 / $Ca_2CuO_2Cl_2$ intergrowth is $Bi_2Ca_2CuO_4Cl_4$. This also happens to be the formula for a Sillen X1X3 phase. Reaction of this stoichiometry in N2 yields the Sillen X1X3 phase which was again seen to hydrate.

Evidence for Cu being located in the central halgen layer of the X3 section is enhanced by the observation that reaction of the X1X3 material with an excess of $CuCl_2$ forms a Sillen X3 structure.

Tentative attempts to synthesise an ideal Cu containing X3 phase alternatively formed $Bi_6Ca_5O_{11}Cl_6$ with an Arppe related structure [17].

Attempts to intergrow X2 and X1X2 phases with La_2CuO_4 and Nd_2CuO_4 showed the formation of compounds Bi_2LaO_4Cl and Bi_2NdO_4Cl to be preferred. These materials contain triple fluorite metal oxide layers separated by a single halogen layer [18].

References for Chapter 3.

[1] Sillen L.G., *Naturewissenschaften* **26**, 612 (1938).

[2] Sillen L.G., *Naturewissenschaften* **28**, 396 (1940).

[3] Sillen L.G., *Naturewissenschaften* **30**, 318 (1942).

[4] Sillen L.G., *Zeitschrift fur Anorganische und Allgemeine Chemie* **242**, 41 (1939).

[5] Sillen L.G., *Zeitschrift fur Anorganische und Allgemeine Chemie* **246**, 115 (1941).

[6] Sillen L.G. and Gjorling-Husberg A.S., *Zeitschrift fur Anorganische und Allgemeine Chemie* **248**, 121 (1941).

[7] Sillen L.G. and Gjorling-Husberg A.S., *Zeitschrift fur Anorganische und Allgemeine Chemie* **248**, 133 (1941).

[8] Aurivillius B., *Arkiv. Kemi* **1**, 463 (1941).

[9] Ackerman J.F., *Journal of Solid State Chemistry* **62**, 92 (1986).

[10] Kusainova A.M., Lightfoot P., Zhou W.Z., Stefanovich S.Y., Mosunov A.V. and Dolgikh V.A., *Chem. Mater.* **13(12)**, 4731 – 4737 (2001).

[11] Zhu W.J., Huang Y.Z., Liang J.K. and Zhao Z.X., *Materials Research Bulletin* **27**, 885 (1992).

[12] Argyriou D.N., Jorgensen J.D., Hitterman R.L., Hiroi Z., Kobayashi N. and Takano M., *Phys. Rev. B* **18**, 1978 (1995).

[13] Werner P.-E., Eriksson L. and Westdahl M., *J. Appl. Crystallogr.* **18**, 360 (1989).

[14] LeBail A., Duroy H. and Fourquet L., *Materials Research Bulletin* **23**, 447 (1989).

[15] Fray S.M., Milne C.J. and Lightfoot P., *Journal of Solid State Chemistry* **128**, 115 (1997).

[16] Kennard M.A., Darriet J., Grannec J. and Tressaud A., *Journal of Solid State Chemistry* **117**, 201 (1995).

[17] Eggenweiler U., Keller E. and Kramer V., *Acta Cryst.* **B56**, 431 (2000).

[18] Milne C.J., Lightfoot P., Short S. and Jorgensen J.D., *Journal of Materials Chemistry* **5(9)**, 1419 (1995).

4. Quadruple Perovskites.

4.1 Introduction

The next set of compounds to be investigated as potential superconductors were the quadruple perovskites. In chapter 1 the 1-2-3, $YBa_2Cu_3O_{7-\delta}$, compound was shown to be a layered perovskite with ordering of oxygen vacancies. This ordering allows the formation of suitably spaced CuO_2 planes and the achievment of superconductivity through control of oxygen non – stoichiometry. This material is known as an oxygen deficient triple perovskite.

The quadruple perovskite structure was first reported by Anderson et al. [1] for a material of composition $La_2Ba_2Cu_2Sn_2O_{11}$. In this material $1/12^{th}$ of the oxygen sites are vacant. These vacancies are located in the sites that coordinate the Cu^{2+} ions giving them a five fold, square pyramidal, coordination. The Sn^{4+} ions retain the normal six fold, octahedral, coordination of a B – site cation in the perovskite structure.

In the quadruple perovskite structure the different B – cation coordination preferences, and a complete ordering of associated oxygen vacancies leads to the structure shown overleaf.

From Figure 4.1 we see that this material contains the CuO_2 sheets requisite of high T_c superconductivity. This material however has a reported a – axis of 3.9893 Å which is slightly longer than the corresponding parameter for known superconductors [2].

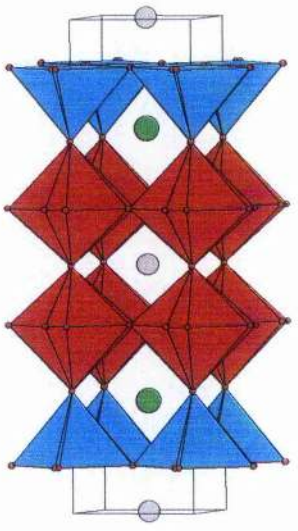

Figure 4.1. The quadruple perovskite structure of $La_2Ba_2Cu_2Sn_2O_{11}$ with ordered oxygen vacancies lending to a unit cell of space group P4/mmm with a = 3.9893(3) Å and c = 16.232(1) Å. CuO_5 square pyramids are shown as Cyan and B'' cation octahedra are shown as red. La positions are shown as grey with the Ba site shown as green.

Table 4.1 Selected Bond Distances for $La_2Ba_2Cu_2Sn_2O_{11}$ [1].

La 1 – O 4 2.486(4) Å x 4	La 3 – O 1 2.821(1) Å x 4
La 1 – O 4 2.592(4) Å x 4	La 3 – O 2 3.041(2) Å x 4
La 2 – O 4 2.830(5) Å x 4	Cu – O 4 2.007(1) Å x 4
La 2 - O 3 2.843(5) Å x 4	Cu – O 3 2.222(3) Å x 1
La 2 – O 4 2.925(1) Å x 2	Sn – O 3 1.998(4) Å x 1
La 2 – O 2 3.026(3) Å x 2	Sn – O 2 2.035(1) Å x 4
La 2 – O 2 3.464(3) Å x 2	Sn – O 1 2.115(2) Å x 1
La 3 – O 2 2.531(2) Å x 4	

Gormenzano and Weller [3,10] then showed that this quadruple perovskite structure could be retained with the use of the smaller lanthanides Nd, Sm and Gd and a cooperative substitution of Ti^{4+} for Sn^{4+}. They synthesised the compounds $Nd_2Ba_2Cu_2SnTiO_{11}$, $Sm_2Ba_2Cu_2Sn_{0.5}Ti_{1.5}O_{11}$ and $Gd_2Ba_2Cu_2Ti_2O_{11}$ and reported an associated contraction of the a – parameter. The $Gd_2Ba_2Cu_2Ti_2O_{11}$ phase contains O – Cu – O linkages of 1.951 Å, similar to those of the high temperature superconductors [2].

Table 4.2. Lattice parameters of samples prepared by Gormezano and Weller .

Compound	a	c
$Nd_2Ba_2Cu_2SnTiO_{11}$	3.9299(2) Å	15.964(8) Å
$Sm_2Ba_2Cu_2Sn_{0.5}Ti_{1.5}O_{11}$	3.9064(1) Å	15.839(5) Å
$Gd_2Ba_2Cu_2Ti_2O_{11}$	3.8873(2) Å	15.7335(7) Å

4.1 Ordering Oxygen Vacancies.

In the quadruple perovskite structure the oxygen vacancies are associated with the Cu^{2+} ions rather than the larger, more electropositive Sn^{4+} or Ti^{4+}. This coordination preference however does not in itself lend to the formation of the quadrupled structure, rather there must also be a complimentary ordering of the A – cations.

The A – cations (Ln and Ba in $Ln_2Ba_2Cu_2(Sn/Ti)_2O_{11}$) occupy 3 different sites in the structure.

1. 8 coordinate site between CuO_2 planes
2. 12 coordinate site between $(Sn/Ti)O_2$ planes
3. 12 coordinate site between $(Sn/Ti)O_2$ and CuO_2 planes.

The lanthanide will reside on the two smaller sites (1 and 2) preferentially, and does so exclusively (giving a totally ordered quadruple perovskite) if sufficiently smaller than Ba [3,4].

The paper of Gormenzano and Weller [3] summarized the dependance of the quadrupled structure on ionic size with an amended Goldsmith tolerance factor [5] equation:

$$t = \frac{\left(\frac{ra_1 + ra_2}{2}\right) + r_o}{\sqrt{2}\left[\left(\frac{rb_1 + rb_2}{2}\right) + r_o\right]}$$

With ra_1 = radius of A' cation, ra_2 = radius of A''cation, rb_1 = radius of B' cation, rb_2 = radius of B'' cation and r_o = radius of oxygen

They stated that the quadrupled structure is observed only in the narrow range of 0.97=>t=>0.965.

4.2 Cu^{2+} and Ti^{4+} quadruple perovskites.

A series of compounds of general formula $Ln_2Ba_2Cu_2Ti_2O_{11}$ have been reported in the literature with members such that Ln = La, Nd, Eu, Gd and Tb.[3,4,6-10]

These materials crystallise in the tetragonal space group P4/mmm and possess a super structure of $a = a_p$, $b = a_p$ and $c = 4 \times a_p$ where a_p is the normal unit cell for a cubic perovskite.

The La member is quite ambiguous in that x – ray diffraction data tends to show that the quadruple perovskite superstructure does not exist but rather a cubic

disordered structure is produced [7,10]. However, electron diffraction studies have revealed the existence of some quadruple nature. A publication by Palacin et al. shows the x – ray diffraction patterns for the La, Nd and Eu versions [6]. These show an increasing quadruple nature with the splitting of cubic peaks non apparent in the La compound but quite pronounced in the Eu version. The article goes on to show that electron diffraction photographs for these materials show a gradually increasing c = 4 x a_p superstructure spot thus ordering increases through the series as the A' cation gets smaller.

A recent publication by Palacin et al. [9] has confirmed that the La member is to an extent quadrupled, with prolonged heating of the sample resulting in a greater degree of ordering. However there remains slight disorder over the Cu and Ti sites.

The Nd analogue, $Nd_2Ba_2Cu_2Ti_2O_{11}$, was reported to be fully quadrupled in a paper by Gomez – Romero et al. [7]. This was however contradicted by work done by Jennings and Greaves [11] who observed disorder in this material with up to 10 % of Cu and Ti exchanging sites.

The disorder is not present for the Eu, Gd and Tb members, with electron diffraction data showing strong 4 x a*p* superstructure spots and hence Goldsmith tolerance factor limits must encompass these members. This observation could be a result of the reduction of the size of the lanthanide reducing the space for oxygen to enter the (0,0,0) site giving more quadrupled nature.

With a Cu – O (basal) bond distance of 1.947(3) Å this Tb member gives an a-parameter more favourable to the yielding of p – type superconductivity in this structure type.

4.3 Doping studies of Quadrupled perovskites.

The aim of my work on these materials was to determine the effect of different substitution methods in the quadruple perovskite structure. The main two problems hindering the observation of superconductivity in the quadruple perovskite system are :

1. Slightly too large in – plane O – Cu – O linkages in the CuO_2 sheets.
2. Lack of mixed valence of the Copper in the CuO_2 sheets.

We aimed to investigate doping strategies to overcome these problems.

The first set of experiments involved the substitution of Sr for Ba in the $Nd_2Ba_2Cu_2Ti_2O_{11}$ system. It was hoped that we would see a decrease in the a – parameter upon such a substitution thus bringing the material closer to the size noted for high T_c superconductors. We hoped to monitor any structural changes occurring upon substitution. The Nd system was chosen as Eu and Gd compounds are unsuitable for neutron diffraction experiments due to the absorption of neutrons by these elements.

4.3.1 $Nd_2Ba_{2-x}Sr_xCu_2Ti_2O_{11}$

Samples corresponding to the formula $Nd_2Ba_{2-x}Sr_xCu_2Ti_2O_{11}$ (x = 0, 0.1, 0.2, 0.3) were preheated, to decompose carbonates, at 950°C for 5 hours. They were then treated in air at 1050°C, and checked by powder x – ray diffraction every 24 hours against a standard pattern for $Nd_2Ba_2Cu_2Ti_2O_{11}$, until no impurity peaks were left. This was achieved after approximately 72 hours of heat treatment.

X – ray diffraction patterns for such samples are shown overleaf.

These materials were made into batches of approximately 5g and sent for neutron diffraction analysis on the SEPD instrument at the IPNS facility at the Argonne National Laboratory, Illinois, U.S.A

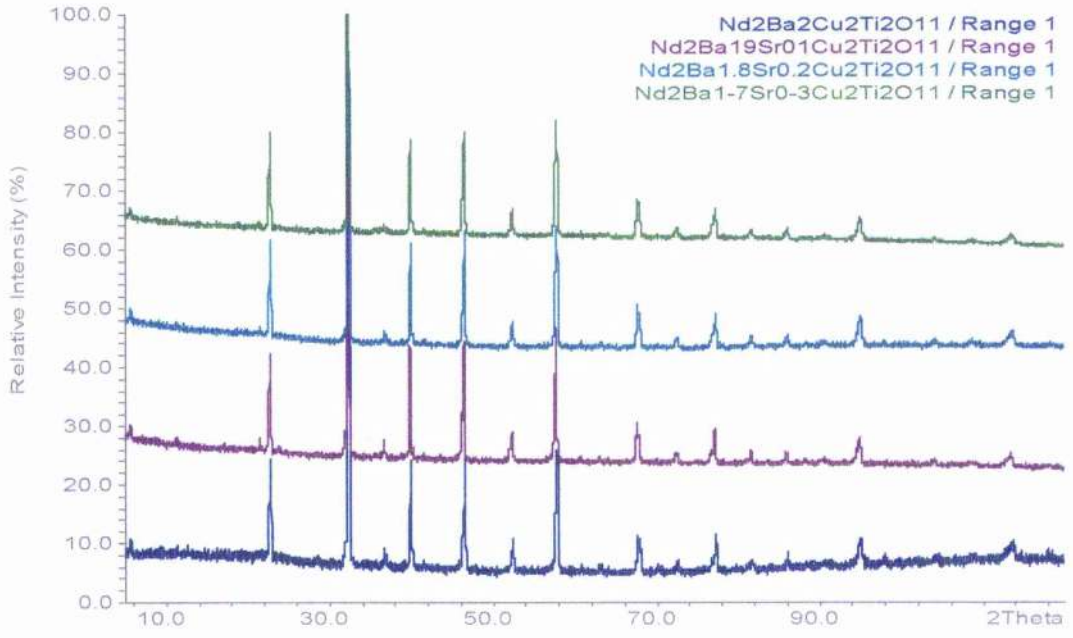

Figure 4.2. X – ray diffraction profiles for $Nd_2Ba_{2-x}Sr_xCu_2Ti_2O_{11}$.

The x – ray diffraction patterns were indexed using TREOR [12] with their a – parameters determined as :

Table 4.3. a - axis for Sr substituted $Nd_2Ba_{2-x}Sr_xCu_2Ti_2O_{11}$.

x	a
0	3.91003 Å
0.1	3.9094 Å
0.2	3.9085 Å
0.3	3.90749 Å

Simultaneous Rietveld refinement of the neutron and x - ray data intimated that Sr was incorporated into the structure, however along with the decrease in the a – parameter we found there was a decrease in the quadrupled nature of the materials with increasing occupancy of the (0,0,0) site by oxygen. This site is completely vacant in a fully quadrupled system.

The refinement strategy involved taking a starting model from Jennings and Greaves [11]for the x = 0 member. Subsequent refinements involved using the refined model of the previous compound as input. Final χ^2 values for the refinement of these data are shown in Table 4.4. The oxygen content of the (0,0,0) site is shown in Table 4.5.

Table 4.4. Final χ^2 values following refinement of data for $Nd_2Ba_{2-x}Sr_xCu_2Ti_2O_{11}$

x	*χ^2
0	4.050
0.1	4.697
0.2	4.808
0.3	3.639

* see section 2.2.11

Table 4.5. Oxygen occupancy of the (0,0,0) site in $Nd_2Ba_{2-x}Sr_xCu_2Ti_2O_{11}$.

x	Oxygen occupancy of (0,0,0)
0	0.138
0.1	0.195
0.2	0.197
0.3	0.239

We can see from Table 4.5 that our results for the x = 0 sample are in accordance with Jennings and Greaves [11] in that they show this compound not to be fully quadrupled.

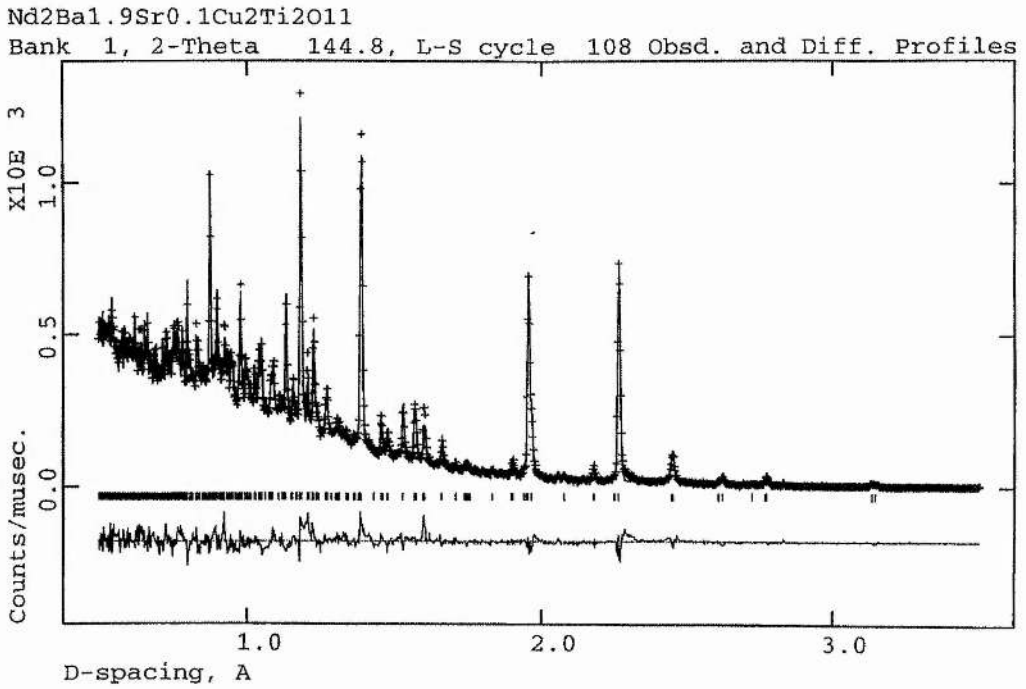

Figure 4.3. Rietveld plot for neutron data of $Nd_2Ba_{1.9}Sr_{0.1}Cu_2Ti_2O_{11}$.

4.3.2 $Gd_2Ba_{2-x}Sr_xCu_2Ti_2O_{11}$

. The same substitution mechanism was tried on the analogous $Gd_2Ba_2Cu_2Ti_2O_{11}$. Precursors of stoichiometries : x = 0, 0.1, 0.2, 0.3 in $Gd_2Ba_{2-x}Sr_xCu_2Ti_2O_{11}$, were heated at 950°C for 5 hours to decompose the carbonate. The mixture was then reground, palletised and treated at 1025°C for 24 hour periods. After each period the sample was cooled, reground and x – rayed. If impurities persisted the cycle was repeated. Final x – ray diffraction patterns for the members x = 0, 0.1, 0.2, 0.3 are shown overleaf with no apparent impurity peaks:

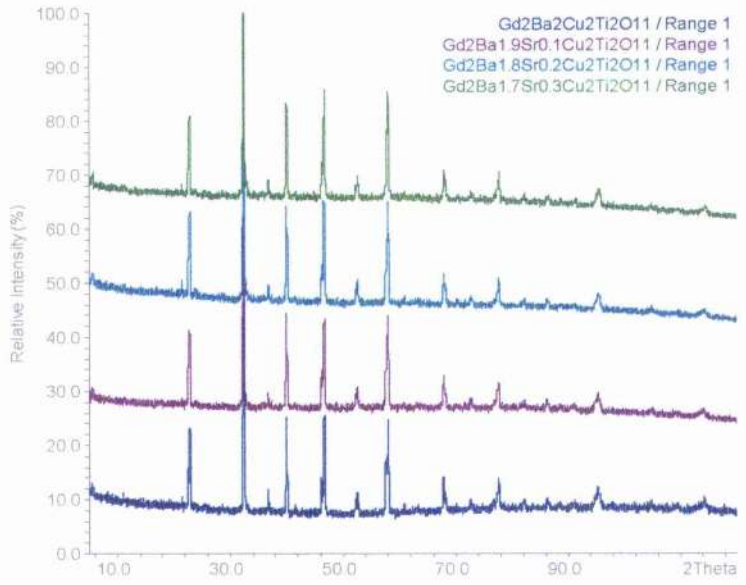

Figure 4.4. X – ray diffraction patterns for the series $Gd_2Ba_{2-x}Sr_xCu_2Ti_2O_{11}$: x = 0, 0.1, 0.2, 0.3. The bottom profile is that of x = 0 with increasing x as you move upwards.

Lattice parameters for these patterns were obtained, however they showed no decrease in the a – parameter with increasing Sr content. i.e.

Table 4.6. Lattice parameters for $Gd_2Ba_{2-x}Sr_xCu_2Ti_2O_{11}$.

x	a	c
0	3.8872 Å	15.733 Å
0.1	3.8880 Å	15.720 Å
0.2	3.8881 Å	15.739 Å
0.3	3.8848 Å	15.740 Å

Neutron data for these samples was not taken as gadolinium absorbs neutrons, however we hoped that analysis of the x – ray diffraction patterns would show a decrease in the quadrupled nature of the series with increasing Sr content. We

anticipated that there would be a decrease in the separation of the {008} and {200}peaks as the mismatch between the A' and A'' cations was decreased. These peaks are shown below in Figure 4.5.

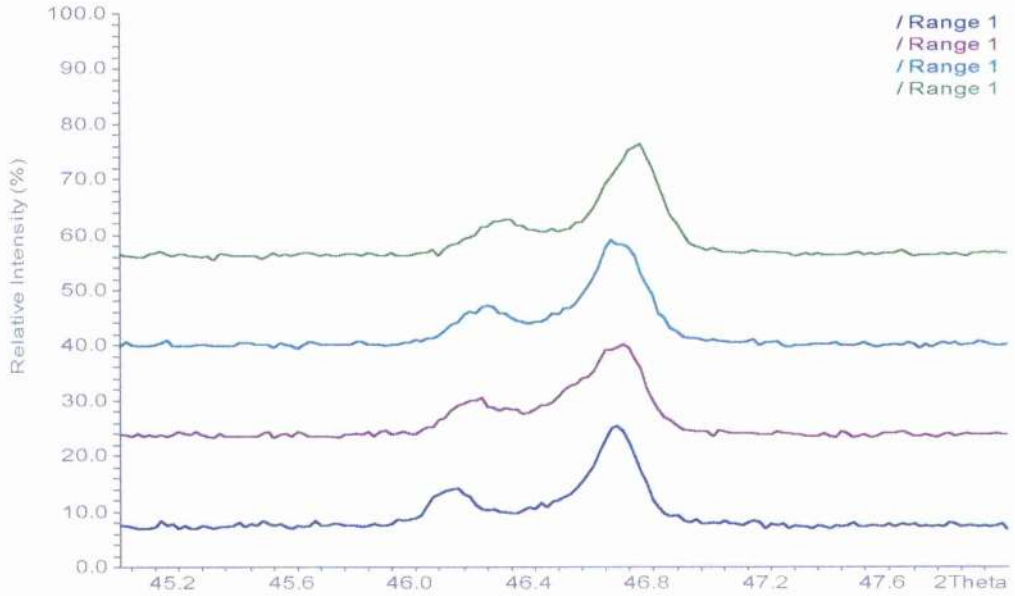

Figure 4.5. {008} and {200} peaks for samples $Gd_2Ba_{2-x}Sr_xCu_2Ti_2O_{11}$. X increases as you move up.

Analysis of these peaks gives no conclusive evidence for increased disorder.

4.3.3 $Tb_2Ba_{2-x}Sr_xCu_2Ti_2O_{11}$.

Samples of the above stoichiometries with x = 0, 0.1 and 0.2, were heated to 950°C for 5 hours to decompose the carbonates and then reacted at 1100°C in air for 48 hours. The following x – ray patterns were yielded with only the x = 0 sample giving an impurity free product :

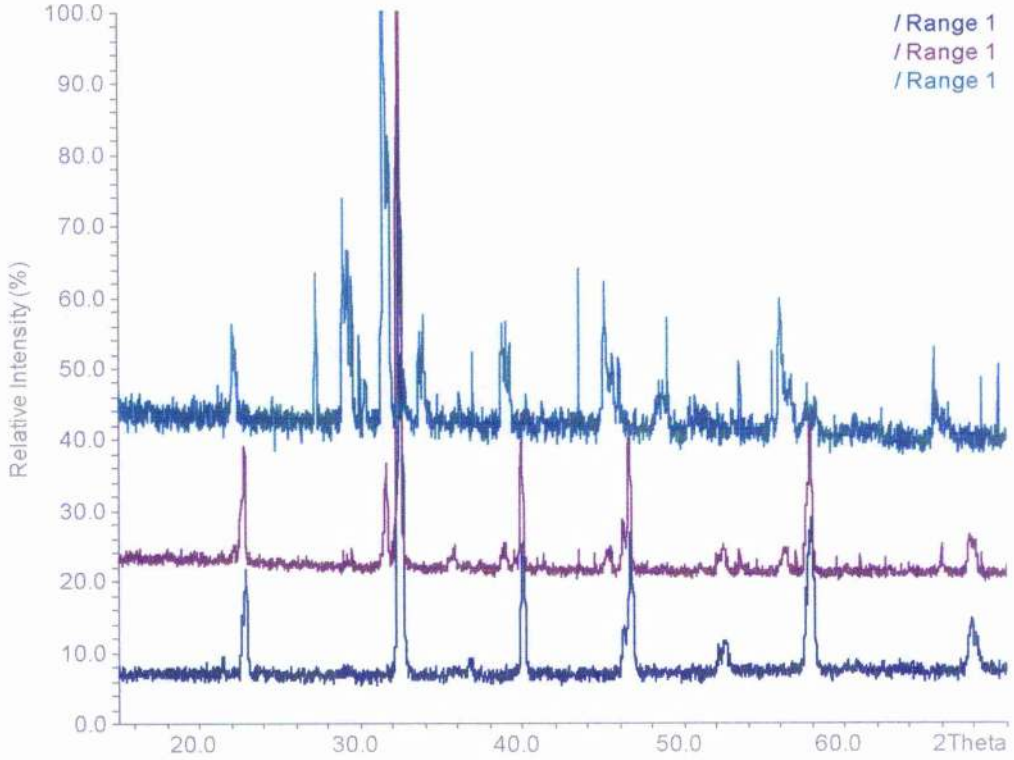

Figure 4.6. Final x– ray diffraction profiles for $Tb_2Ba_{2-x}Sr_xCu_2Ti_2O_{11}$ with x = 0, 0.1, 0.2. Member x = 0 is the bottom profile with x = 0.2 at the top.

From this it appears that Sr substitution is not possible in this system. It seems that the stoichiometric $Tb_2Ba_2Cu_2Ti_2O_{11}$ is at the limit of stability for the quadruple perovskite structure and that a reduction in size of the A'' cation cannot be accommodated. The mismatch between the different cations may be such that a quadruple perovskite of such formulae are not within tolerance factor limits.

4.3.4 $Nd_2Ba_2Cu_{2+x}Ti_{2-x}O_{11}$.

The next stage of investigation in to this system was to evaluate the ability to dope the CuO_2 sheets in this structure by aliovalent substitution. Our doping strategy was to substitute Cu^{2+} for Ti^{4+}, Cu^{2+} can occupy six fold coordinate sites as well as five fold, trying to introduce holes into the CuO_2 sheets.

5g samples of the above stoichiometries, with x = 0.1 and 0.2 (the member x = 0.3 showed impurity peaks on x –ray analysis), were prepared by reaction in air, firstly at 950°C to decompose carbonates and then at 1100°C for 72 hours, with intermediate grindings every 24 hours. Lattice parameters and sample purity were determined from data collected on the STOE x – ray diffractometer with the remaining sample sent to the IPNS at Argonne U.S.A. where neutron data was collected on the S.E.P.D. instrument. These data were then refined using G.S.A.S [13]

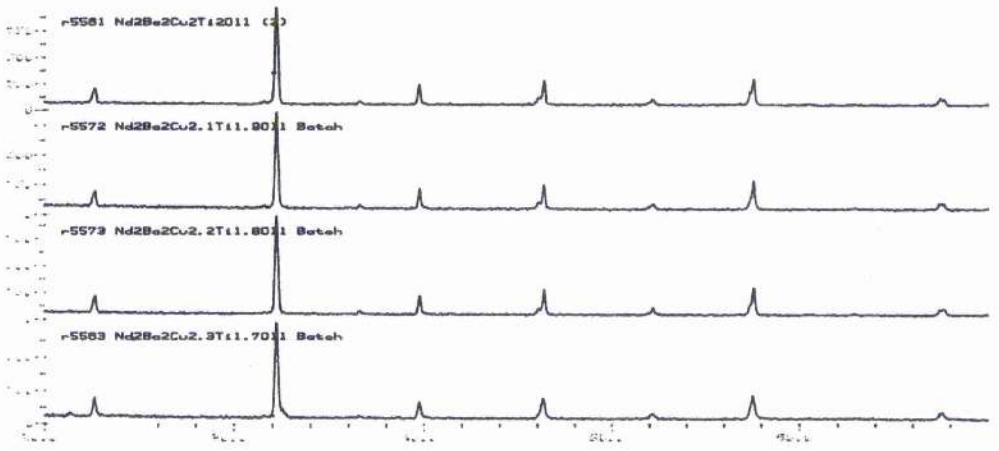

Figure 4.7. X – ray diffraction patterns for samples of $Nd_2Ba_2Cu_{2+x}Ti_{2-x}O_{11}$. The x = 0.3 member at the bottom shows a slight impurity at the base of the most intense peak.

Rietveld refinement was carried out on these data with the ideal $Nd_2Ba_2Cu_2Ti_2O_{11}$ [7] structure used as a starting model. Refinement of these data encompassed 27 parameters with final χ^2 values of 3.317 and 2.328 for members x = 0.1 and 0.2 respectively.

The major observation from these refinements was that the CuO_2 planes were more intact with less Ti^{4+} ions occupying the Cu^{2+} site. i.e. :

Table 4.7. Increasing copper occupancy of (0,0,0.1077) site with increasing copper content.

x	Cu occupancy of (0,0,0.1077) site
0	0.84
0.1	0.888
0.2	0.951

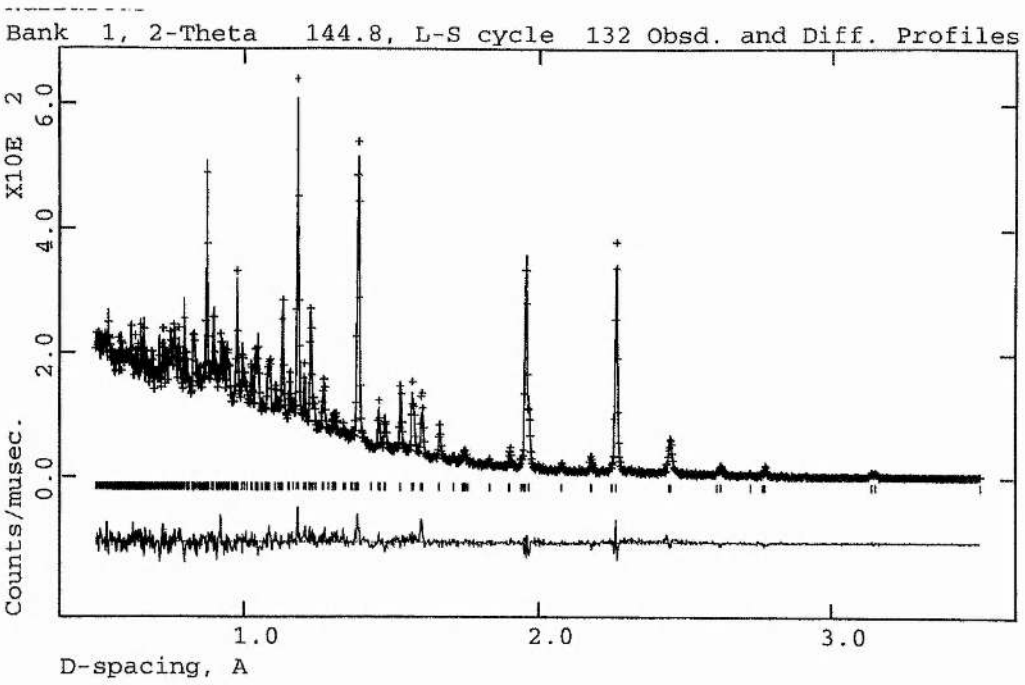

Figure 4.8. Rietveld plot for neutron data of $Nd_2Ba_2Cu_{2.1}Ti_{1.9}O_{11}$

4.4 Discussion and Summary.

The ideal quadruple perovskite structure has the potential to support superconductivity due to the presence of CuO_2 sheets. No member of this structure type has been rendered superconducting due to (i) slightly long in plane O – Cu – O linkages, and (ii) lack of ability to suitably dope these compounds to give the necessary mixed valence nature to the copper.

I have investigated strategies to overcome these problems with (i) Sr substitution for Ba to reduce the O – Cu – O distance, and (ii) Cu^{2+} substitution for Ti^{4+} to alter the valence of copper in the CuO_2 sheets.

My x – ray and neutron powder diffraction study of the $Nd_2Ba_{2-x}Sr_xCu_2Ti_2O_{11}$ system shows that there is the anticipated reduction in the unit cell size, however there is a cooperative increase in the oxygen occupancy of the (0,0,0) site which is vacant in the ideal quadruple perovskite structure. This suggests Cu and Ti are exchanging sites to a greater degree on increasing Sr content. This reduces the intact nature of the CuO_2 sheets stopping any chance of superconductivity. Oxygen occupancy of the (0,0,0) site also allows communication between Cu ions in the structure which does not allow superconductivity.

X – ray studies of the $Gd_2Ba_{2-x}Sr_xCu_2Ti_2O_{11}$ system again implies that Sr is incorporated into the structure due to the absence of any impurity peaks up to and including x = 0.3. Indexing of the diffractograms of this system however shows no trend for a reduction in size of the unit cell. Analysis of the {008} and {200} peaks shows no evidence for increasing disorder as there appears to be no convergence of them.

Analysis of powder x – ray diffraction traces for the $Tb_2Ba_{2-x}Sr_xCu_2Ti_2O_{11}$ system shows that only the x = 0 member is impurity free. Additional peaks are observed in the diffractograms of the x = 0.1 and 0.2 members.

Powder x – ray and neutron diffraction studies of the $Nd_2Ba_2Cu_{2+x}Ti_{2-x}O_{11}$ system show that the CuO_2 sheets become more intact with increasing x. The x = 0.1 and 0.2 members appear to be impurity free with low levels of impurity in the x = 0.3 member. Thus substitution of Cu^{2+} for Ti^{4+} may be a way of doping this system. However there may be communication between Cu in the five fold sites and Cu in the six fold sites causing a breakdown in any superconductivity.

References for Chapter 4.

[1] Anderson M.T., Poeppelmeier K.R., Zhang J.-P., Fan H.-J. and Marks L.D., *Chemistry of Materials* **4**, 1305 – 1313 (1992).

[2] Tokura Y. and Arima T., *Japanese Journal of Applied Physics* **29**, 2388 (1990).

[3] Gormezano A. and Weller M.T, *Journal of Materials Chemistry* **3(9)**, 979 – 982 (1993).

[4] Palacin M.R., Krumeich F., Caldes M.T. and Gomez-Romero P., *Journal of Solid State Chemistry* **117**, 213-216 (1995).

[5] Goldschmidt V.M., *Str. Ner. Vidensk Akad. Oslo* **1**, 1, (1926).

[6] Palacin M.R., Fuertes A., Casan-Pastor N. and Gomez-Romero P., *Advanced Materials* **6(1)**, 54 (1994).

[7] Gomez-Romero P., Palacin M.R. and Rodriguez-Carrajal J., *Chemistry of Materials* **6**, 2118 (1994).

[8] Palacin M.R., Fuertes A., Casan-Pastor N. and Gomez-Romero P., *Journal of Solid State Chemistry* **119**, 224 (1995).

[9] Palacin M.R., Krumeich F. and Gomez-Romero P., *Solid State Ionics* **101**, 1079 (1997).

[10] Gormezano A. and Weller M.T., *Journal of Materials Chemistry* **3(7)**, 771 (1993).

[11] Jennings R.A. and Greaves C., *Physica C* **235 –240**, 989 – 990 (1994).

[12] WernerP.-E., Eriksson L. and Westdahl M., *J. Appl. Crystallogr.* **18**, 360 (1989).

[13] Larson A. C. and Von Dreele R. B., Los Alamos National Laboratory Report No. LA-UR-86-748 (1987).

5. Ruthenates

5.1 Background

Interest in ordered copper – ruthenium perovskites has been fuelled by the observation of both ferromagnetism and superconductivity in the material $RuSr_2GdCu_2O_8$ [1]. This material was first prepared by Bauernfeind et al. [2] and is of the structure shown below :

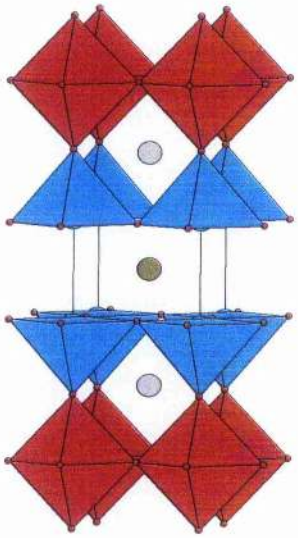

Figure 5.1. The structure of $RuSr_2GdCu_2O_8$ with RuO_6 octahedra shown as red and CuO_5 pyramids shown as cyan. Strontium positions are shown as grey with the gadolinium site shown as olive.

This material belongs to the tetragonal P4/mmm space group with a ~ 3.84 Å and c ~ 11.6 Å and shows a Curie transition at T_M = 132 K and T_c onset at 46 K [3].

In an annealed sample prepared by McLaughlin et al.[3] they found no evidence for cation disorder or oxygen non – stoichiometry. This allows the formal oxidation states of Cu and Ru to be written as 2 + p and 5 – 2p, respectively, with p denoting the

amount of charge tranferred between the CuO_2 and RuO_2 planes through the interaction of Cu $d_x2_{-y}2$ and Ru t_{2g} bands.

For p = 0 both CuO_2 and RuO_2 planes would be antiferromagnetically ordered and hence insulating. In the case of the upper limit with p = 0.5 we would expect itinerant electron behaviour with the CuO_2 planes overdoped for superconductivity but with the RuO_2 layers able to show ferromagnetic ordering as in $SrRuO_3$ [4,5]. The observation of both superconductivity and ferromagnetism in $RuSr_2GdCu_2O_8$ shows that p lies somewhere between these two extremes : $0 < p < 0.5$.

The value of p was calculated by McLaughlin et al. by means of bond valence summations which utilise the sensitivity of Cu – O bond lengths to hole concentration. They used a technique outlined by I.D. Brown [6] and calculated a high value of p ~ 0.4 based on bond lengths derived from diffraction data taken at 295 K. The authors state that this is in contrast to a value of p ~ 0.1 derived from transport measurements.

The difference in p values suggests that a large number of holes may be trapped by defects or the ferromagnetic order in the material.

Klamut et al. [7] investigated the $Ru_{1-x}Sr_2GdCu_{2+x}O_{8-y}$ system and successfully synthesised members x = 0, 0.1, 0.2, 0.3, 0.4 and 0.75 in a high pressure oxygen atmosphere. They showed a change in T_c with varying x with a maximum value of T_c (onset) at 72 K for x = 0.3 and 0.4. There was however an associated loss of the ferromagnetic signal of the Ru sublattice with members x = 0 and 0.1 the only ones showing even a small signature which could not even be attributed to the bulk of the sample. ie Cu dilution of the Ru site breaks up the ferromagnetic communication.

Bauernfeind et al. [2] also published the structure of materials of general composition $RuSr_2(Ln_{1+x}Ce_{1-x})Cu_2O_{10}$ with Ln = Sm, Eu and Gd. They showed that

variation of x in these systems resulted in bulk superconductivity for $0.3 =< x =< 0.5$ with T_c onset at ~40 K. The structure of these materials is shown below in Figure 5.2.

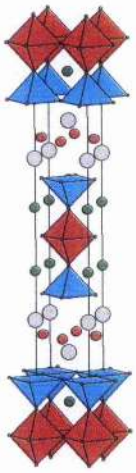

Figure 5.2. Structure of $RuSr_2Ln_{1+x}Ce_{1-x}Cu_2O_{10-\delta}$ with RuO_6 octahedra shown as red and CuO_5 pyramids shown as cyan. Sr positions are shown as green with the Ln/Ce site shown as grey and the O position in the $(Ln/Ce)_2O_2$ fluorite layer shown as red.

Felner et al. [8] showed that materials $RuSr_2(Ln_{1.4}Ce_{0.6})Cu_2O_{10-\delta}$ (Ln = Eu and Gd) were magnetically ordered as well as superconducting with T_M ~180 and 122 K and T_c ~ 42 and 32 K respectively. They used magnetic susceptibility measurements and Mössbauer spectroscopy to show that superconductivity was confined to the CuO_2 planes with ferromagnetism originating from the Ru sublattice. NB. RuO_2 sheets are the seat of superconductivity in Sr_2RuO_4.

5.2 Aims

With the coexistence of ferromagnetism and superconductivity in the triple perovskite related 1 – 2 – 1 – 2 structure of $RuSr_2GdCu_2O_8$, we sought extend the

range of the family, $RuSr_2LnCu_2O_8$, with the synthesis of the Ln = Tb variant (Ln = Sm, Eu and Gd were characterised by Bauernfeind et al. [2]). We also hoped to produce similar properties on incorporation of ruthenium into the quadruple perovkite structure.

5.3 $RuSr_2TbCu_2O_8$

A sample of the above stoichiometry was prepared from precursor oxides and carbonates. These powders were intimately mixed in an agate mortar and pestle and heated in air to 970°C for 24 hours to decompose the carbonates.

The sample was then pelletised and heated at 1000°C, in air, for 72 hours with intermediate grindings. The sample after this teatment rendered an x – ray powder diffraction profile shown below :

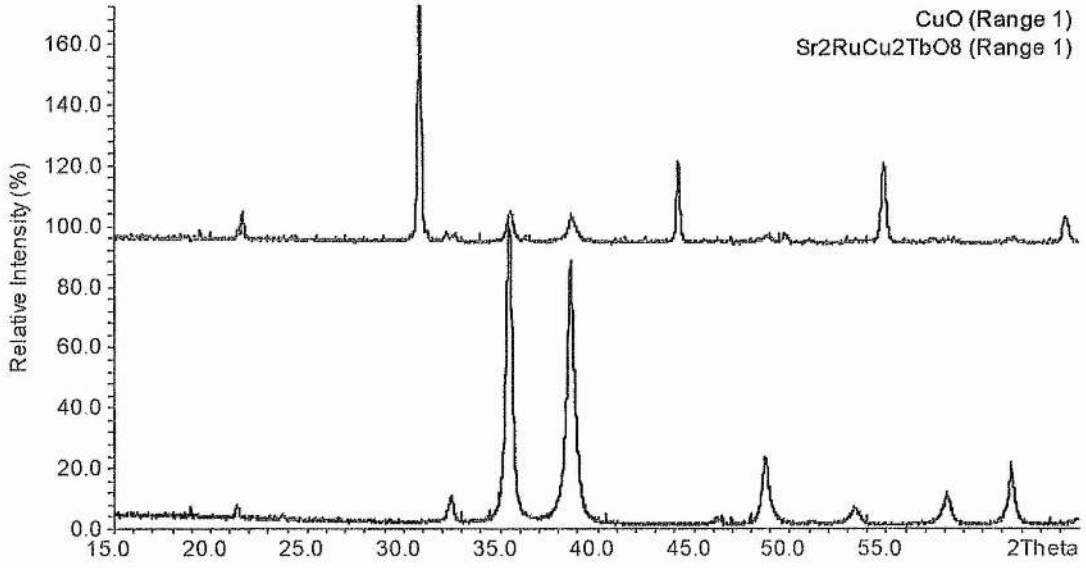

Figure 5.3. The powder X – ray diffraction pattern for the treated sample of $RuSr_2TbCu_2O_8$. The bottom profile is that of CuO.

Inspection of this pattern showed that CuO was present whilst the remainder of the peaks were indexed, using TREOR [9], on the basis of a cubic unit cell with a = 8.1943 Å. A similar result was noted by Bauernfeind et al.[2] when they attempted to synthesise Dy and Y analogues of the 1-2-1-2 structure. CuO and cubic phases, of a = 8.17 Å and 8.16 Å respectively, being produced on treatment. The authors state that these cubic phases are ordered cubic perovskites of composition Sr_2DyRuO_6 and Sr_2YRuO_6.

5.3.1 Sr_2TbRuO_6

Crystal structure data for perovskite type materials with similar stoichiometries exists for compounds Sr_2YRuO_6 [10], Sr_2LuRuO_6 [11], Sr_2FeRuO_6 [12] and Sr_2ErRuO_6 [13]. All these materials, bar Sr_2FeRuO_6 (structure shown in Figure 5.5), crystallise in the $P2_1/n$ space group with structures like that shown below in Figure 5.4.

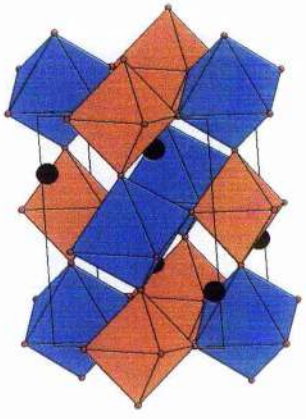

Figure 5.4. The monoclinic structure of Sr_2ErRuO_6 [13], with RuO_6 octahedra shown as orange, ErO_6 octahedra shown as blue with A – site Sr ions shown as black.

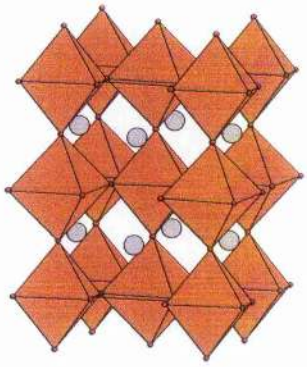

Figure 5.5. Structure of Sr_2FeRuO_6 with total disorder of Fe and Ru on the B – site.

A search of the PDF for materials with cubic unit cells of similar volume showed two promising candidates for a structural model in Sr_2LuTaO_6 [14] and Sr_2DyReO_6 [15]. These cubic materials belong to the space group Fm3m with a = 8.195 Å and 8.21 Å respectively. Crystallographic data was available for Sr_2DyReO_6 [16] and examination of an ideal pattern for this compound against the diffraction pattern obtained for Sr_2TbRuO_6 shows a good match (Figure 5.6). The structure of Sr_2DyReO_6 is shown in Figure 5.7 :

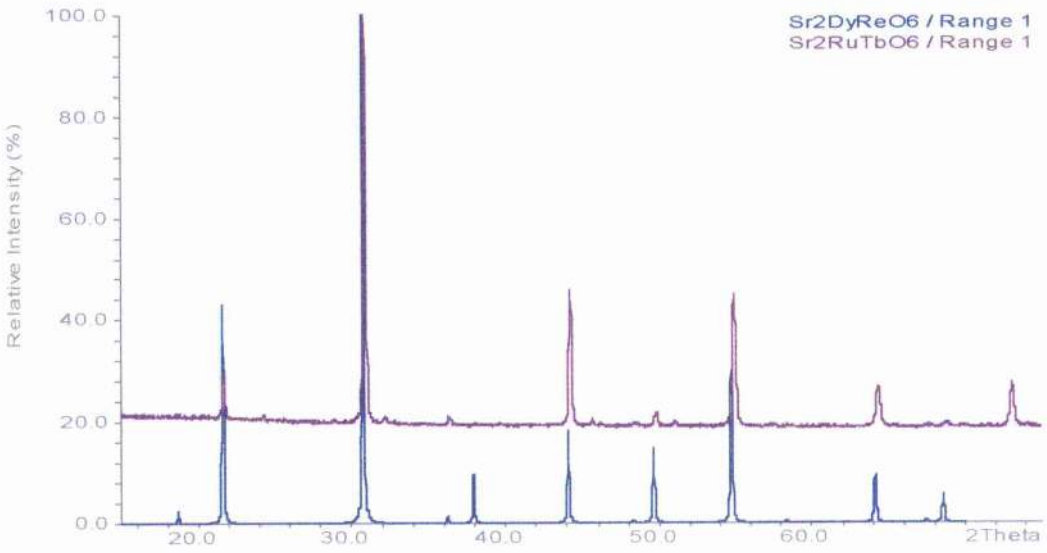

Figure 5.6. Comparison of the collected data for Sr_2TbRuO_6 (top profile) and an ideal pattern for Sr_2DyReO_6 (bottom profile).

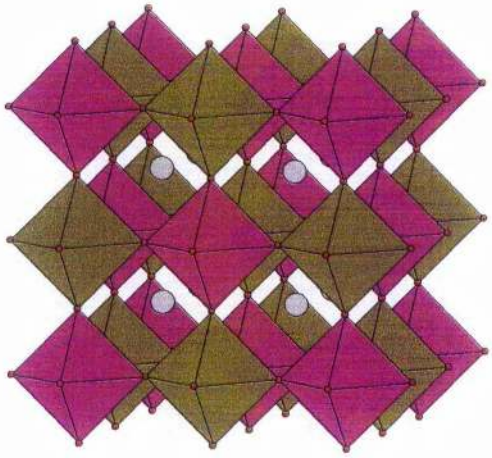

Figure 5.7. Structure of cubic Sr_2DyReO_6. ReO_6 octahedra are shown as purple with DyO_6 octahedra shown as olive. Sr positions are shown as grey.

5.4 Quadruple perovskites

The first set of experiments attempting to incorporate ruthenium into the quadruple perovskite structure involved the attempted synthesis of a series $Ln_2Ba_2Cu_2Ru_2O_{11}$ with members Ln = La, Nd, Gd and Tb.

5.4.1 $La_2Ba_2Cu_2Ru_2O_{11}$

Stoichiometric amounts of oxides and carbonates corresponding to the above formula were intimately mixed in an agate mortar and pestle and heated to 950°C, for 5 hours, to decompose the carbonate. The sample was then reground, made into a pellet and treated at 1000°C in air for 24 hour periods with x- ray analysis at the end of each treatment.

The resulting x – ray diffractogram of this procedure is shown below in Figure 5.8. This pattern shown was indexed on the basis of a cubic unit cell with a = 3.9858 Å.

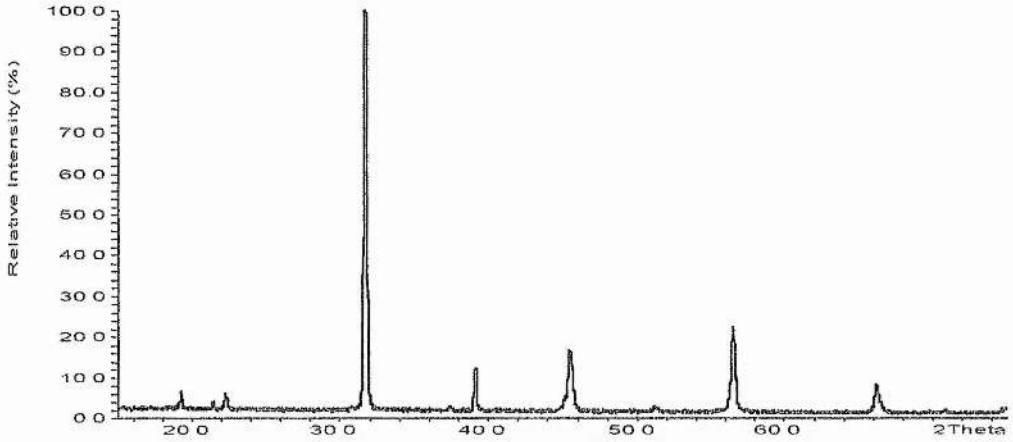

Figure 5.8. The x – ray pattern of the single phase realised on reaction of stoichiometric precursors corresponding to the formula $La_2Ba_2Cu_2Ru_2O_{11}$.

The observation of this cubic cell suggested we had a simple perovskite structure(Figure 1.5) with total disorder of La and Ba on the A – site and Cu and Ru

on the B - site. This is in contrast to the perovskite material, $LaBaCuRuO_{5.13}$ which shows B – site ordering to give the structure shown below in Figure 5.9.

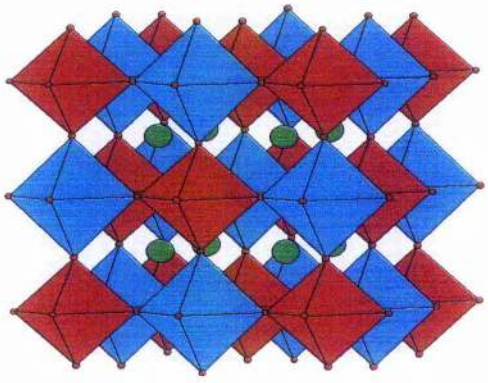

Figure 5.9. Structure of tetragonal $LaBaCuRuO_{5.13}$ [15]

This material is not completely ordered with about 6 % of Cu and Ru exchanging sites.

5.4.2 $Nd_2Ba_2Cu_2Ru_2O_{11}$

Stoichiometric amounts of binary oxides and carbonate corresponding to the above formula were intimately mixed in an agate mortar and pestle, pelletised and heated to 950°C for 5 hours to decompose the carbonate. The mixture was then heated for 36 hours at 1000°C. The resulting x- ray diffraction pattern is shown overleaf :

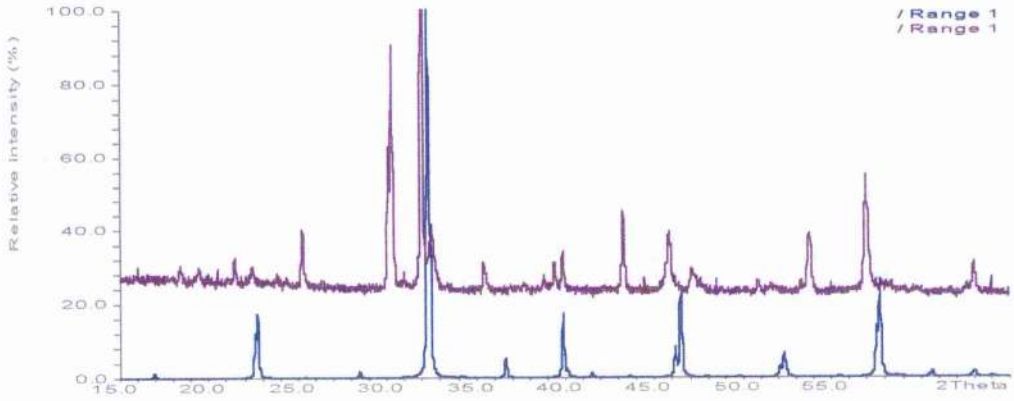

Figure 5.10. X – ray diffraction pattern of $Nd_2Ba_2Cu_2Ru_2O_{11}$ treated at 950°C for 5 hours, and 1000°C for 36 hours, in air. The bottom profile is of $Nd_2Ba_2Cu_2Ti_2O_{11}$

Analysis of the diffractogram in Figure 5.10 shows the product bearing little resemblance to the pattern for the isostructural $Nd_2Ba_2Cu_2Ti_2O_{11}$. The sample was thus heated for a further 36 hours at 1050°C with the following powder x – ray diffraction pattern realised :

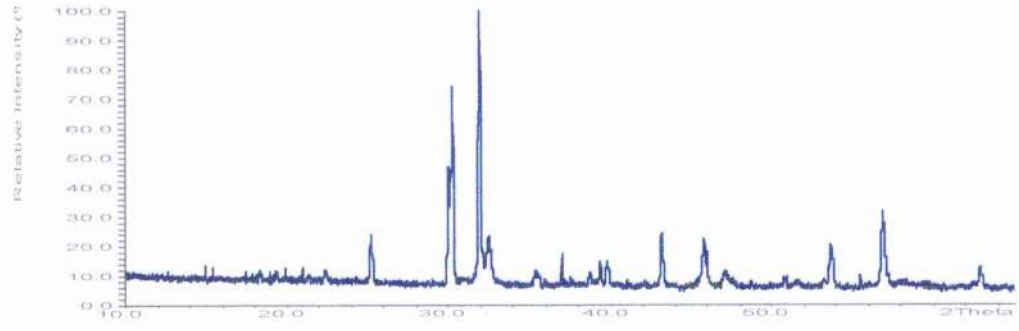

Figure 5.11. Powder x – ray diffraction pattern for $Nd_2Ba_2Cu_2Ru_2O_{11}$ following second heat treatment.

The sample was then treated at 1075°C for 36 hours with the following pattern realised :

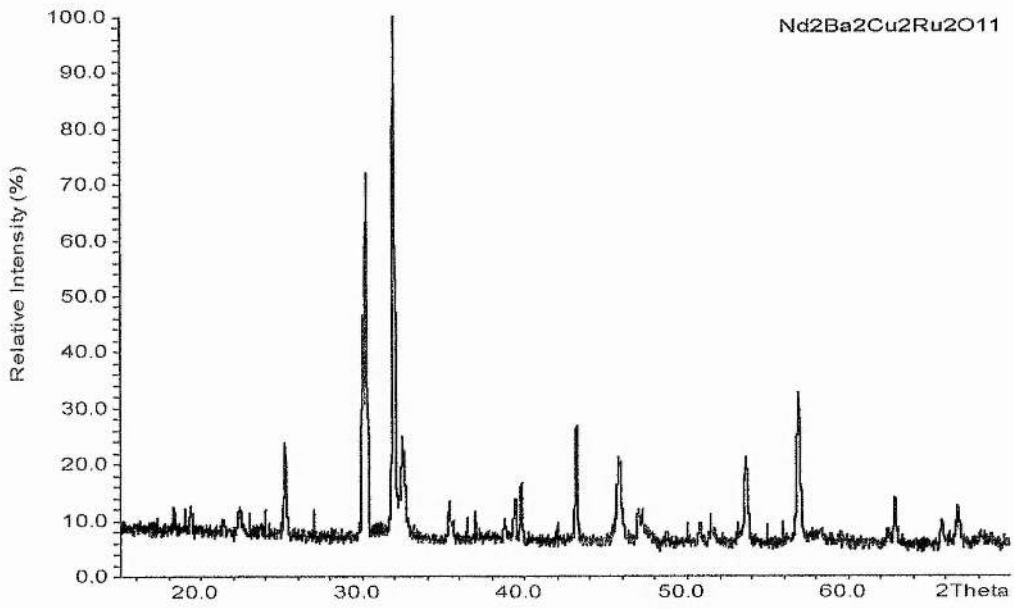

Figure 5.12. Powder x – ray diffraction pattern for $Nd_2Ba_2Cu_2Ru_2O_{11}$ following third heat treatment.

We observe that the progressive heat treatments of this stoichiometry doesn't produce the layered quadruple perovskite desired.

5.4.3 $Gd_2Ba_2Cu_2Ru_2O_{11}$

Stoichiometric amounts of binary oxides and carbonate corresponding to the above formula were mixed, pelletised and again heated for 5 hours at 950°C and 36 hours at1000°C. The product yielded the diffractogram shown overleaf in Figure 5.13.

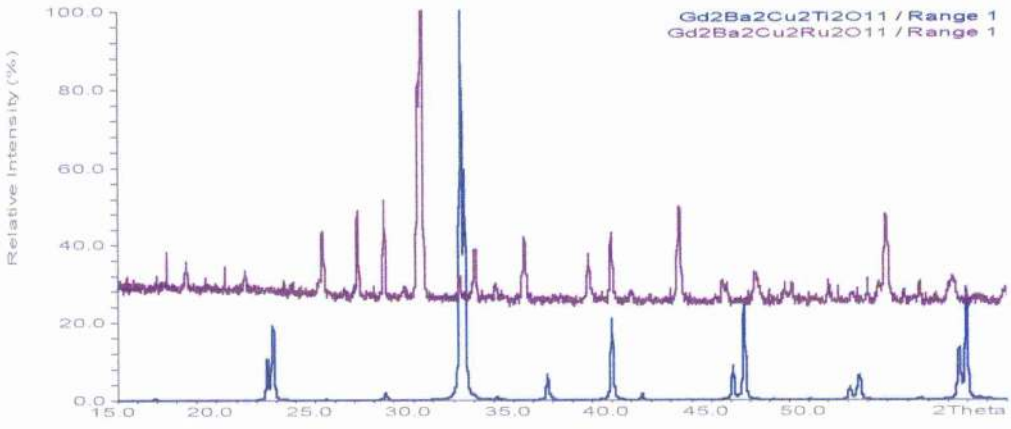

Figure 5.13. Product of $Gd_2Ba_2Cu_2Ru_2O_{11}$ after first heat treatment.

The sample was then treated at 1050°C for 36 hours with the diffractogram in Figure 5.14 realised. There appears little difference in the profiles obtained from progressive heat treatments.

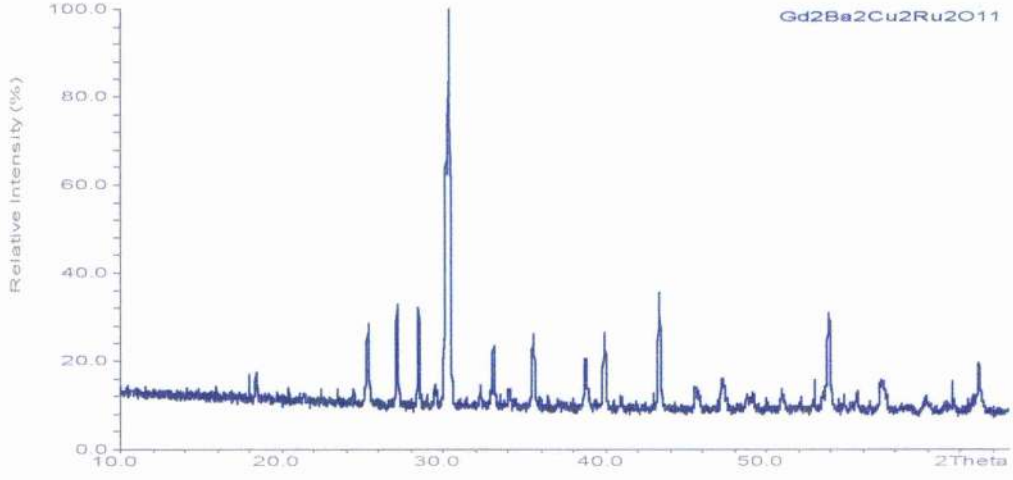

Figure 5.14. Product of $Gd_2Ba_2Cu_2Ru_2O_{11}$ after second heat treatment.

Further heat treatment at 1075°C for 36 hours realised the diffractogram shown in Figure 5.15. Again little change in the diffractogram is noticed with the desired quadruple perovskite structure not realised.

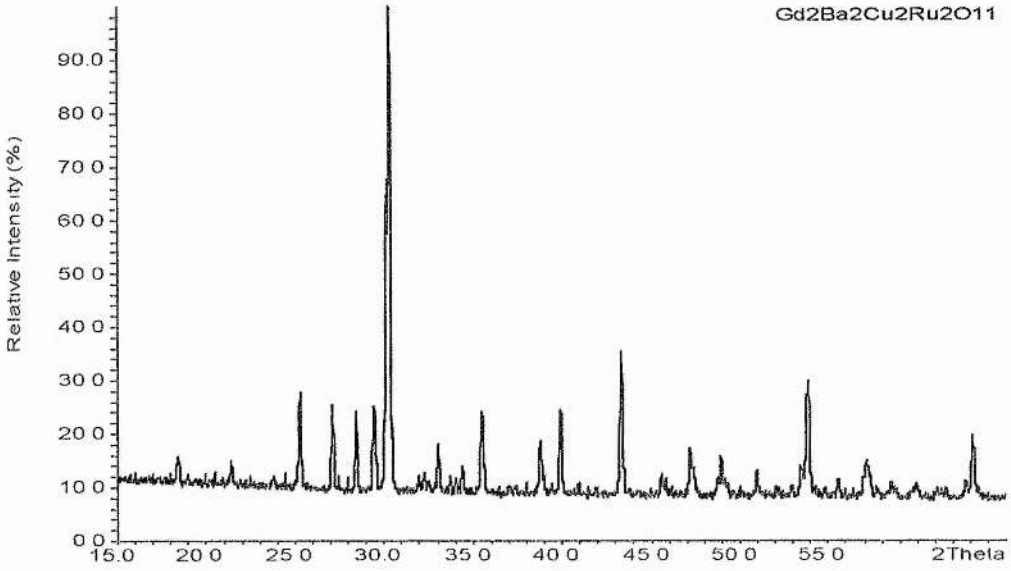

Figure 5.15. Product of $Gd_2Ba_2Cu_2Ru_2O_{11}$ after third heat treatment.

5.4.4 $Tb_2Ba_2Cu_2Ru_2O_{11}$

Stoichiometric amounts of binary oxides and carbonate corresponding to the above formula were mixed and pelletised. The sample was then treated at 950°C for 5 hours and 1000°C for 36 hours. The realised product showed a similar trace to that of $Gd_2Ba_2Cu_2Ru_2O_{11}$. ie.

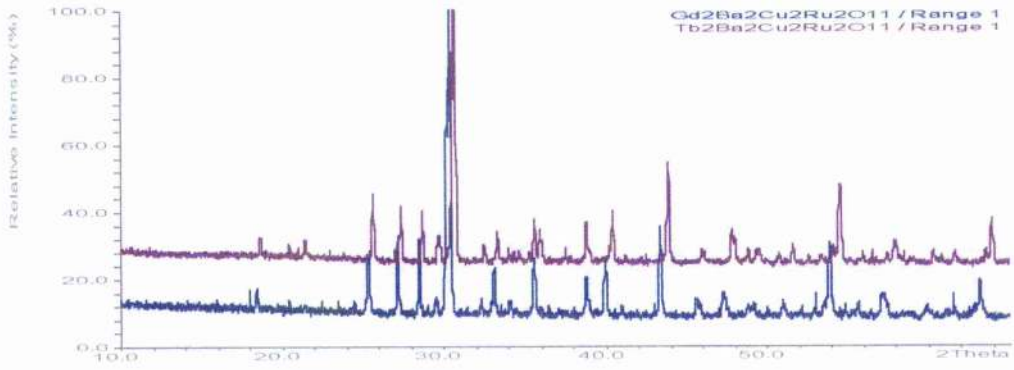

Figure 5.16. Product of reaction of above stoichiometry at 950°C for five hours and 1000°C for 36 hours.

5.4.5 Rentschler's Quadruple Perovskite

In 1995 T. Rentschler reported the structure of $NdBa_3Cu_2TiNbO_{11}$ showing it to be a quadruple perovskite, as discussed in Chapter 4, with ordering of oxygen vacancies and associated B site cations.ie.

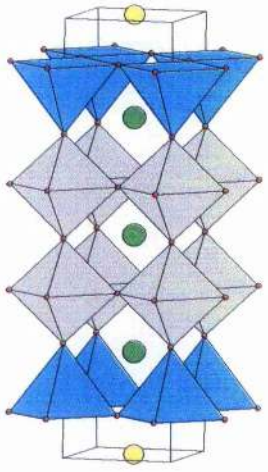

Figure 5.17. The structure of $NdBa_3Cu_2TiNbO_{11}$. Disordered Ti/Nb octahedra are shown as grey with CuO_5 pyramids shown as cyan. Ba sites are shown as green and Nd sites are shown as yellow [17].

We hoped that we could substitute ruthenium for niobium in this new quadruple perovskite stoichiometry, with the smaller Ru ions lending to products with lattice parameters suitable for superconductivity.

The publication by Bauernfeind et al. [2] showed that ruthenium and niobium were able to substitute for each other in the 1 – 2 – 1 – 2 structure with the publication of lattice parameters shown overleaf :

Table 5.1. Lattice parameters of $RuSr_2LnCu_2O_8$ in comparison to $NbSr_2LnCu_2O_8$.

Compound	A	c
$RuSr_2SmCu_2O_8$	3.852 Å	11.56 Å
$NbSr_2SmCu_2O_8$	3.877 Å	11.64 Å
$RuSr_2EuCu_2O_8$	3.843 Å	11.55 Å
$NbSr_2EuCu_2O_8$	3.872 Å	11.63 Å
$RuSr_2GdCu_2O_8$	3.838 Å	11.53 Å
$NbSr_2GdCu_2O_8$	3.869 Å	11.62 Å

5.4.5.1 $NdBa_3Cu_2TiNb_{1-x}Ru_xO_{11}$

Experiments involved the investigation of the $NdBa_3Cu_2TiNb_{1-x}Ru_xO_{11}$ system with stoichiometries of x = 0, 0.5 and 1 prepared by reaction of suitable amounts of precursor oxides and carbonates. The mixtures were treated at 950°C for five hours to decompose the carbonates and then at 1050°C for twenty four hour periods. The

twenty four hour heating periods were followed by x – ray analysis with repeated heating until the diffraction profiles, from one heating to the next, showed no change. Final x – ray diffraction plots for the aforementioned stoichiometries are shown below in Figure 5.18. We see from inspection of these profiles that the x = 0 member gives a profile suggesting partial accomplishment of the desired quadruple perovskite structure. The x = 0.5 member also shows partial accomplishment, however there is an increase in impurities when compared to the x = 0 member.

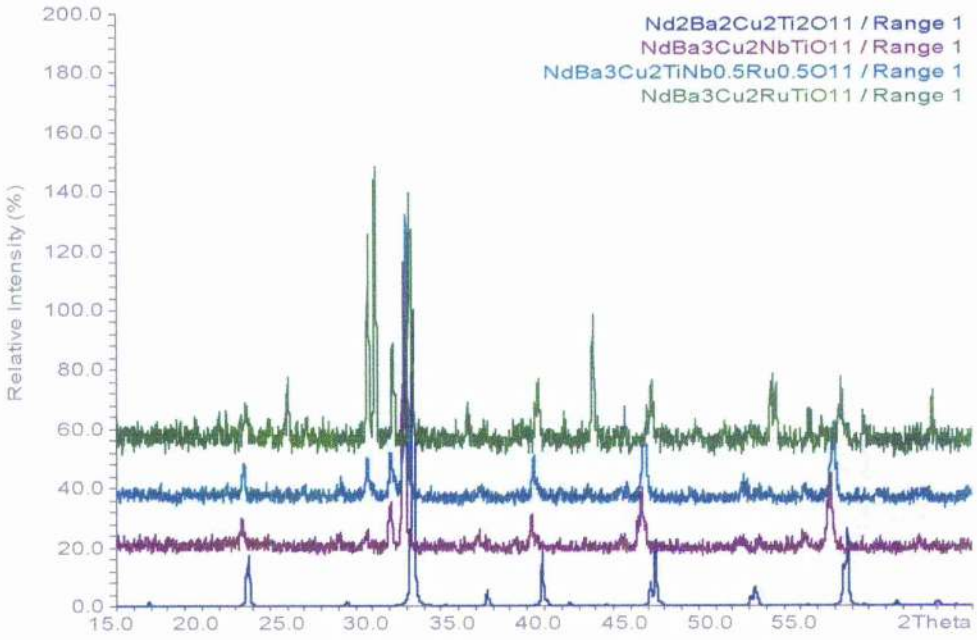

Figure 5.18. X – ray patterns for the stoichiometries $NdBa_3Cu_2TiNb_{1-x}Ru_xO_{11}$: x = 0, 0.5, 1. The bottom profile shows a pattern for $Nd_2Ba_2Cu_2Ti_2O_{11}$ with the structure desired.

Comparison of the profiles of $NdBa_3Cu_2TiNbO_{11}$ and $NdBa_3Cu_2TiNb_{0.5}Ru_{0.5}O_{11}$ is quite interesting :

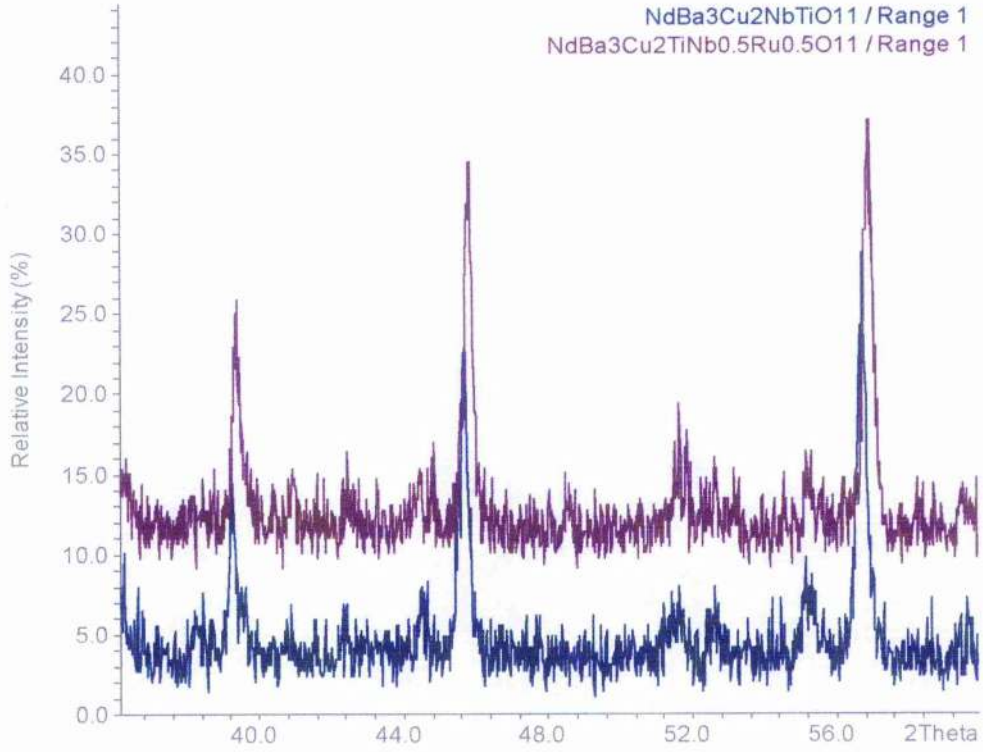

Figure 5.19. Section of diffractograms of $NdBa_3Cu_2TiNbO_{11}$ (bottom) and $NdBa_3Cu_2TiNb_{0.5}Ru_{0.5}O_{11}$.

Although both these traces show impurities in the three most intense peaks show similarity to those of the desired quadruple perovskite with a shift to lower d spacing intimating some substitution of the smaller Ru for Nb.

To see if substitution of the smaller Ru (ionic radius in coordination number of six = 0.565 Å) for Nb (0.64 Å) [18] could be achieved with a coopertative reduction in the size of the lanthanide species the stoichiometry $GdBa_3Cu_2TiRuO_{11}$ was prepared and reacted as described for $NdBa_3Cu_2TiNb_{1-x}Ru_xO_{11}$.

5.4.5.2 $GdBa_3Cu_2TiRuO_{11}$.

Reaction of the above stoichiometry at 1050°C for seventy two hours (following a five hour treatment at 950°C) realised the profile shown in Figure 5.20.

Analysis of this diffractogram by searching for matches to the major peaks in the JCPDS.PDF shows that the majority of the peaks can be attributed to a 6H – hexagonal perovskite type structure, observed by the family $Ba_3MRu_2O_9$ (M = Ni and Zn)[19] as shown below in Figure 5.20.

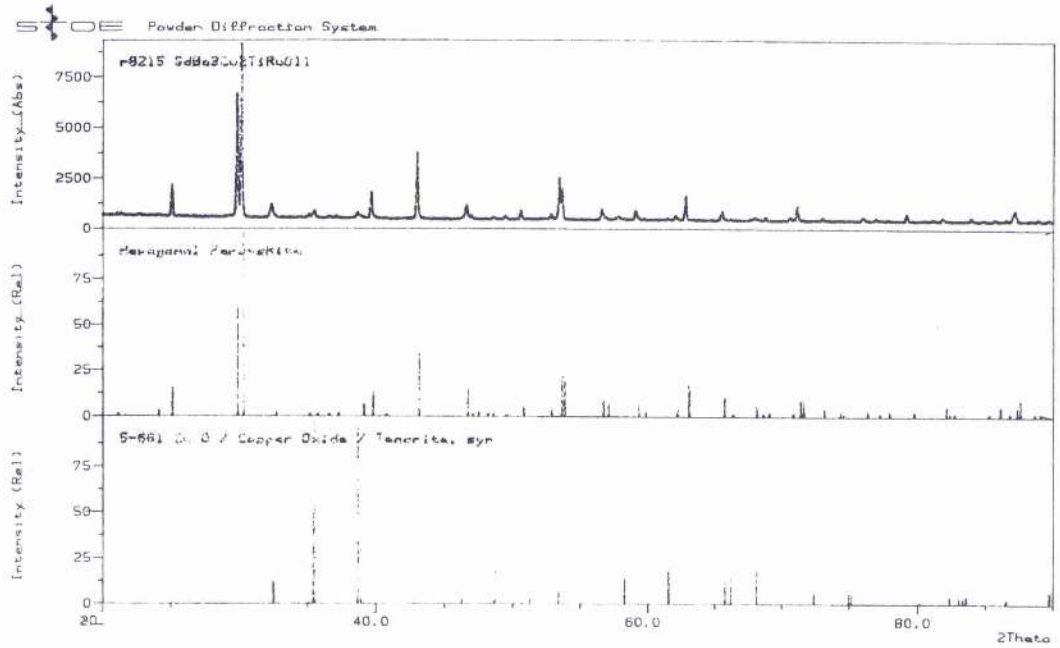

Figure 5.20. Comparison of the profiles of reacted $GdBa_3Cu_2TiRuO_{11}$ with that of the 6H – perovskite $Ba_3GdRu_2O_9$.

5.5 Discussion and Summary.

Ruthenates have been investigated with a view to producing materials that exhibit both superconductivity and ferromagnetism as in the 1-2-1-2 type $RuSr_2GdCu_2O_8$.

I sought to expand the range of this structure type by substituting Tb for Gd. My experiments to this end showed that, as in the Dy and Y analogues, instead of the

desired structure we obtain a cubic material of nominal stoichiometry Sr_2RuTbO_6 and CuO.

I then tried to produce quadruple perovskites of formula $Ln_2Ba_2Cu_2Ru_2O_{11}$ with Ln = La, Nd, Gd and Tb. I found that solid state reaction did not yield the desired quadruple perovskite structure but rather a simple cubic perovskite for Ln = La and a mixture of non identifiable phases for the other members.

With the inability to substitute Ru for Ti in the above mentioned system I moved to work on a stoichiometry outlined by Rentschler [17].

This $NdBa_3Cu_2TiNbO_{11}$ stoichiometry was shown to have a quadruple perovskite structure. Ru has been shown to readily substitute for Nb by Bauernfiend [2] and thus I sought to substitute Ru for Nb in the mentioned stoichiometry.

Samples of stoichiometry $NdBa_3Cu_2TiNb_{1-x}Ru_xO_{11}$, x = 0, 0.5 and 1, were prepared. Partial substitution appears to take place with peaks shifted to lower d spacing when comparing the x = 0 and 0.5 members, however both the x = 0.5 and 1 members show significant impurities.

Trying a cooperative reduction in the size of the lanthanide with the substitution of Ru for Nb, i.e. $GdBa_3Cu_2TiRuO_{11}$, forms an alternative 6H – perovskite.

References for Chapter 5.

[1] Tallon J.L., Bernhard C., Bowden M.E., Stoto T.M., Walker B., Gilberd P.W., Presland M.R., Attfield J.P., McLaughlin A.C. and Fitch A.N., unpublished results.

[2] Bauernfeind L., Widder W. and Braun H.F., *Physica C* **254**, 151 (1995).

[3] McLaughlin A.C., Zhou W., Attfield J.P., Fitch A.N. and Tallon J.L., *Phys. Rev.* **B60**, 7512 (1999).

[4] Bernhard C., Tallon J.L., Niedermayer Ch., Blasius Th., Golnik A., Brucher E., Kremer R.K., Noakes D.R., Stronach C.E. and Ansaldo E.J., *Phys. Rev.* **B59**, 14099 (1999).

[5] Cho J.H., Jia Q.X., Wu X.D., Foltyn S.R. and Moley M.P., *Phys. Rev.* **B54**, 37 (1996).

[6] Brown I.D., *J. Solid State Chem.* **82**, 122 (1989).

[7] Klamut P.W., Dabrowski B., Kolesnik S., Maxwell M. and Mau J., *Phys. Rev.* **B63**, 224512 (2001).

[8] Felner I., Asaf U., Levi Y. and Millo O., *Phys. Rev.* **B55**, R3374 (1997).

[9] Werner P.-E., Eriksson L. and Westdahl M., *J. Appl. Crystallogr.* **18**, 360 (1989).

[10] Battle P.D. and Macklin W.J., *J. Solid State Chem.* **52**, 138 (1984).

[11] Battle P.D. and Jones C.W., *J. Solid State Chem.* **78**, 108 (1989).

[12] Battle P.D., Gibb T.C., Jones C.W. and Studer F., *J. Solid State Chem.* **78**, 281 (1989).

[13] Battle P.D., Jones C.W. and Studer F., *J. Solid State Chem.* **90**, 302 (1991).

[14] PDF card no. 24 – 1126.

[15] PDF card no. 24 – 1195i.

[16] Baud G. and Capestan M., *Bull de la Soc. Chimique de France*, p 1872 (1969).

[17] Rentschler T., *Physica C* **276**, 109 (1997).

[18] Shannon R.D., *Acta Crystallographica* **A32**, 751 (1976).

[19] Lightfoot P. and Battle P.D., *J. Solid State Chem.* **89**, 174 (1990).

6. Conclusions and Further Work.

6.1 Bismuth Oxyhalides

The aim of my work on bismuth oxyhalides was to synthesise and characterise a new series of Sillen / Ruddlesden Popper intergrowths. The possibility of such an intergrowth system was intimated by a publication by Zhu et al. [1]. They claimed to have made a Sillen X1X2 / Ruddlesden Popper intergrowth phase of composition $Bi_{2.4}Ca_{3.1}CuO_{6-y}Cl_5$. The structure they postulated was such that a T type $Ca_2CuO_2Cl_2$ unit was sandwiched between the halide layers of the X2 section of an X1X2 Sillen phase.

I attempted to produce a stoichiometric compound of such a structure type by reaction of quantities equating to a formula of $Bi_3Ca_3CuO_6Cl_5$. Attempts at such a synthesis were initially carried out in air, however it was found that a new compound of formula $CaBiO_2Cl$ was preferentially formed. I therefore conclude that the desired structure cannot be synthesised in air.

In their paper Zhu et al. reported that the structure type was formed on reaction in an inert atmosphere and hence the experiment was repeated under flowing N_2. I observed that a pattern similar to that for the desired compound was only formed after exposure of the product to air. This exposed compound was of a grey / green colour and not the black expected of a compound containing CuO_2 sheets. These observations led me to conclude that instead of the desired product Zhu et al. were actually observing the formation of the hydrated analogue of an X1X3 phase. Synthesis of compositions pertaining to the formation of such an X1X3 product was carried out with varying Cu : Ca ratios. X - ray diffraction pattern analysis and lattice parameter calculations appear to confirm that Cu can be incorporated into the Sillen

X1X3 structure and that this structure hydrates to give a crystalline product of dimensions similar to the desired intergrowth system.

Attempts to incorporate T type La_2CuO_4 and T' type Nd_2CuO_4 between chloride layers in Sillen phases were shown to be hindered by the alternative formation of a novel variant of the Sillen X1 structure with the halide layer sandwiched between triple fluorite layers of composition Bi_2LaO_4Cl and Bi_2NdO_4Cl thus allowing me to conclude that these desired structures cannot be formed by conventional solid state synthesis.

Further work could involve alternative synthetic strategies such as use of sealed silica tubes or preformation of the Ruddlesden Popper unit before reacting with a Sillen phase.

Had such a Sillen / Ruddlesden Popper intergrowth existed I would have attempted to incorporate n = 2 Ruddlesden Popper units such as $Ca_3Cu_2O_4Cl_2$ [2] and T* compounds, $MLnCuO_3Cl$ outlined by Fuller and Greenblatt[3] with M = Ca, Sr and Ln = Nd, Sm, Eu and Gd.

6.2 Quadruple Perovskites

I feel that a lot more work could be done on this system.When preparing my samples I only reacted until there were no impurity peaks. A publication by Palacin et al.[4] showed that prolonged heating of these compounds results in a greater degree of ordering. Had I employed such a tactic I feel that more useful information on the response of this system to the doping strategies tried could have been realised.

What I do feel I can conclude is that Sr can be substituted for Ba in the $Nd_2Ba_{2-x}Sr_xCu_2Ti_2O_{11}$ system and in the $Gd_2Ba_{2-x}Sr_xCu_2Ti_2O_{11}$ as the x = 0.1 member of the Tb analogue shows noticable impurity peaks and hence low levels of Sr based

impurities are not completely masked by the strong scattering nature of these phases. ie Had Sr not been incorporated in to the Nd and Gd members impurity peaks would be observed.

My investigation of the $Nd_2Ba_2Cu_{2+x}Ti_{2-x}O_{11}$ system arrives at the same conclusions as a Den et al.[5] in that the copper site becomes less tainted by disorder with Ti^{4+} on increasing x. However they claim that a value of x = 0.09 is enough to give totally intact CuO_2 sheets whereas I observed disorder even in the x = 0.2 phase.

Further work would thus again involved more prolonged heating of these samples to try to reach the maximum ordering possible. I would also like to investigate the $Tb_2Ba_2Cu_{2+x}Ti_{2-x}O_{11}$ system to see if copper can still exist in excess in the structure even though the stoichiometric compound is fully quadrupled. Successful incorporation may be enough to dope the CuO_2 planes with enough holes to induce superconductivity. The response of oxygen content to such doping would be investigated to determine if the holes are trapped by oxygen vacancies. Bond valence sums, neutron diffraction studies and iodometric titrations could be employed to investigate any suitably doped compounds.

6.3 Ruthenates

In chapter 5 a new composition (Sr_2RuTbO_6) with an old structure (double perovskite, Fm3m, a = 8.194 Å) was produced on attempting to produce a new 1-2-1-2 structure. This result allows the conclusion that this 1-2-1-2 structure is at its smallest as the Gd version ($Sr_2GdCu_2RuO_8$).

Attempts to produce quadruple perovskites of general formula $Ln_2Ba_2Cu_2Ru_2O_{11}$ were unsuccessful however the simple cubic material produced when compared with

the structure of $LaBaCuRuO_{5.13}$ shows that perovskite structures and in particuliar B – site cation ordering are affected by oxygen stoichiometry.

The pattern for $NdBa_3Cu_2TiNb_{0.5}Ru_{0.5}O_{11}$ is interesting as there appears to be a small amount of Ru actually incorporated into the structure, further work would involve longer reaction times to obtain better patterns and further investigation as to the amount of Ru that can be accomodated. In order to even stand a chance of exhibiting superconductivity and ferromagnetism we would require to fully substitute Ru for Nb and also see layered ordering of the Ti and Ru sites.

One such way of trying to accommodate more of the smaller Ru was to reduce the size of the lanthanide species however there is competitive formation of a material with the 6H- perovskite structure. Investigation of systems with different lanthanide to barium ratio's may allow greater amounts of Ru to be incorporated in the quadruple perovskite structure.

References for Chapter 6.

[1] Zhu W.J., Huang Y.Z., Liang J.K. and Zhao Z.X., *Materials Research Bulletin* **27**, 885 (1992).

[2] Sowa T., Hiratani M. and Miyauchi K., *J. Solid State Chem.* **84**, 178 (1990).

[3] Fuller R.L. and Greenblatt M., *J. Solid State Chem.* **92**, 386 (1991).

[4] Palacin M.R., Krumeich F. and Gomez – Romero P., *Solid State Ionics* **101**, 1079 (1997).

[5] Den T., Kobayashi T., Izumi F., Kamiyama T., Shimakawa Y., Jorgensen J.D., Rotella F.J. and Hitterman R.L., *Physica C* **255**, 37 (1995).